FINAL TECHNICAL REPORT
THERMAL ENERGY STORAGE
RESEARCH AND DEVELOPMENT PROGRAM

6 December 1960 to 1 December 1961

E. F. Batutis

Prepared for National Aeronautics and Space Administration
Contract No. NAS 5-826
G-E Requisition No. 214-787

Missile and Space Vehicle Department
GENERAL ELECTRIC

FINAL TECHNICAL REPORT
THERMAL ENERGY STORAGE
RESEARCH AND DEVELOPMENT PROGRAM

6 December 1960 to 1 December 1961

E. F. Batutis

Prepared for National Aeronautics and Space Administration
Contract No. NAS 5-826
G-E Requisition No. 214-787

Missile and Space Vehicle Department
GENERAL ELECTRIC

FINAL TECHNICAL REPORT
THERMAL ENERGY STORAGE
RESEARCH AND DEVELOPMENT PROGRAM

6 December 1960 to 1 December 1961

by: E. F. Batutis, Chemist, Energy Conversion Materials
Approved by: B. Klawans, Program Manager, Space Power

Missile and Space Vehicle Department
GENERAL ELECTRIC
3198 Chestnut Street, Philadelphia 4, Penna.

ACKNOWLEDGEMENTS

The technical work on this program has been done by Dr. E. Feingold, Dr. F. Bowman, Dr. G. Kibler, Dr. P. Gorsuch, Messrs. R. Frank, W. Flanigan, M. Lapides, D. Purdy, and E. Ray as well as by the author.

The aid of Mr. Thomas A. Moss, Project Engineer, National Aeronautics and Space Administration, Lewis Research Center, is gratefully recognized.

CONTENTS

CONTENTS (Cont'd)

LIST OF ILLUSTRATIONS

TABLES

ABSTRACT

ABSTRACT

Silicon and a number of refractory oxide mixtures were studied in an investigation of materials having the properties of high heat of fusion and melting temperatures ranging from 1600 to 2100^{o}K. These thermal energy storage (TES) materials were examined for usage in solar collector-thermionic converter electrical power systems employed in space vehicles.

Successful refractory oxide mixture containment in refractory matals up to 500 hours was achieved. Adequate containment of silicon was obtained for 100 hours. However, silicon container sealing and fabrication has not been completely resolved. Recommended additional effort is described herein.

In a limited directive system study, the oxide materials and silicon were evaluated as part of a solar thermionic electric power system. Calculated specific system weights ranged from 75 to 127 pounds per kilowatt for four of the most attractive oxide materials as compared to 160 pounds per kilowatt using silicon. The higher operating temperatures possible using oxides was the major parameter resulting in specific system weights lower than that calculated for silicon.

1. SUMMARY

1. SUMMARY

This program was directed toward the development of materials useful for thermal energy storage application in the range of 1600 to 2100° K. The experimental effort involved containment of these materials as well as determination of certain thermophysical properties including heat of fusion, melting point and density. A limited directive system study was also included.

Silicon with a heat of fusion of 200 watt-hours per pound (wh/lb) was studied with respect to containment only, since most of its thermophysical properties were known. A good measure of success was accomplished using boron nitride and pyrolytic graphite as container materials for periods to 100 hours and indications were that containment to the order of 1,000 to 10,000 hours could be attained. Fabricating sealed vessels and joining containers to thermionic coverter cathode materials remain major problems. Possible solutions to these materials problems were studied and continued study areas are suggested.

Additional thermal energy storage materials were uncovered and include a wide variety of stable oxide binary and ternary compounds and eutectics with melting points ranging from 1630 to 2145° K. The basic oxide combination with most potential use is BeO-MgO, which, as a binary or in ternary mixtures, has provided heats of fusion ranging from 179 to 264 wh/lb. These BeO-MgO base mixtures are:

	Heat of Fusion (wh/lb)	M.P. (°K)
$4BeO \cdot 4MgO \cdot Al_2O_3$	179	1910
$4BeO \cdot MgO \cdot Al_2O_3$	190	2020
$3BeO \cdot 2MgO$	264	2145

Other oxide mixtures found in this study and of interest are:

	Heat of Fusion (wh/lb)	M.P. (°K)
$3MgO \cdot B_2O_3$	95	1630
$3BeO \cdot 2CaO$	117	1685

	Heat of Fusion (wh/lb)	M.P. (^{o}K)
$3CaO \cdot B_2O_3$	69	1770
$3BeO \cdot Al_2O_3 \cdot 2TiO_2$	121	1883
$2BeO \cdot Al_2O_3 \cdot 4TiO_2$	127	1883
$Al_2O_3 \cdot 3MgO \cdot 4TiO_2$	85	1910
$2BeO \cdot 3TiO_2$	100	1930
$2BeO \cdot 5Al_2O_3 \cdot 2TiO_2$	80	1960
$5BeO \cdot 4MgO \cdot 3ZrO_2$	113	1973
Silicon	227	1693

Note: Silicon for comparison.

From those given above, several oxide mixtures approach the heat of fusion of silicon. In addition, the higher melting temperatures would allow operation of converters in the regions of higher efficiencies. Directive systems studies show that this increase in converter efficiency can make these oxides much more attractive (as TES materials) than silicon. Other properties which have an effect on choice of materials are: density, containment, materials compatibility, thermal conductivity. The oxides score well in all of these areas except for the last. However, it is believed that thermal conductivity might be improved by using fins or some other kind of arrangement. The oxides are more dense than silicon (less volume needed); compatibility-wise, the converter and container can be made from the same metal. Containment on the order of 500 hours has been attained in molybdenum; tungsten shows even better resistance.

Directive systems studies of limited scope have been made. These studies do show that select oxide mixtures appear more attractive for use as thermal energy storage materials than silicon. The systems studies have shown that system specific weights (excluding orientation components) on the order of 75 to 125 lb per kilowatt are possible with a number of the oxides uncovered as compared to a silicon system weight of 160 lb/kw. Thermal energy storage, using heat of fusion, favorably compares with the estimated 225 lb/kw utilizing storage

batteries in lieu of thermal energy storage in a solar thermionic power system satellite whose orbit passes into shadow zones. Comparison with a present-day photovoltaic system using rechargeable batteries shows weight advantage by factors of five to ten times for the postulated system.

2. INTRODUCTION

2. INTRODUCTION

The work covered in this report was a study of fusible materials, and containers for such materials, that would be suited for high temperature thermal energy storage. The Lewis Research Center of the National Aeronautics and Space Administration supported this effort which is part of a larger program conducted by the Missile and Space Vehicle Department of the General Electric Company to develop a direct conversion solar thermionic electrical power system for use in space applications.

The objectives of the work reported here were:

a. To provide a thermal energy storage (TES) material which could store up to 200 wh/lb when used in conjunction with a solar thermionic electric power system (1600 to 2100^{O}K cathode temperature).

b. To indicate a containment life of 60 days at temperature.

c. To indicate life of 100 cycles between liquid and solid states of TES material.

d. To conduct a limited directive system study.

Initially, the major emphasis was on use of silicon as the TES material, in either a pure or a doped state, and silicon containment was a primary objective. As a secondary objective, various ceramic oxides were also investigated as potential alternate TES materials; specifically included were the binaries, BeO-MgO and BeO-CaO. Because of the sealing problems encountered with silicon, emphasis shifted first to the oxide thermophysical properties determinations and, when these proved attractive, to containment and sealing of the oxides.

Specifically, a more concentrated effort on oxides was made (1) to determine if oxide eutectic melting was sharp and congruent, (2) to establish heat of fusion valves experimentally, and finally (3) to get some data on corrosion rates and

compatibility with refractory metals. These areas were delved into for a number of oxide eutectics which were chosen from existing phase diagrams found in the literature, and which represented best choices from myriad possible oxide combinations.

The experimental effort will be reported in a chronological sequence for the most part. The studies of silicon containment are reported first, followed by the oxide studies and finally the directive system study. The work was also reported in a series of monthly progress letters and an Interim Report was written mid-way in the program. (See Reference 19).

3. SILICON CONTAINMENT MATERIALS STUDIES

3. SILICON CONTAINMENT MATERIALS STUDIES

In earlier phases of GE-sponsored effort in this area, possibility of silicon containment was indicated for approximately 100 hours with a variety of ceramic-coated metals. Longer life extrapolations could not be made from this data. Therefore, in the early phases, materials screening tests were planned, to be followed by diffusion or corrosion rate studies to permit assessment of long operating life capability.

3.1 Discussion

The data given in Figure 1 indicate the prominence of silicon as a potential TES medium. The melting point of silicon, 1683°K, lies within the limits set for thermionic converter operation. It has a heat of fusion (energy per unit mass, or weight) roughly four times that of titanium, the next most attractive element in the 1600°K-2100°K melting point interval. Beryllium falls below 1600°K and was not considered. Listed in Table I are the generally accepted values of important TES parameters for silicon.

TABLE I

SELECTED THERMODYNAMIC AND PHYSICAL PROPERTIES OF SILICON

H_f(1)	M.P. (2)	K_T(3)	ρ
395 cal gm^{-1}	1683°K	0.06 cal $(sec\text{-}cm\text{-}^{o}C)^{-1}$	2.33 gm cm^{-3}
209 watt-hr lb^{-1}	2571°R	0.35 watt $(in^{o}F)^{-1}$	0.084 lb in^{-3}

The use of silicon as a TES medium presented two major problems: (1) Molten silicon is a reactive material and hence is difficult to contain for long periods of time. (Reference 5) Berezhnoi, in his excellent review of the binary systems of silicon, states that "silicon reacts with 79 percent of the elements, forming numerous compounds (more than 160 of them are known at present). This is an indication of the high chemical activity of silicon." (2) Silicon

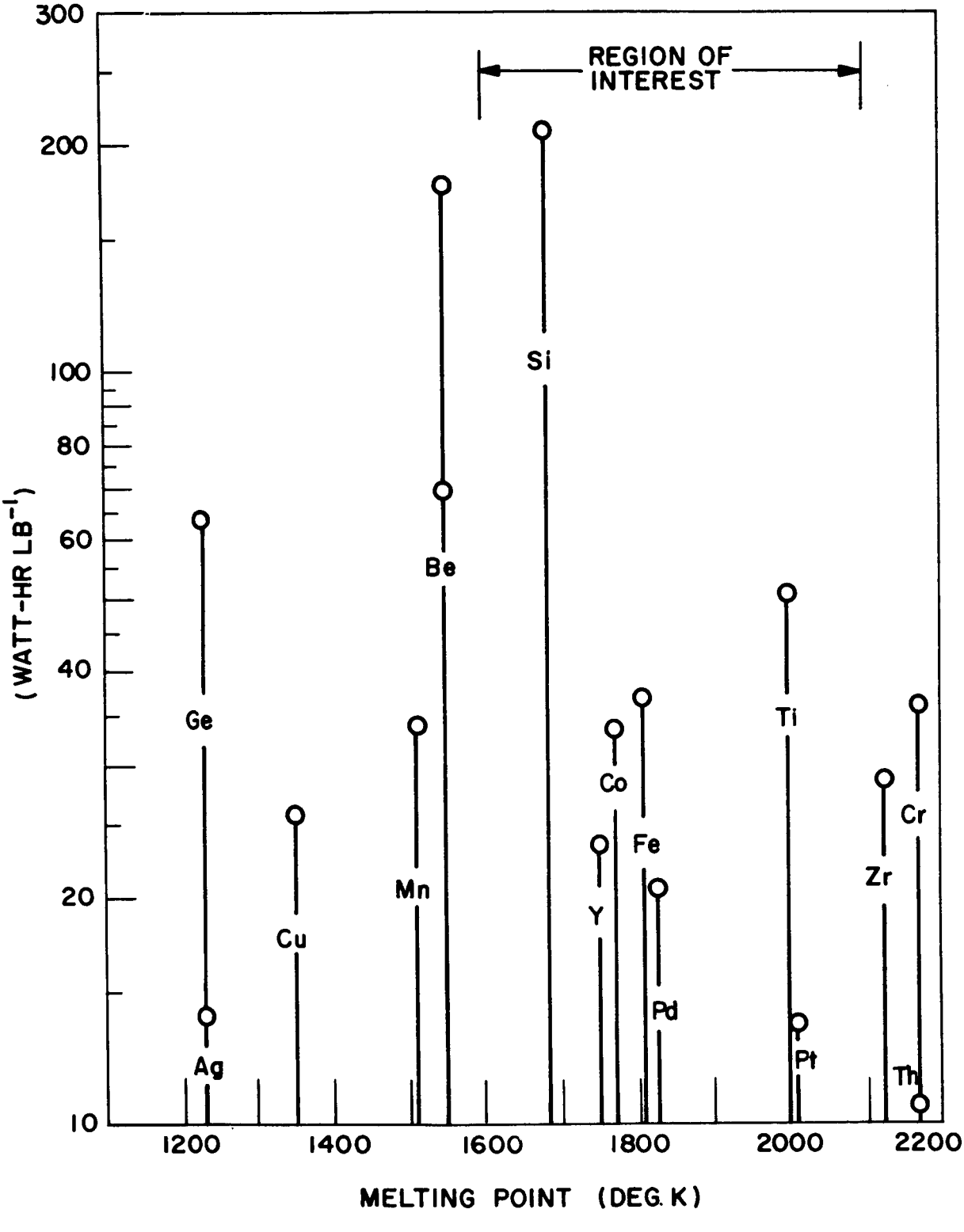

Figure 1. Heat of Fusion of Some Selected Elements (Data from Ref. 4)

exhibits an anomalous volume expansion when it freezes (a volume increase of approximately 10 percent).

The latter problem was not thought to be insurmountable. If necessary, one could compensate for anomalous expansion effects by proper container design By introducing fins inside the container, one could provide adequate thermal paths between the contained silicon and the container walls to avoid thermal impedances caused by voids in the silicon melt. The fins could also be arranged to control the freezing pattern to prevent any internal pressure build-up within the mass.

The containment study was begun by engaging in a comprehensive survey of pertinent literature as well as investigating sources in industry, and research activities. The following observations were made after careful digestion of these sources.

The containment of molten silicon has been a problem of concern in the semiconductor industry. There it has been imperative that the impurity content in silicon be maintained controllably low during processing. Hence considerable effort was directed toward studies concerning the choice of materials for crucibles to be used in silicon purification. For the most part, containment did not involve long time periods.

Although thermodynamic considerations (Ref. 6) indicated that beryllia, magnesia or alumina would not be reduced by silicon, it was found that silicon prepared in crucibles of these materials showed metallic contamination. Other investigators have reported that thermodynamic studies (Ref. 7) indicated that silicon will somewhat reduce all pure oxides. Where oxygen contamination is preferred to metallic contamination, i.e., in the production of rectifiers, fused silica crucibles have been employed (Ref. 8, 9, and 10). Seitz (Ref. 11) has concluded that silicon has an appreciable solubility for silica and becomes saturated with oxygen when melted in fused silica crucibles. Zirconia, alumina and magnesia contain sufficient silica due to commercial processing methods to offer no advantage over pure silica.

Seitz (Ref. 12) also demonstrated that high-purity silicon ingots could be made in high-purity magnesia crucibles. Others have had little success in using magnesia crucibles in the purification of silicon. Johnson and Hansen (Ref. 13) found that with rapid melting in crucibles of high-purity alumina there was very little attack of the crucible by the molten silicon.

In a private communication, Runyan (Ref. 14) stated that he has used silicon nitride in short term molten silicon containment experiments (1-3 hours). He found some contamination of the silicon but had negligible evidence of solution. He also reported that silicon did not wet the container.

Coated refractory metals were studied at General Electric Company previous to this effort since the fabricability of metals was more desirable than with nonmetallic containers. In one case, using a General Electric System 400* coating on columbium, containment for 78 hours was shown. However, serious problems were encountered in maintaining coating integrity under cycling conditions. Therefore other coatings and techniques were evaluated in this effort.

3.2 Experimental Effort

Two types of high-temperature vacuum equipment were used in the screening studies. These are discussed in Appendix A. The apparatus which departs from conventional equipment is described in more detail.

3.2.1 Screening Tests

3.2.1.1 Test Procedures

All tests were made in vacuum (10^{-6} mm Hg) at temperatures between 1500°C and 1550°C for periods of one hour, two hours, five hours and in certain cases one hundred hours.

*Flame-sprayed alumina, silica binder

Whenever possible, crucibles and caps of the materials under investigation were used. In all other cases tests were made in capped boron nitride crucibles. As will be discussed later, it was found that boron nitride contained molten silicon for long periods of time (at least one hundred hours) without evidence of chemical attack.

In all screening tests Electromet high purity (99.8 percent)* silicon powder, supplied by Union Carbide, High Purity Metals Division, Niagara Falls, New York, was used. This type of silicon was employed because it was of commercial quality, readily obtained and typical of the material that might be used in TES applications.

In most cases where molten silicon was observed to attack the test material, the attack was found to be so severe that visual examination alone was sufficient to rule out that material for long time molten silicon containment. In other cases where chemical compatibility was questionable, an optical microscope was used to investigate the degree of attack.

The crystal character of the materials before and after screening tests was determined by x-ray diffraction methods when changes were suspected to have occurred.

X-ray fluorescence techniques, in particular the use of a Heinrich miniature probe, were used to determine qualitatively the solubility of the test specimens in silicon.

3.2.1.2 Materials Evaluated

A list of the materials evaluated for molten silicon containment during this study is presented in Table II. Single crystals of certain materials were included in the testing program because they represent the most dense (least surface per unit mass) form. If the single crystals were to show signs of attack, then certainly any other less dense form should be correspondingly less resistant.

---

*Major impurities Fe and Al.

TABLE II
A LIST OF MATERIALS EVALUATED AND THEIR SOURCE

Material	Polycrystal	Single Crystal	Form
Alumina			
Lucalox Ceramic (a)	x		plate
Sapphire (b)		x	rod, crucible
Aluminum Nitride			
Hot Pressed (b)	x		crucible
Sintered (b)	x		crucible
Boron Nitride	x		crucible
Pyrolytic (a)	x		cylinder
Chromium Oxide (b)		x	A
Graphite			
High Density	x		crucible
ZT7001 (c)	x		crucible
ZT0707 (c)	x		crucible
Pyrolytic (a)	x		crucible
Recrystallized (c)	x		A
Molybdenum Disilicide (b)		x	A
Niobium Carbide (b)		x	A
Silica			
Recrystallized Quartz (d)	x		crucible
Silicon Carbide			
Crystolon R (e)	x		crucible
GRB (f)	x		crucible
Pyrolytic (g)	x		A
Titanium Carbide (b)		x	A
Titanium Diboride (b)		x	A
Titanium Diboride (b)	x		crucible

NOTE: A = crystal fragment approximately $(1/4 \text{ inch})^3$

Materials obtained from:

a = General Electric
b = Linde
c = National Carbon
d = Thermal American
e = Norton
f = Carborundum
g = Raytheon

3.2.1.3 Results of Screening Tests

1. Alumina

   a. Lucalox Ceramic

   b. Sapphire

   Both types of Al_2O_3 showed evidence of rather severe molten silicon attack. Figures 2 and 3 are photomicrographs of sections of Lucalox Ceramic and sapphire after one hour of molten silicon attack at 1500°C. The Lucalox Ceramic sample tested was in the form of a thin (0.0535 cm) sheet while the sapphire was in rod form (0.254 cm diameter). Several cracks appeared in the sapphire rod. The Lucalox Ceramic sheet did not fracture as severely as did the rod.

   Very severe molten silicon attack was observed in the case of a tested single crystal sapphire crucible. The wall thickness, originally 1/16 inch, was found to be less than 0.010 inch after a five hour test (at 1500°C). This corresponded to an average attack rate during this period of approximately 55 mils/hour. A photograph of the before and after condition of the sapphire crucible is shown in Figure 4.

2. Aluminum Nitride (hot pressed and sintered)

Crucibles of each of the above two mentioned materials were obtained. The hot pressed crucible was provided with a BN cap while the sintered sample had a cap of sintered aluminum nitride. These samples were each run for five hours at 1500°C in vacuum. Both materials failed because the silicon seeped through the crucible walls.

Optical microscopy revealed, after the screening test, that the sintered aluminum nitride employed was extremely porous. Some of the larger pores had diameters of 0.2 mm (and greater) and all pores appeared to be interconnected. See Figure 5a.

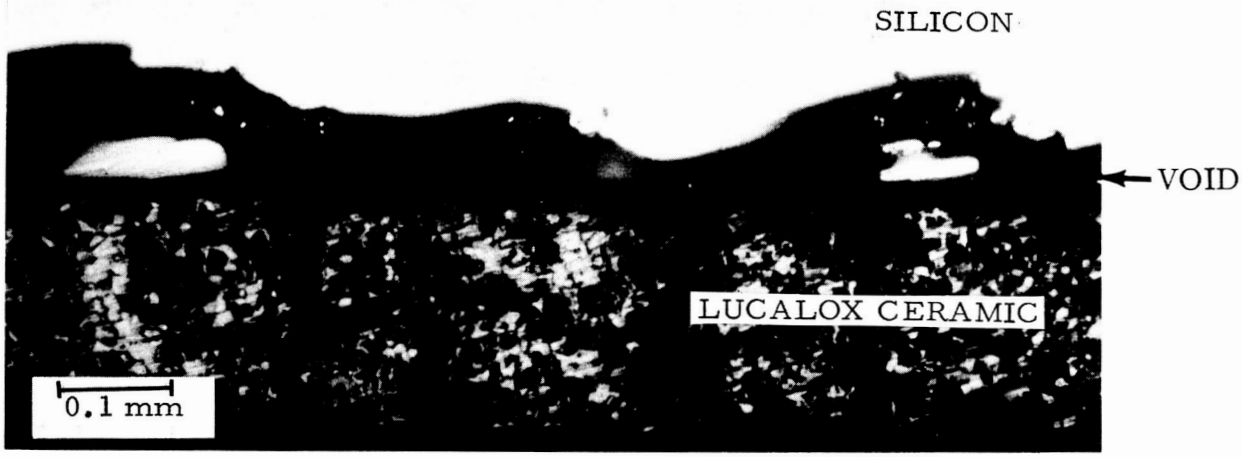

Figure 2. Screening Test: Lucalox Ceramic - Silicon Interface After 1 Hr., 1500°C, Vacuum 10^{-6} mm Hg

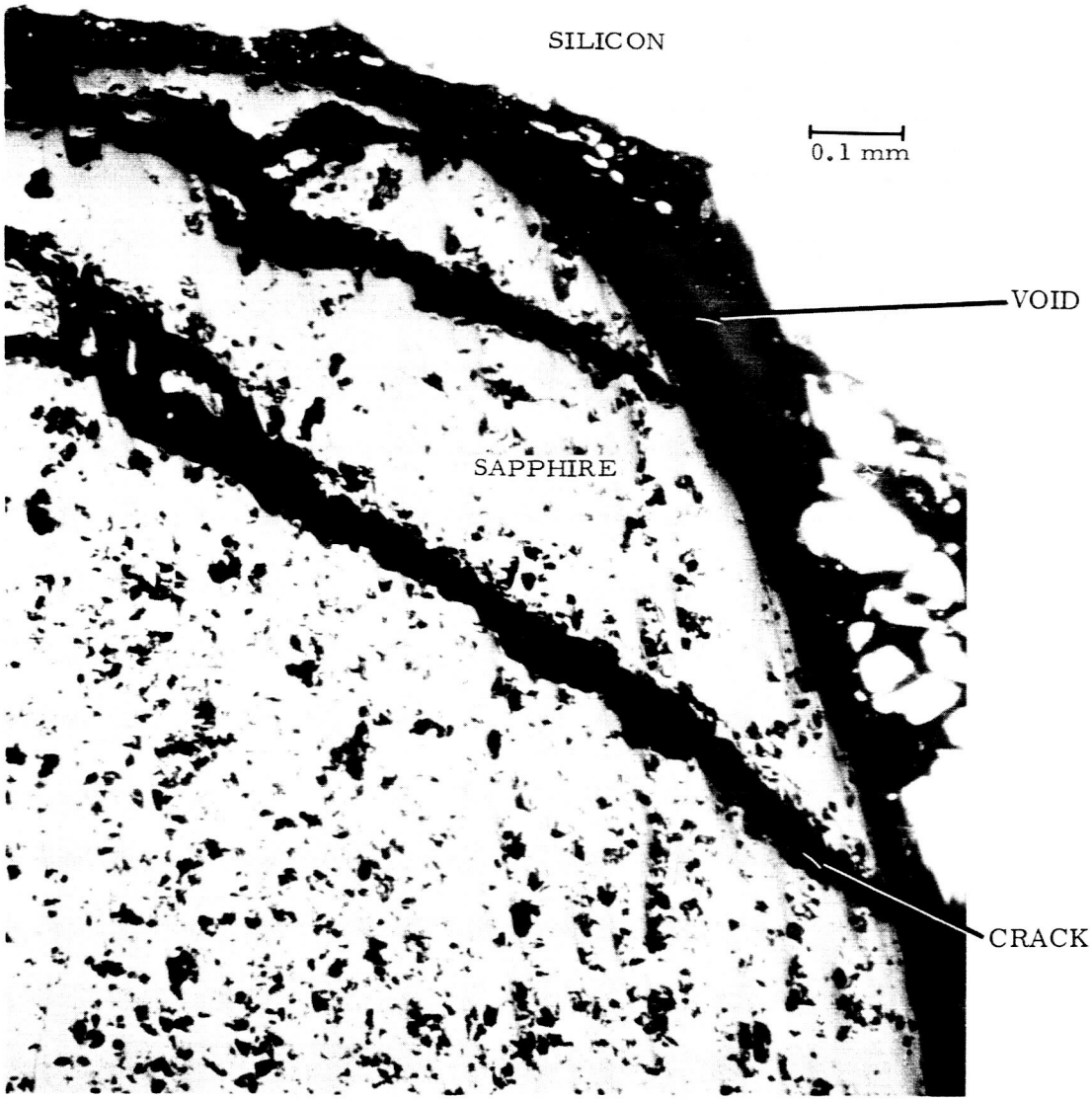

Figure 3. Screening Test: Sapphire - Silicon Interface After 1 Hr., 1500°C, Vacuum 10^{-6} mm Hg

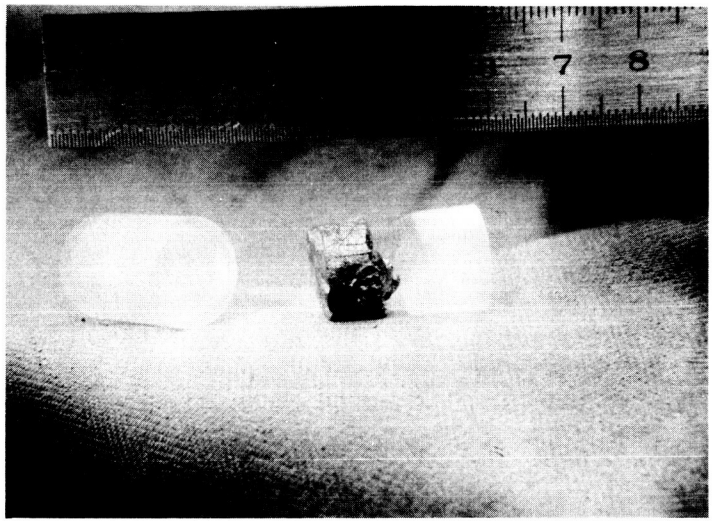

Figure 4. Screening Test of Silicon in Sapphire Crucible Shown After 5 Hr., 1500° C, Vacuum 10^{-6} mmHg.

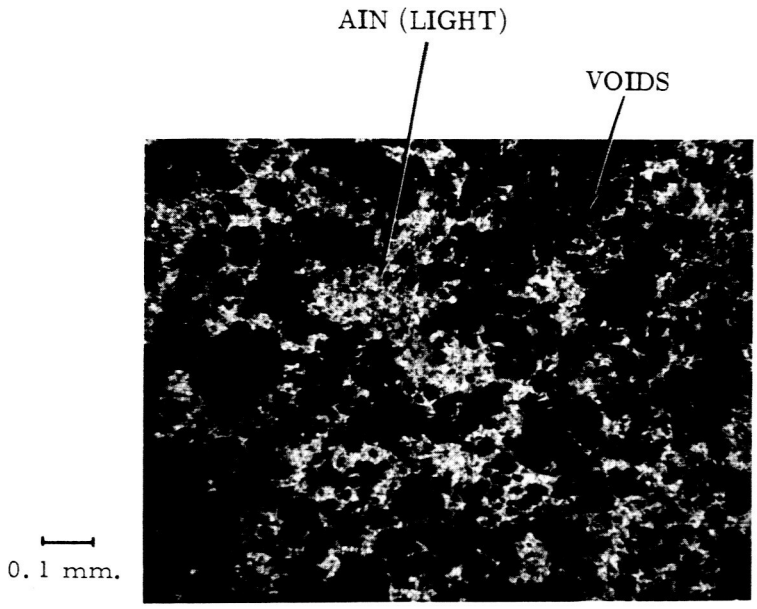

a - SINTERED

Figure 5. Screening Test of Aluminum Nitride Crucibles Containing Silicon After 5 Hr., 1500°C, Vacuum 10^{-6} mmHg.

The average pore diameter in the hot pressed aluminum nitride specimen after test was found to be considerably less than that of the sintered sample. The photomicrograph of Figure 5b shows silicon diffused into the pores of this specimen.

3. Boron Nitride

a. Hot Pressed BN

BN appeared to be one of the most promising of the potential materials studied for long time containment of molten silicon. This material was found to survive screening tests for as long as 100 hours at 1500°C in vacuum without showing any evidence of chemical attack possibly because molten silicon did not wet the BN under these conditions. In one experiment a BN crucible was found to contain a few hair-line cracks and since there was no evidence of silicon "leakage" from these cracks, it is believed that they resulted from the anomalous expansion (10 percent) which silicon experiences upon freezing. BN crucibles containing silicon did not crack if cooled relatively slowly. Therefore, where at first glance the fracture problem might be considered serious in the case of BN, it probably can be controlled by proper container design.

The interface between silicon and boron nitride after a one hour run in vacuum at 1500°C is shown in the photomicrograph of Figure 6. Figure 7 shows "before and after" photographs of a BN crucible used in a 100-hour screening test. The threaded BN crucible cap was easily removed after the 100 hour run. A deposit of dark powder was found inside the cap. X-ray analysis proved this deposit to be silicon.

As can be seen in the "after test" photograph in Figure 7, a dark deposit was also found on the outside of the BN crucible and cap. This deposit was SiC which probably formed when silicon lost

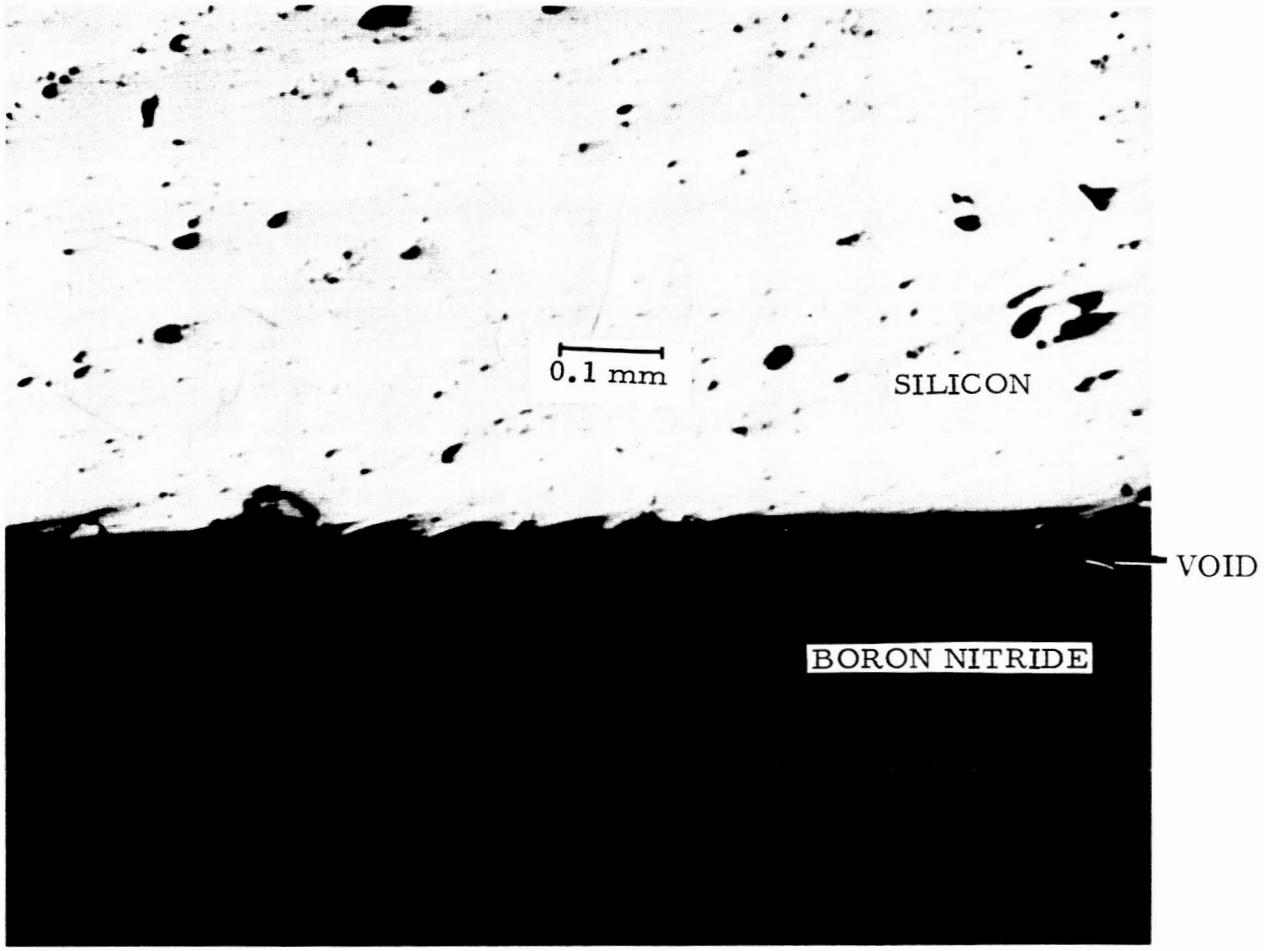

Figure 6. Silicon-Boron Nitride Interface After Screening Test
(1 Hr., 1500°C, Vacuum)

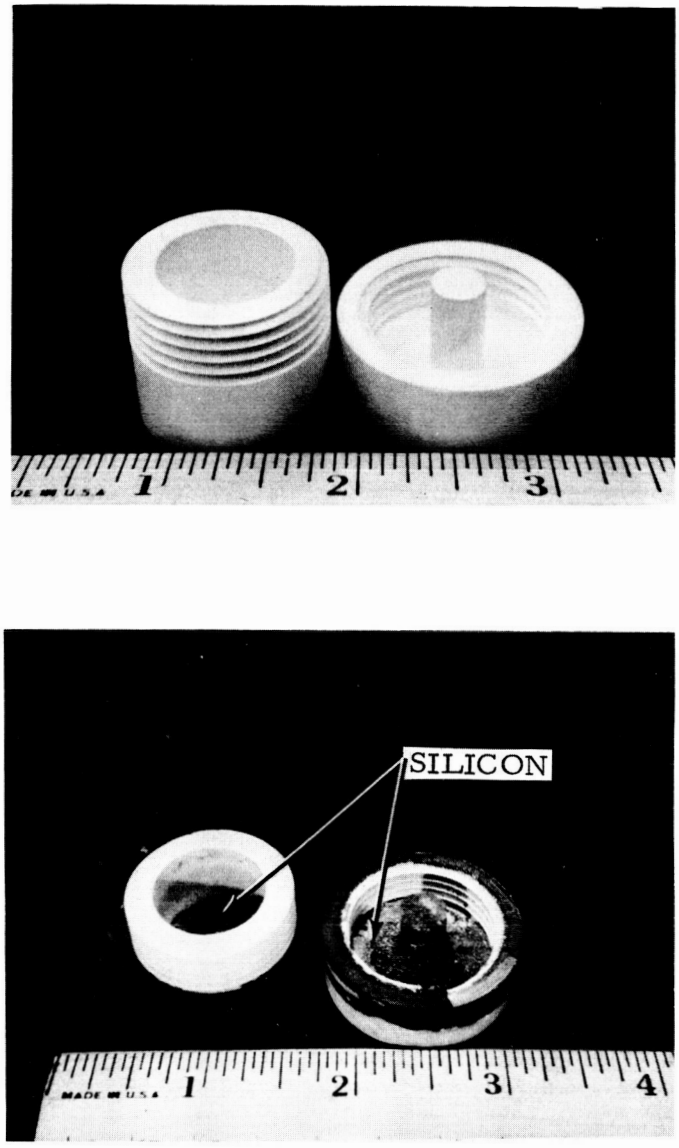

Figure 7. Disassembled Boron Nitride Crucible Before and After 100 Hour Silicon Containment Screening Test (1500^{o}C, Vacuum)

(24 percent) past the loosely fitted cap reacted with a carbon heater liner located in close proximity to the test crucible.

Figure 8 shows a photomicrograph of the BN-Si interface and a photograph of the sectioned BN crucible. As may be noted there is no metallographical evidence of chemical attack.

The BN used came from National Carbon Co and a typical assay is 95.5 - 97 percent BN and 3 - 4.5 percent B_2O_3

ultimate analysis:		
	N %	53.8
	B %	42.9
	C %	0.2
	0	3.1

b. Pyrolytic BN

A small sample of pyrolytic boron nitride, supplied by the General Electric Research Laboratory, showed no evidence of attack by molten silicon. This sample was run in a hot pressed BN crucible for five hours at 1500°C in vacuum. Photomicrographs of sections of the pyrolytic BN specimen, before and after testing, are shown in Figure 9.

4. Chromium Oxide

A single crystal of chromium oxide was found to be severely attacked by molten silicon (1500°C, 5 hours, in vacuum). The photomicrograph of Figure 10 shows the severity of the attack.

5. Graphite

a. High Density Graphite, ZT7001 and ZT0707

Small crucibles and caps were machined from these materials. Some crucibles and caps were formed with their symmetry axes in the direction of pressing and others at right angles to this direction. None of these crucibles survived one hour screening tests. These materials were found to be severely

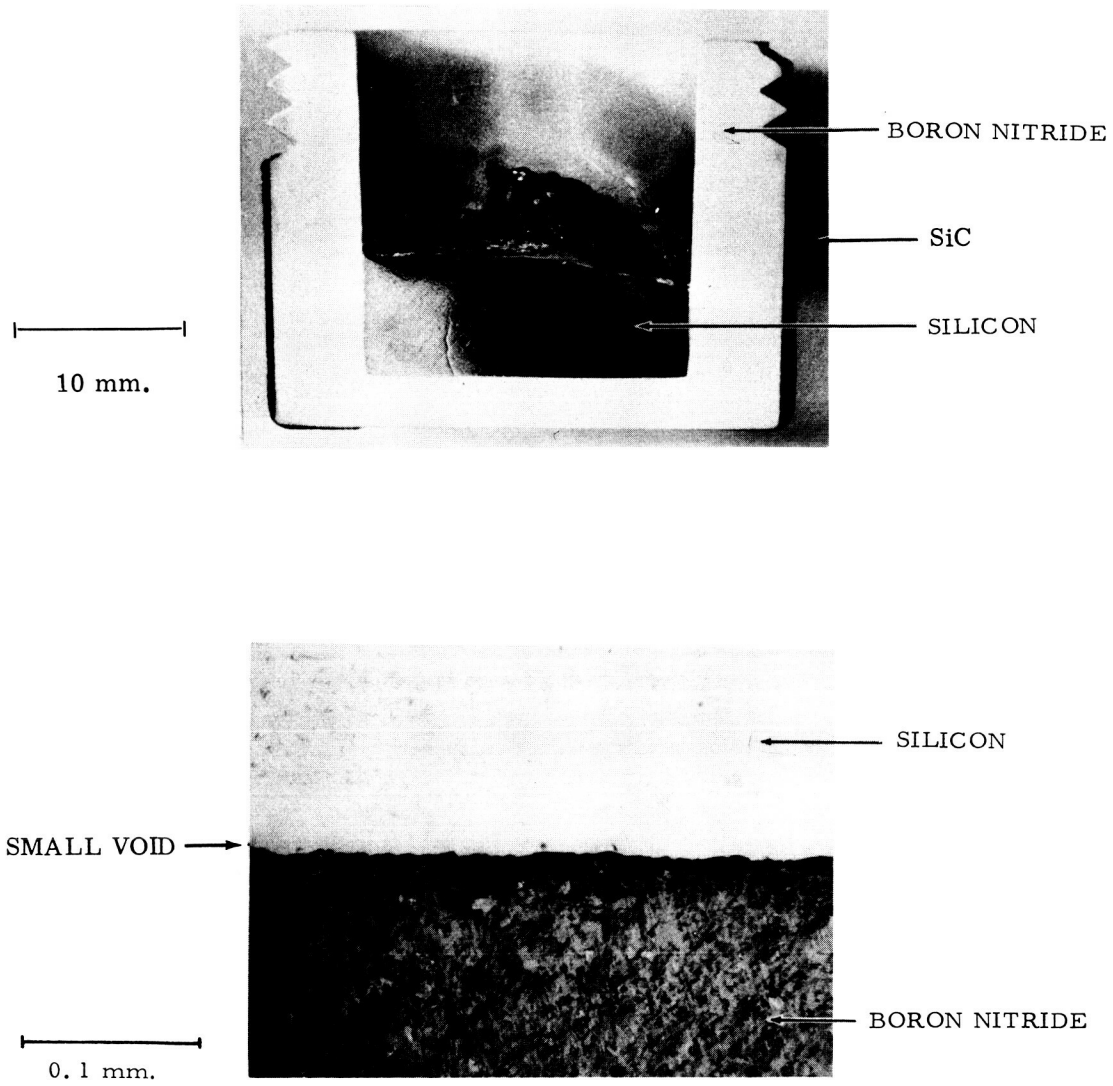

Figure 8. Compatibility Test: Boron Nitride - Silicon After 100 Hours (1500^{O} C, Vacuum)

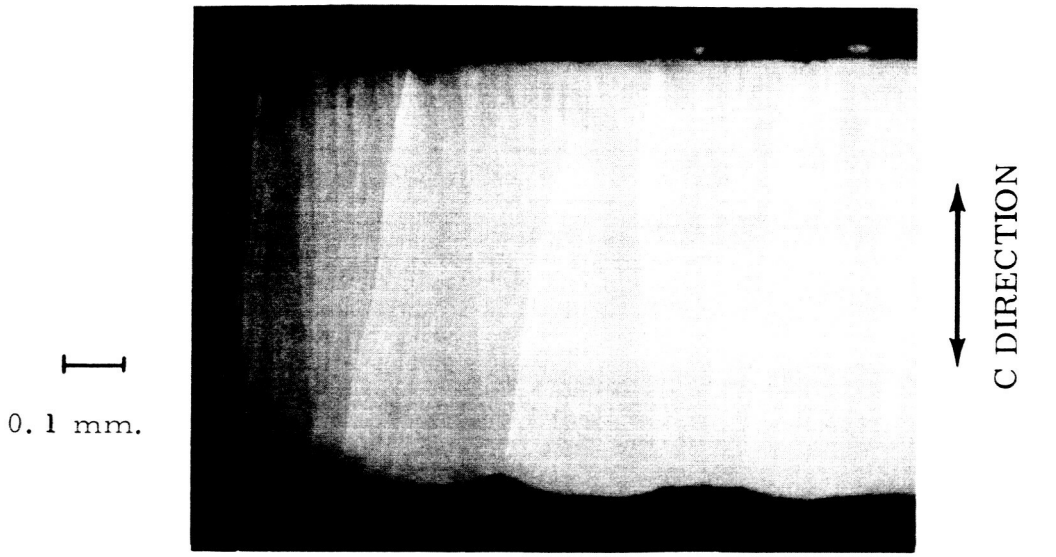

BEFORE TEST

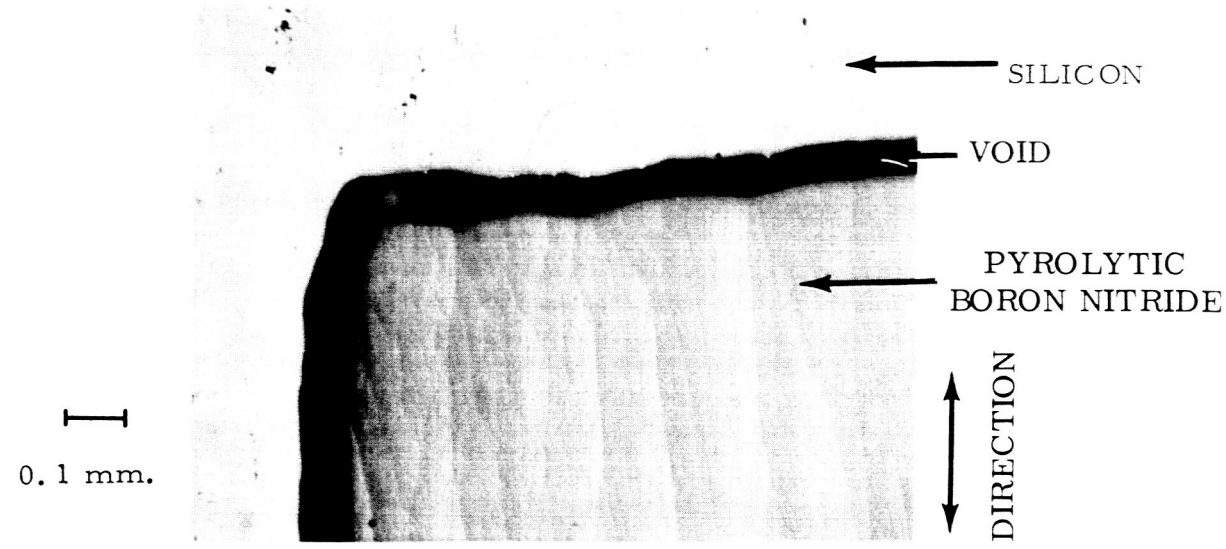

AFTER TEST

Figure 9. Screening Test - Pyrolytic Boron Nitride - Silicon Interface Shown After 5 Hr., 1500° C, Vacuum 10^{-6} mmHg.

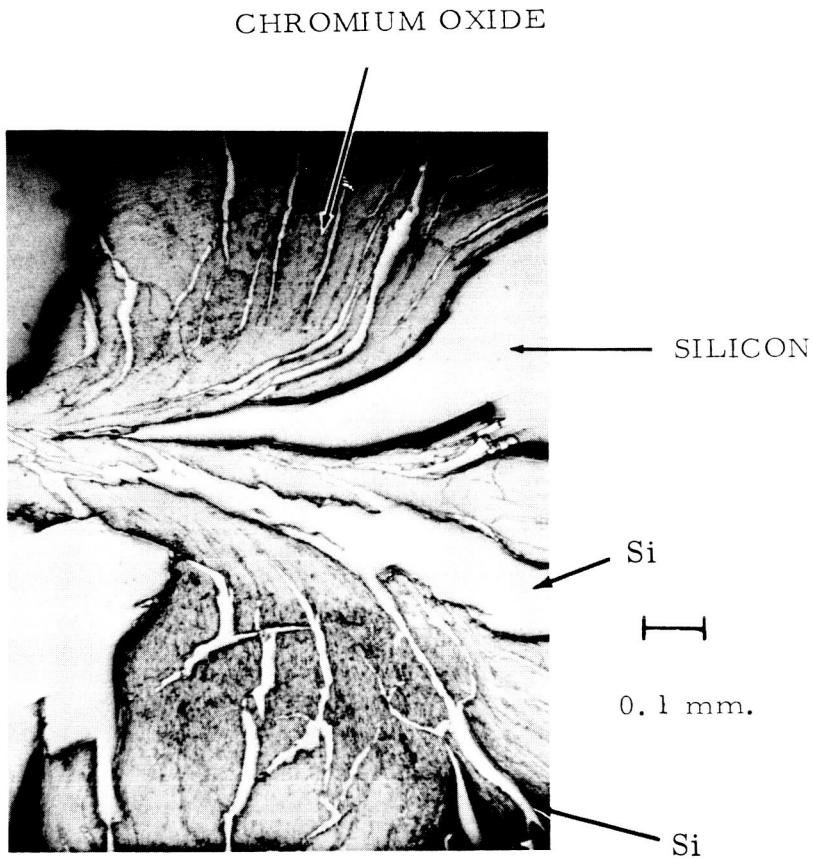

Figure 10. Screening Test of Chromium Oxide - Silicon, After 5 hr., 1500°C, Vacuum 10^{-6} mm Hg

attacked by molten silicon. Photographs of representative ZT0707 and ZT7001 graphite crucibles after a one hour screening test (1500°C in vacuum) are shown in Figure 11. X-ray diffraction showed silicon carbide formation.

b. Pyrolytic Graphite

Small pyrolytic crucibles were prepared. Since pyrolytic graphite is normally highly anisotropic, two crucible types were prepared. One type consisted of a flat bottomed cylindrical cavity (about 1/4 inch diameter and 3/8-inch deep) drilled in the "c" crystallographic direction of a flat piece of pyrolytic graphite. In this case the edges of the stacked carbon planes, of which pyrolytic graphite is composed, were exposed in the cylinder walls. The bottom of the cylindrical cavity thus formed was essentially free of stacked plane edges. The second kind of pyrolytic graphite crucible was made in such a way that the stacked carbon planes everywhere enveloped the crucible cavity (about 3/16 inch diameter and 3/4 inch deep).

In some preliminary short-time experiments, the crucibles were not covered. Since the vapor pressure at the melting point of silicon had been reported to be about 30 microns and since the inside diameter of the crucible was relatively small (3/16 inch), it was not thought that silicon loss by vaporization would be unreasonably great. About 20 percent weight loss was found after a one-hour run at 1550°C (the crucibles were originally charged with about one gram of silicon).

As was suspected, molten silicon attack on pyrolytic graphite after one hour was found to be severe in the case where the stacked carbon plane edges were exposed. Prolonged contact with molten silicon resulted in catastrophic delaminations in the walls. Figure 12 is a photomacrograph of a sectioned crucible, after the screening test, showing the large scale

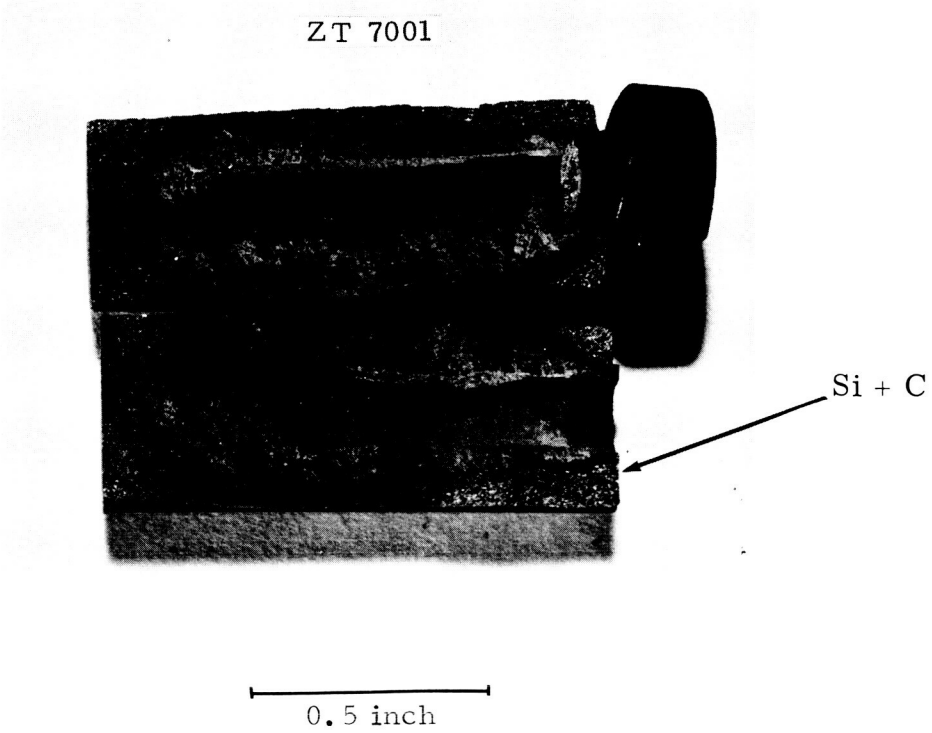

Figure 11. Graphite Crucibles After Silicon Screening Test
(1 Hr., 1500^{O} C, Vacuum)

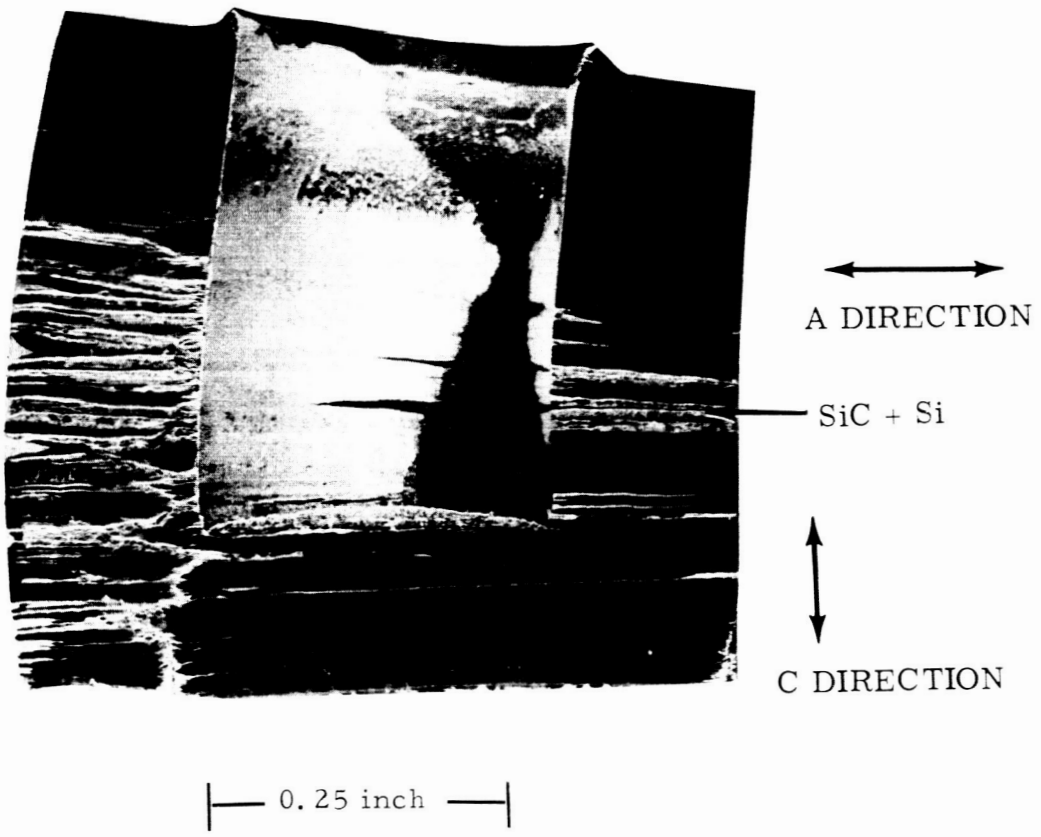

Figure 12. Pyrolytic Graphite Crucible After Molten Silicon Screening Test (1 hr, 1550°C, Vacuum) Showing Poor Crystal Orientation Effects

separations of families of stacked carbon planes. It is to be noted that the bottom of the crucible survived silicon attack to a much higher degree than did the sides. On the other hand, molten silicon attack on the second type of pyrolytic crucible (carbon planes perferentially oriented around the cavity) was found to be extremely mild. Figure 13 is a photomacrograph of a pyrolytic graphite crucible of the second kind after a one hour screening run at 1550°C. It is of interest to note the raised drop of silicon in the center of the crucible cavity. This is due to the fact that silicon experiences a rather large increase in volume (about 10 percent) upon freezing and that the sample froze inward from the crucible walls. Figure 14 indicates that silicon wets the surface of pyrolytic graphite.

Shown in Figure 15 is a photomicrograph of the silicon-pyrolytic graphite interface. In this figure a thin silicon carbide layer (about 4 microns thick) can be observed at the interface. It is this continuous layer that most likely prevents catastrophic attack of pyrolytic graphite by molten silicon.

The pyrolytic graphite employed in the above experiments was of rather poor quality. It was used because it was the only pyrolytic graphite of proper geometry available at the time. An experiment was conducted to establish whether the density of pyrolytic graphite plays an important role in its ability to resist attack by molten silicon. Two specimens of pyrolytic graphite, one with a density of 2.16 gm/cm^3, and the other having a density of 2.20 gm/cm^3, were examined after a two hour exposure to molten silicon at 1500°C. Both samples resisted attack to the same high degree. This is evidenced in the photomicrographs of Figure 16.

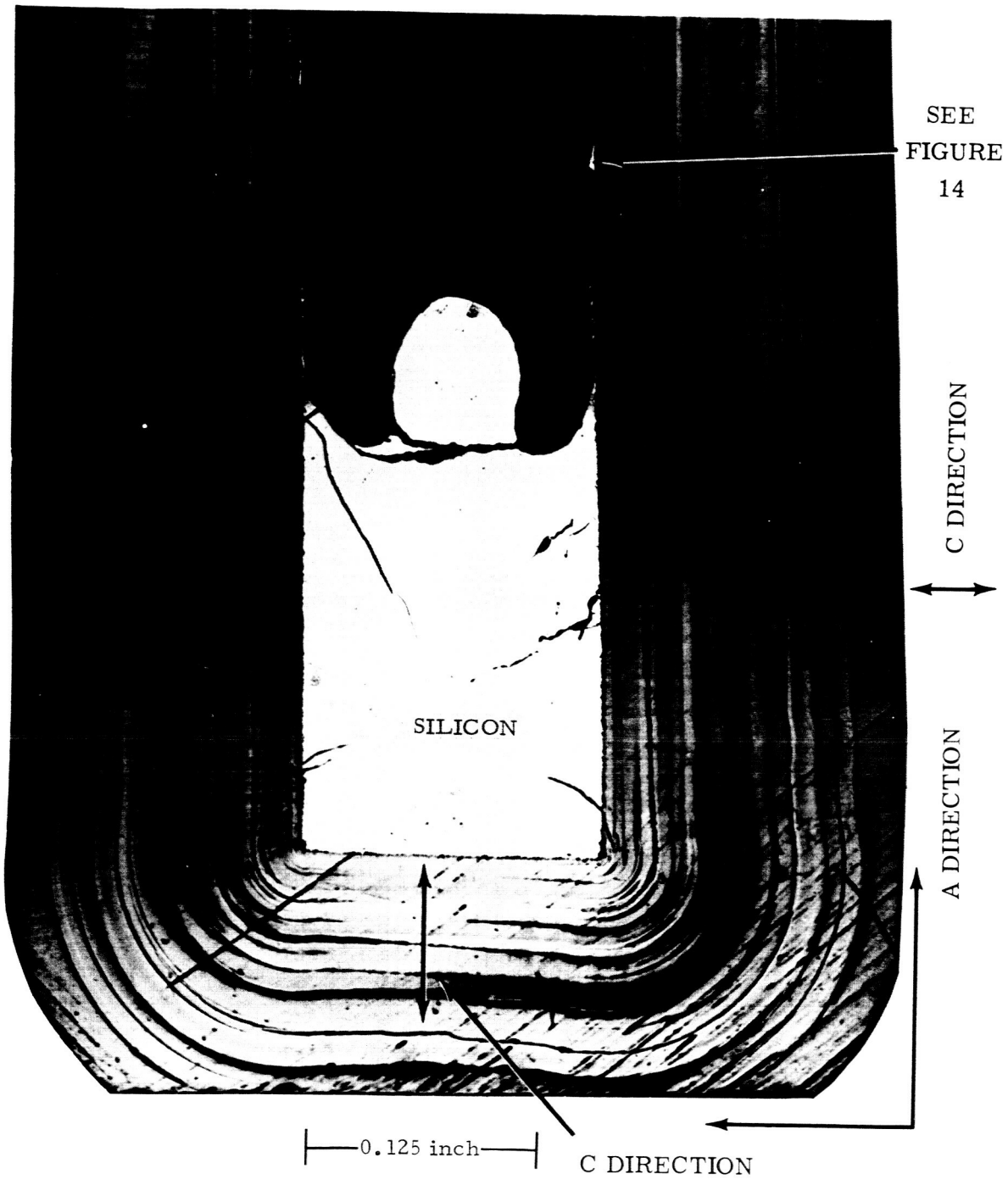

Figure 13. Pyrolytic Graphite Crucible After Molten Silicon Screening Test (1 Hr, 1550°C, Vacuum) Showing Proper Crystal Orientation Effects

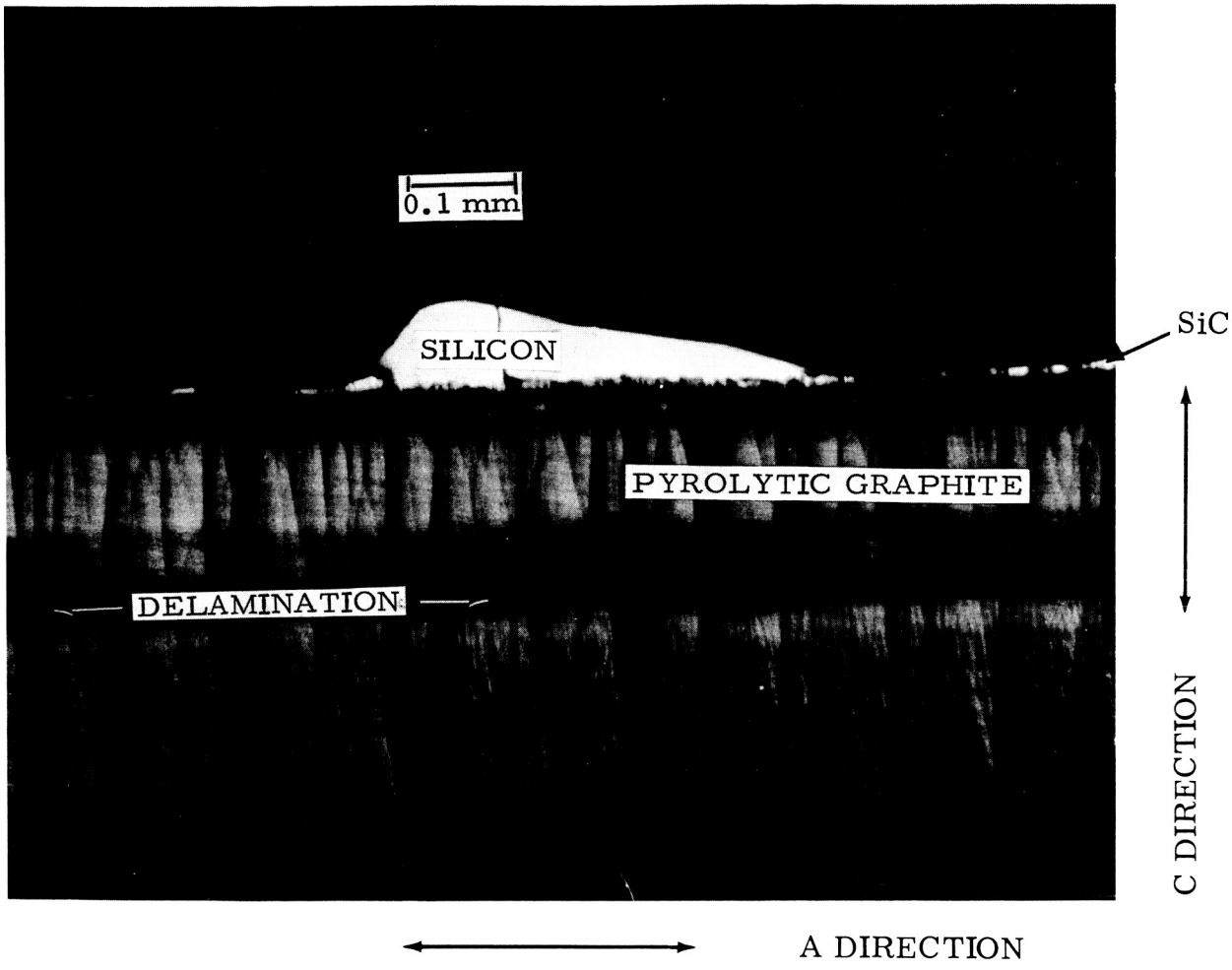

Figure 14. Droplet Showing Wetting of Pyrolytic Graphite by Silicon (See Figure 13)

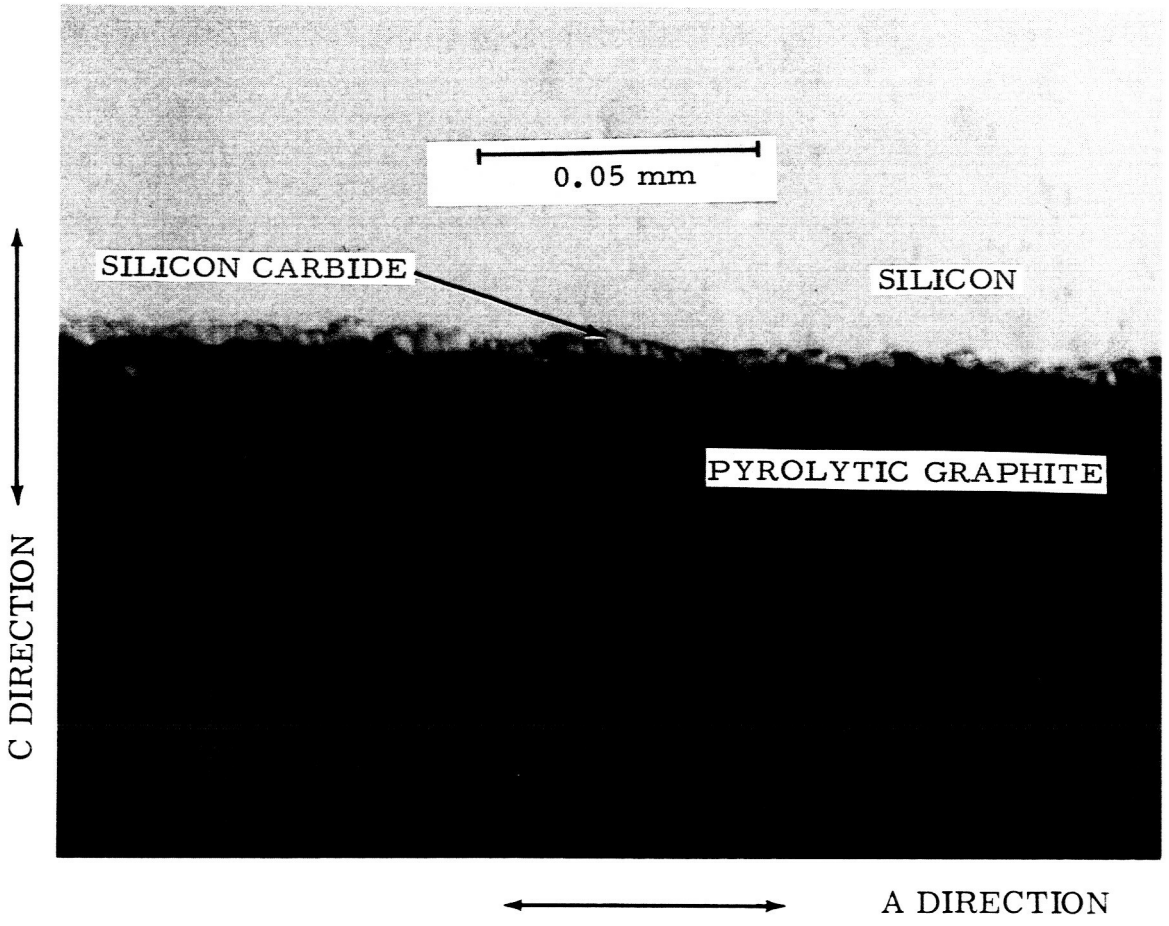

Figure 15. Silicon Carbide Layer at Interface Between Silicon and Pyrolytic Graphite (See Figure 13)

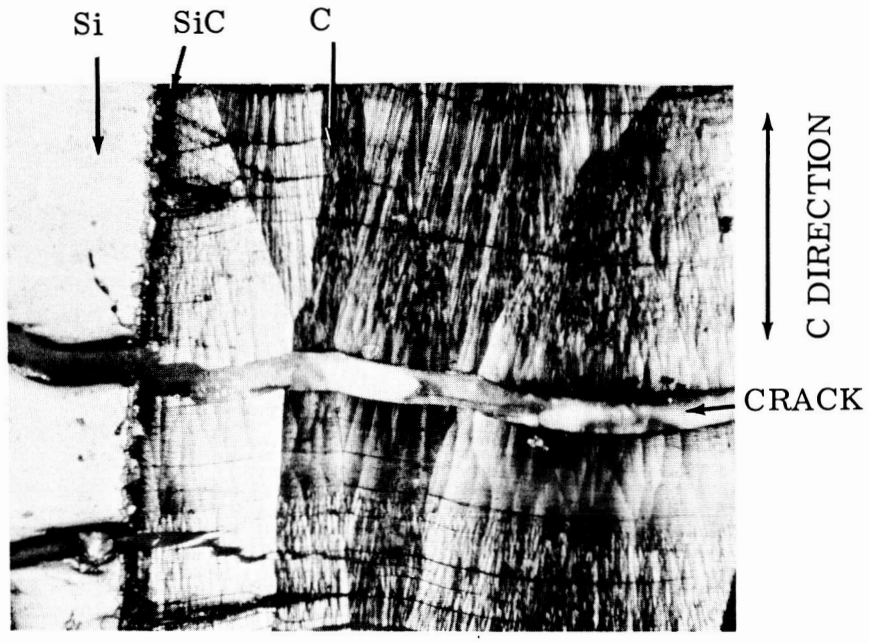

a- Density 2.16 gm cm^{-3}

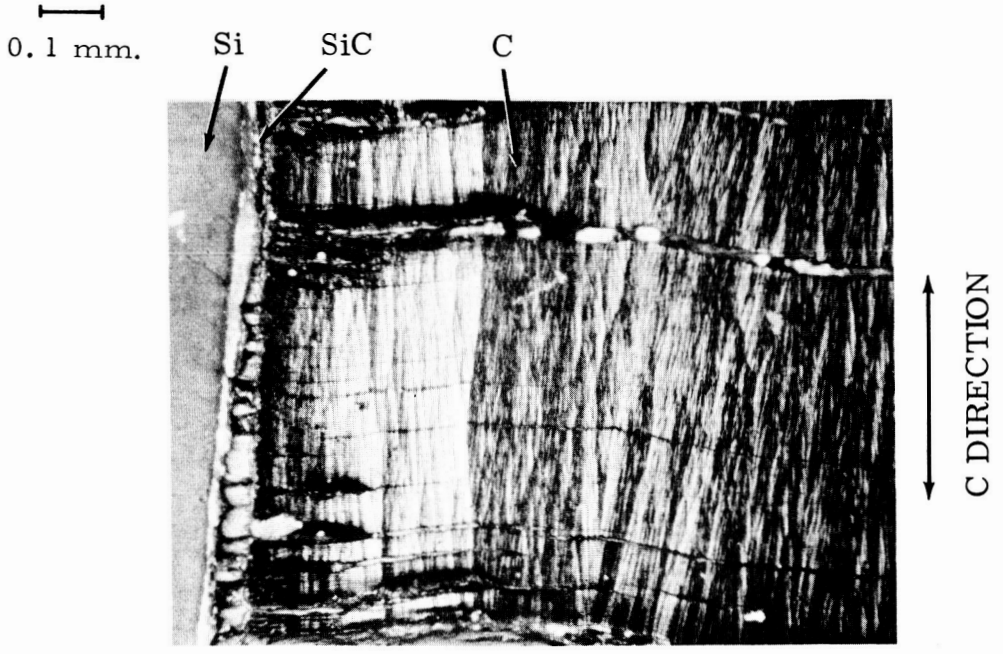

b - Density 2.20 gm cm^{-3}

Figure 16. Density Variation of Pyrolytic Graphite Studied for Silicon Compatibility, Shown After 2 Hr., 1500°C, Vacuum

Since it appeared that low density pyrolytic graphite was as satisfactory as the high density material for molten silicon containment and since it was much easier to fabricate good quality, low density pyrolytic graphite bodies, several low density (2.16 gm/cm^3) pyrolytic graphite crucibles were made. These crucibles were used in two 100-hour screening tests which were run at 1500^{o}C in vacuum.

No silicon remained in the crucible after the first 100 hour test. In this run the crucible had been loosely capped with pyrolytic graphite. Close examination of the crucible, including microscopy of sections, revealed that silicon had not severely attacked the container (a thin layer of SiC had formed on the walls and cap) nor had it passed through it. Therefore it had to be assumed that silicon loss occurred from around the loosely fitted cap.

In the second run a pyrolytic graphite crucible was placed inside a boron nitride container which in turn was covered with a screw cap of BN. During this 100 hour run only 8 percent of the silicon was lost. The BN screw cap was easily removed from the outside container after the run and was found to be quite clean. There was a slight deposit of silicon on the inside of the cap. In addition, a light overgrowth of filamentary silica crystals (whiskers) was found on the cap. No damage to the pyrolytic graphite crucible was observed. Figure 17 is a photograph of the sectioned pyrolytic graphite crucible and a photomicrograph of the pyrolytic graphite-silicon interface.

A 20μ thick layer of silicon carbide was found to have been formed at the silicon-pyrolytic graphite interface after the 100-hour run. Thus the average rate of formation of silicon carbide over a 100-hour period was 0.2 μ/hr, whereas the

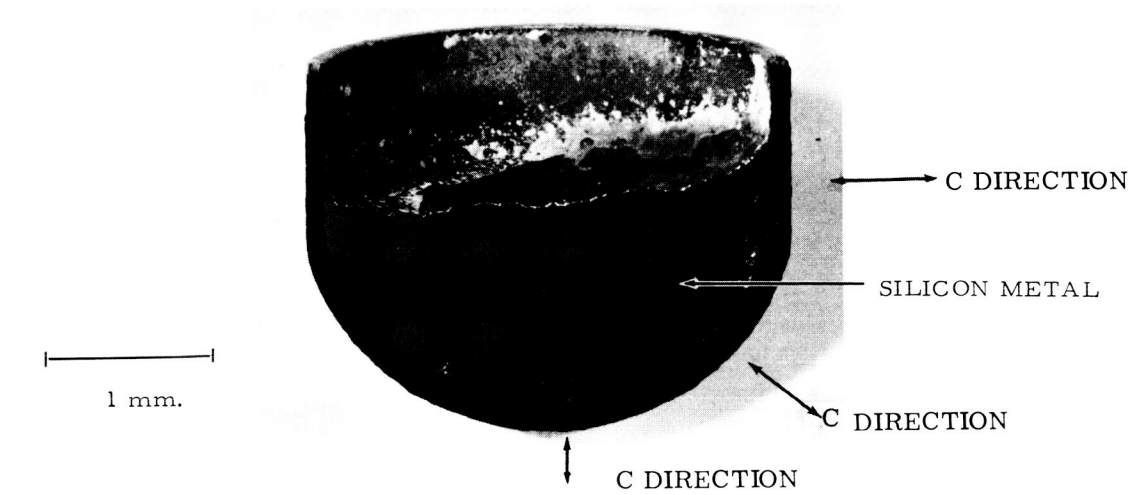

a - SECTIONED CRUCIBLE

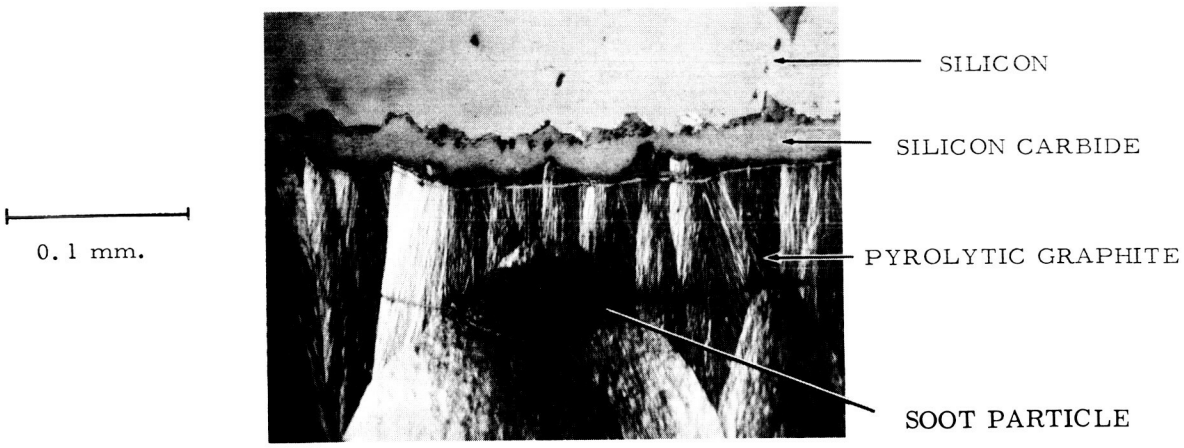

Figure 17. Compatibility Test of Pyrolytic Graphite - Silicon Shown After 100 hr., 1500°C, Vacuum

corresponding average rate of formation from a one-hour test was found to be 4 μ/hr. This appears to be a limiting process. That is, the silicon carbide layer which is formed acts as a barrier to further molten silicon attack.

c. Recrystallized Graphite

A small sample of recrystallized graphite, about $(1/4 \text{ inch})^3$, was tested in a BN crucible. Silicon attack, after a five-hour screening test run at 1500°C in vacuum, was found to be catastrophic. The graphite specimen swelled with a volume increase of about 500 percent. Figure 18 shows "before and after" photographs of the recrystallized graphite specimen.

6. Molybdenum Disilicide

Attack was catastrophic after 5 hours at 500°C (see Figure 19a).

7. Niobium Carbide

The attack of niobium carbide after 5 hours at 1500°C was catastrophic (see Figure 19b).

8. Silica - Recrystallized Quartz

Attack on quartz was fairly severe after one hour at 1500°C. The surface eroded and the material cracked (see Figure 20).

9. Silicon Carbide

a. Crystolon R

Crucibles of this material, although they maintained their integrity, were found unsuitable for molten silicon containment. In periods of even less than 15 minutes at 1500°C almost all of the total charge (about 10.5 grams of molten silicon was found to have seeped through the 1/4 inch thick crucible walls (I.D. of crucible was 1 inch and its depth about 1.25 inch). The photomicrograph of Figure 21a shows a section of the crucible (bottom) after a 15-minute run. Note the porosity of the Crystolon R crucible.

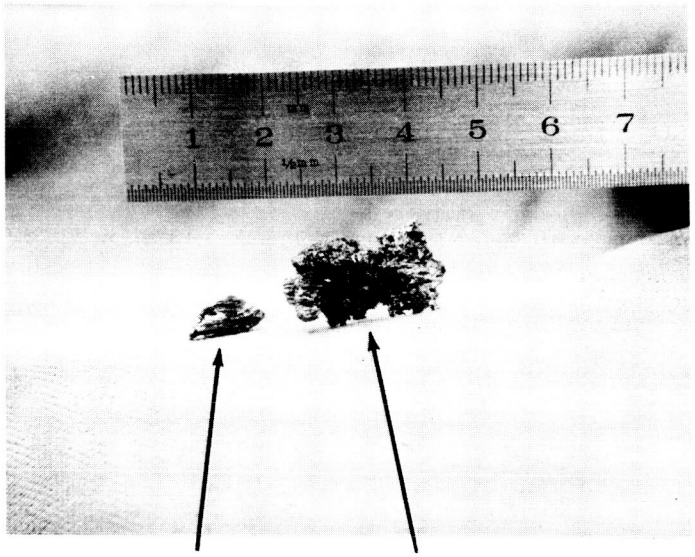

Figure 18. Specimens of Recrystallized Graphite - Before and After Silicon Screening Test (5 Hours, 1500°C, Vacuum)

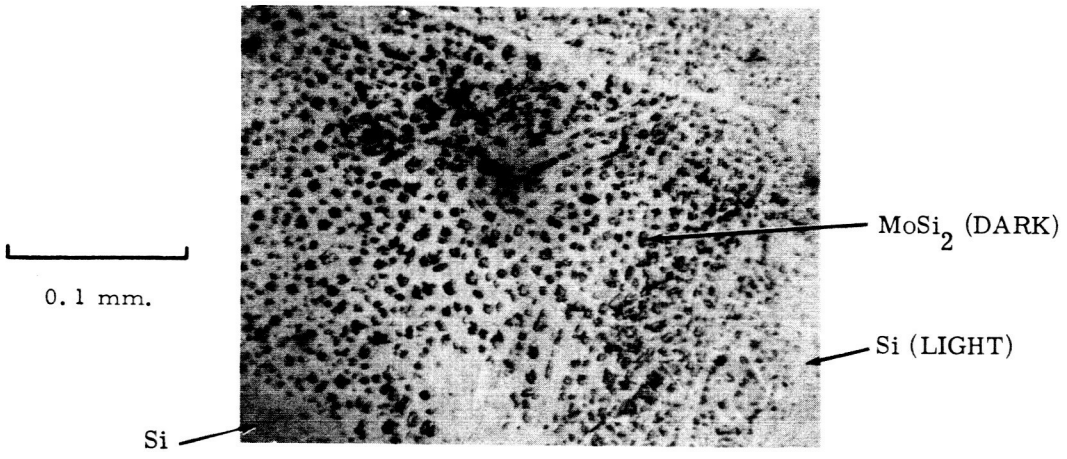

Figure 19a. Molybdenum Disilicide - Silicon Screening Test Shown After 5 Hr., 1500°C, Vacuum

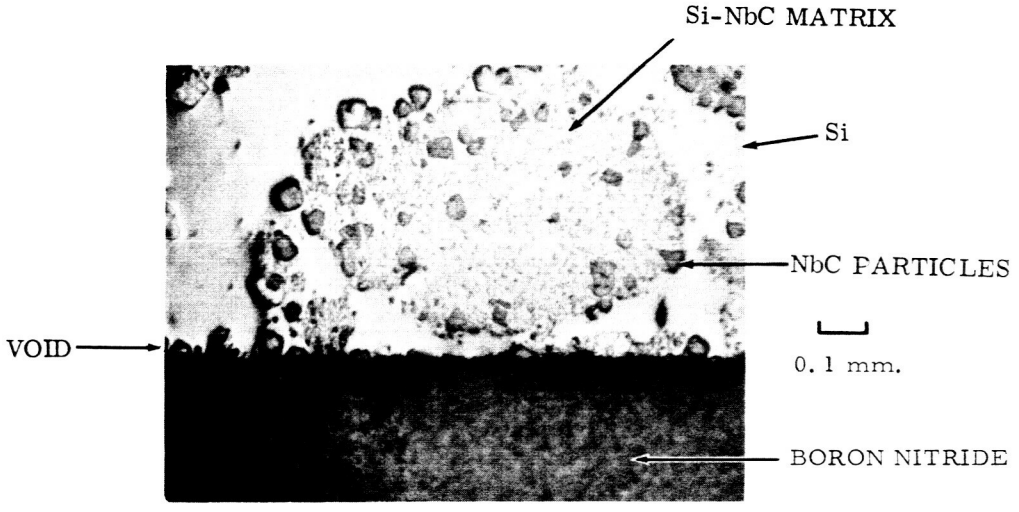

Figure 19b. Niobium Carbide - Silicon Screening Test Shown After 5 Hr., 1500°C, Vacuum

Figure 19

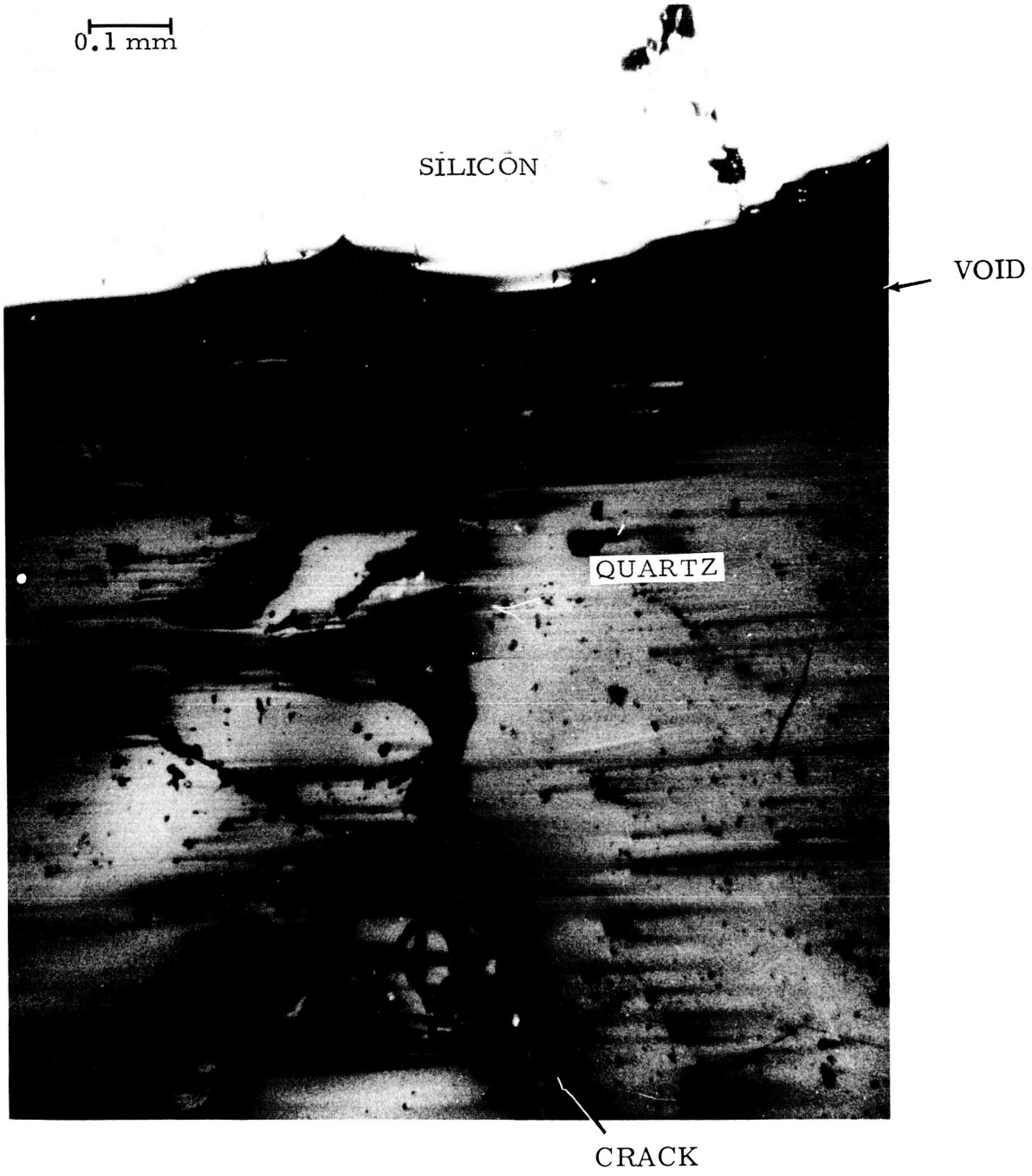

Figure 20. Screening Test, Quartz-Silicon Interface Shown After 1 hr., 1500°C, Vacuum

b. GRB Silicon Carbide

It was found that a crucible of this highly porous material would not contain molten silicon at 1500°C for 5 hours although the crucible maintained its structural integrity. It had been hoped that the molten silicon would react with the free graphite in this material to form silicon carbide, thereby sealing the pores.

c. Pyrolytic Silicon Carbide

A specimen of pyrolytic silicon carbide was obtained and exposed to silicon in a boron nitride crucible for 5 hours at 1500°C. Microscope examination showed some physical changes but penetration apparently was not as severe as for the other two types of silicon carbide (see the preceding paragraphs). A crucible of pyrolytic silicon carbide would have been more appropriate for test purposes than one of boron nitride, but such a container was unavailable (see Figure 21b).

10. Titanium Carbide

A titanium carbide single crystal was found to be severely attacked by molten silicon after 5 hours at 1500°C (see Figure 22).

11. Titanium Diboride

a. Single Crystal

This was the only single crystal that showed little evidence of molten silicon attack after 5 hours at 1500°C. In all other cases, single crystal constituents were found to be dispersed throughout the silicon. Further studies were undertaken by obtaining crucibles of TiB_2.

b. Polycrystalline Titanium Diboride (Crucible)

A boron nitride capped titanium diboride crucible was heated in vacuum for 5 hours at 1500°C. About 80 percent of the silicon charge was found to have seeped through the pores of the crucible walls (see Figure 23a). The crucible was found

0.1 mm.

Figure 21a. Crystolon R - Silicon Interface After 15 Min., 1500° C, Vacuum

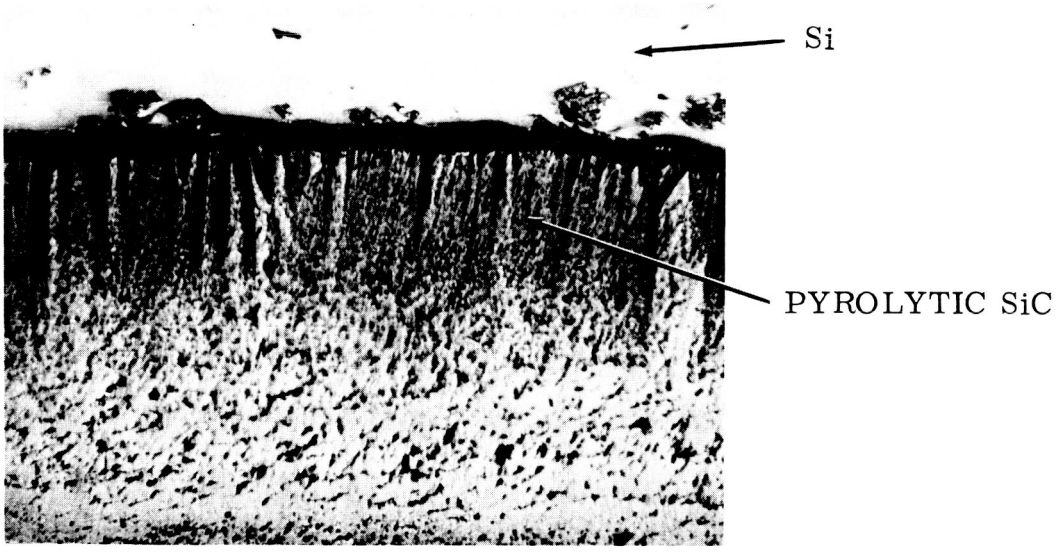

0.1 mm.

Figure 21b. Pyrolytic Silicon Carbide - Silicon Interface After 5 Hr., 1500° C, Vacuum

Figure 21

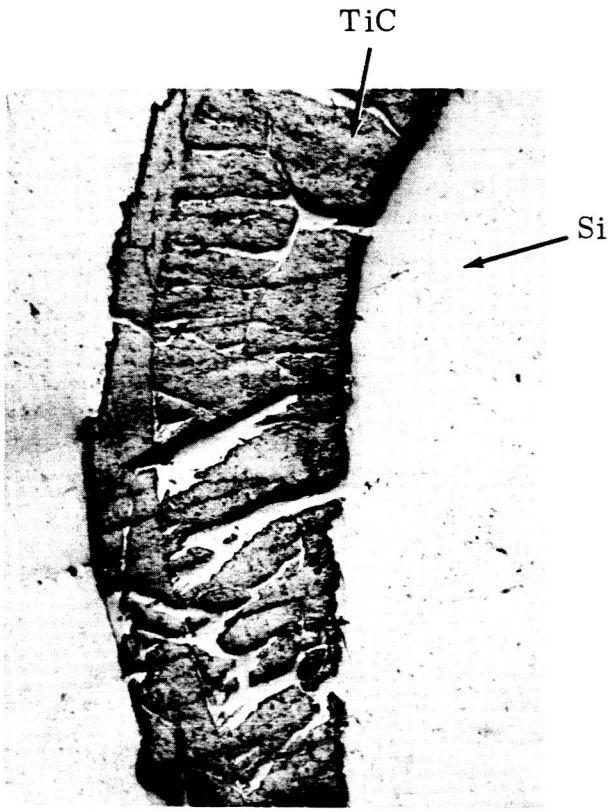

Figure 22. Screening Test, Titanium Carbide - Silicon Interface Shown After 5 hr., 1500°C, Vacuum

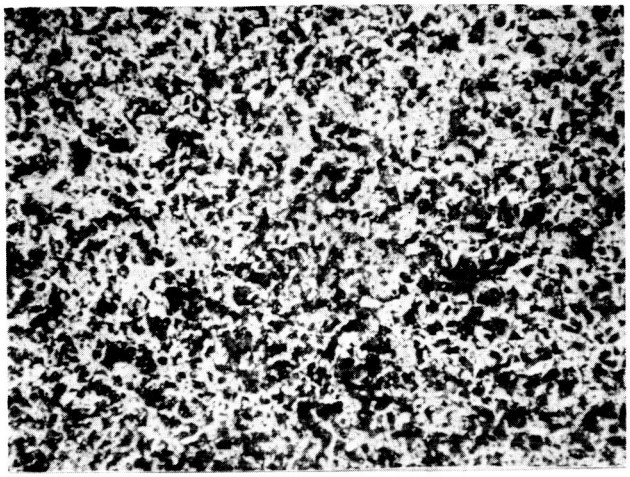

Figure 23a. Titanium Diboride Crucible Wall After Exposure to Molten Silicon for 5 Hrs, at 1500° C in Vacuum.

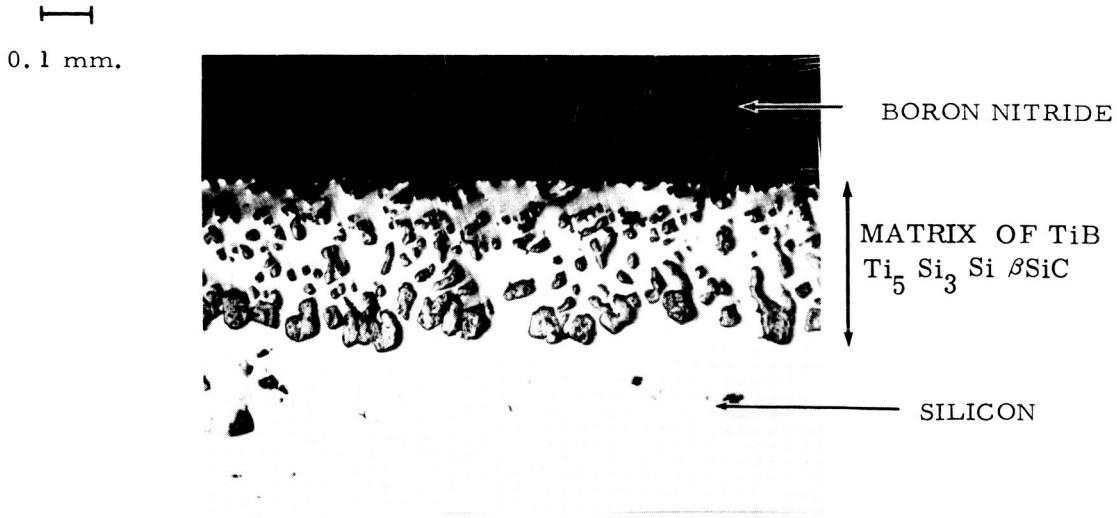

Figure 23b. Boron Nitride Cap - Silicon Interface Found in Above Crucible.

Figure 23

to be mechanically sound after the test. However, there was an unusual occurrence. This was the first time that silicon was found to wet a BN surface. A rather large button of "silicon" was found tenaciously adhered to the inner portion of the BN cap.

Photomicrographs (see Figure 23b) showed a fairly high concentration of a foreign crystalline component at the BN-Si interface. Although not completely analyzed, x-ray diffraction indicated that this material contained large amounts of titanium boride. The origin of the titanium boride must have been an impurity constituent in the titanium diboride crucible. Thus it is indicated that silicon could possibly be made to wet BN by slight additions of titanium boride. This might have an application if silicon used as a TES medium in BN containers is required to wet container walls.

12. System 400 Coating

The magnitude of the problems associated with the sealing of non-metallic containers for use with silicon as a thermal energy storage material are apparent. Therefore, the relatively excellent weldability of the refractory metals created an immediate interest in their possible use in this application. Since it had been known that molten silicon reacts readily with the refractory metals to form silicides, it was obvious that a coating would be required to prevent such attack. Earlier work had been carried out at FPLD[15] to evaluate the effectiveness of several sprayed refractory oxide coatings in protecting columbium from attack of molten silicon. Of these, the System 400 (sprayed Al_2O_3 + glass seal + heat treatment) appeared to be the most attractive of these coatings. However, serious problems were encountered in maintaining the coating integrity under cycling conditions.

13. Silicide Coatings

Silicide coatings which had already been developed for purposes of oxidation resistance appeared to be a possible choice for consideration. Feasibility of silicide coatings to eliminate reaction of silicon with refractory metals is, of course, dependent upon diffusion rates of silicon through the silicide layer with resulting increase in coating thickness. To evaluate this growth rate, 1/4 inch diameter rods of molybdenum, columbium, tantalum, and tungsten were treated by Chance-Vought Corporation, using their cemetation process to provide the appropriate silicide coatings. The resulting impervious coatings were 0.002 inch thick.

A test in which the silicided rods were to be submerged in molten silicon required a suitable container. This container problem was no different from the basic problem under investigation, and it was soon found that all available containers would contaminate the experiment. It was decided to employ crucibles of the metal under test. To minimize the attack on the crucible, as well as solution of the silicide coating on the sample, the silicon was doped with the base metal to provide the eutectic composition or about 5 weight percent.

The metallic crucibles were fabricated by drilling a 7/8 inch diameter hole in a one inch diameter rod of the metal to be tested. Approximately fifteen grams of DuPont Hyperpure Silicon was charged so that essentially one inch of the coated specimens was submerged when the bath was molten during the test. After loading the refractory metal crucible with the doped silicon and the coated rod specimen, the assembly was sealed in vacuum using electron beam welding.

The initial test was run for approximately eight hours at $1720^{o}K$ in a vacuum tungsten resistance furnace, with molybdenum as the base metal. Post test evaluation indicated unsuitability of silicide

coatings to contain molten silicon. The coating thickness increased from 0.002 inch to 0.010 inch or at a rate of approximately 0.001 inch per hour. It was also observed that the silicide layer buildup was essentially the same on both the coated rod and the uncoated crucible wall.

Of major importance, and this applies to all the refractory metals in view of similarity in the phase diagrams, was the spongy nature of the remaining silicon alloy. It is apparent that a congruent melting point material cannot be maintained in a refractory metal-silicon system. The existence of a eutectic in all four such systems results in a change in composition as the ultimate temperature is raised above the eutectic temperature. On this basis, studies of silicide coatings on refractory metals as silicon containment systems were discontinued.

14. Other Coatings

Boron nitride was considered as a possible metal coating material. However, the method of application presented problems which appeared to be beyond the scope of the present program. Plasma spraying was not possible because the sublimation temperature is below that necessary to soften the material. Pyrolytic deposition was considered but the excess nitrogen present in the process would only contaminate the base metal.

Cerium sulphide was considered as a coating material. A preliminary test was conducted using a small cerium sulphide crucible loaded with silicon and enclosed in a vacuum sealed molybdenum capsule. After six hours at 1730^{o}K it was found that the crucible was completely permeated with silicon indicating a relatively high degree of porosity. It is possible that an improved higher density crucible would minimize the problem. However, there was also evidence of a break-down of the CeS, presumably to Ce_3S_4 as predicted by

Brewer[16]. It is apparent that the thermodynamics of the CeS-Si systems are such as to render the combination sufficiently unstable so CeS was eliminated as a possible coating.

The results obtained with these screening tests of coated refractory metals coupled with anticipated problems of welding a coated container suggested that further effort in this area was unwarranted and this particular effort was terminated.

Table III is a summary of all screening tests. As can be seen in Table III, only three of the materials evaluated showed most promise for long time molten silicon containment. These were:

a. pyrolytic and hot pressed boron nitride (BN)
b. pyrolytic graphite (PG) in which only the graphite planes normal to the "c" crystallographic direction were in contact with silicon
c. single crystal titanium diboride (TiB_2).

BN and PG crucibles were found to successfully contain molten silicon (1500°C in vacuum) for at least 100 hours. No evidence of molten silicon attack was found in the case of BN and TiB_2. The attack on PG was found to be self-limiting. A thin protective layer (4 μ thick after one hour and 20 μ after 100 hours) of silicon carbide formed at the PG-Si interface.

Silicon does not wet BN or TiB_2, but it does wet PG. Silicon with a small amount of TiB was found to wet BN.

Some selected physical properties of pyrolytic graphite and boron nitride are presented in Appendix B.

3.2.2 Sealing and Joining Tests

Three conditions at least must be satisfied before any material can be classed as satisfactory for long-time containment of a TES medium (i.e., molten silicon) in a practical solar, thermionic, space-power generator.

TABLE III. SUMMARY OF SCREENING TESTS

Material	Exposure (Hrs.)	Attack
Alumina		
Lucalox Ceramic	1	Mild-severe; sample cracked
Sapphire	5	severe
Aluminum Nitride		
Hot Pressed	5	porous to silicon
Sintered	5	porous to silicon
Boron Nitride		
Hot Pressed	up to 100	no attack; not wetted by silicon
Pyrolytic	5	no attack; not wetted by silicon
Chromium Oxide	5	catastrophic
Graphite		
ZT7001, ZT0707	1	catastrophic
Pyrolytic		
"c" direction	up to 100	extremely mild; self-limiting
"a" direction	1	severe
Recrystallized	5	catastrophic
Molybdenum Disilicide	5	catastrophic
Niobium Carbide	5	catastrophic
Silica	1	mild-severe; sample cracked
Silicon Carbide		
Crystolon R	1/4	porous to silicon
GRB	5	porous to silicon
Pyrolytic	5	mild
Titanium Carbide	5	catastrophic
Titanium Diboride		
Single Crystal	5	no attack
Polycrystal (crucible)	5	porous to silicon
System 400 Coating	78	container failure
Refractory Metal Silicide		
coatings	8	gross attack
CeS	6	permeation, reaction

(a) It must be chemically compatible for long periods with the molten TES medium.

(b) It must be capable of being hermetically sealed.

(c) It must be capable of being mated mechanically and thermally to the cathode of a thermionic converter.

Two of the materials investigated, namely boron nitride and properly oriented pyrolytic graphite, appeared to fulfill condition (a) for molten silicon containment. It was not practical to establish long-time compatibility (upwards of 1000 hours) because of program time limits.

In addition, results from the short-time tests (100 hours and less) indicated that silicon loss for long time tests (1000 hours and longer) would be excessive unless the containers were adequately sealed (condition (b) above). Therefore a preliminary or exploratory sealing and joining program was initiated. This program considered the joining of the following:

(a) pyrolytic graphite to itself

(b) pyrolytic graphite to boron nitride

(c) boron nitride to itself

An early experiment was designed to investigate the feasibility of joining graphite bodies. The top inner portion of a pyrolytic graphite crucible (with proper crystal orientation for molten Si containment) was tapped. A rod of commercial graphite (ATJ) with suitable diameter was threaded and used as a cap for the container. The thread was purposely made to form a "sloppy" fit. The crucible was filled with silicon, placed in the vacuum induction furnace, evacuated, and heated to 1550^{o}C. After one hour at temperature the crucible was taken out of the furnace and examined. The cap which was previously loosely fitted was found to be firmly joined to the body of the crucible. Figure 24 is a photomicrograph of a section of the specimen showing the "brazed" joint of pyrolytic and ATJ graphite.

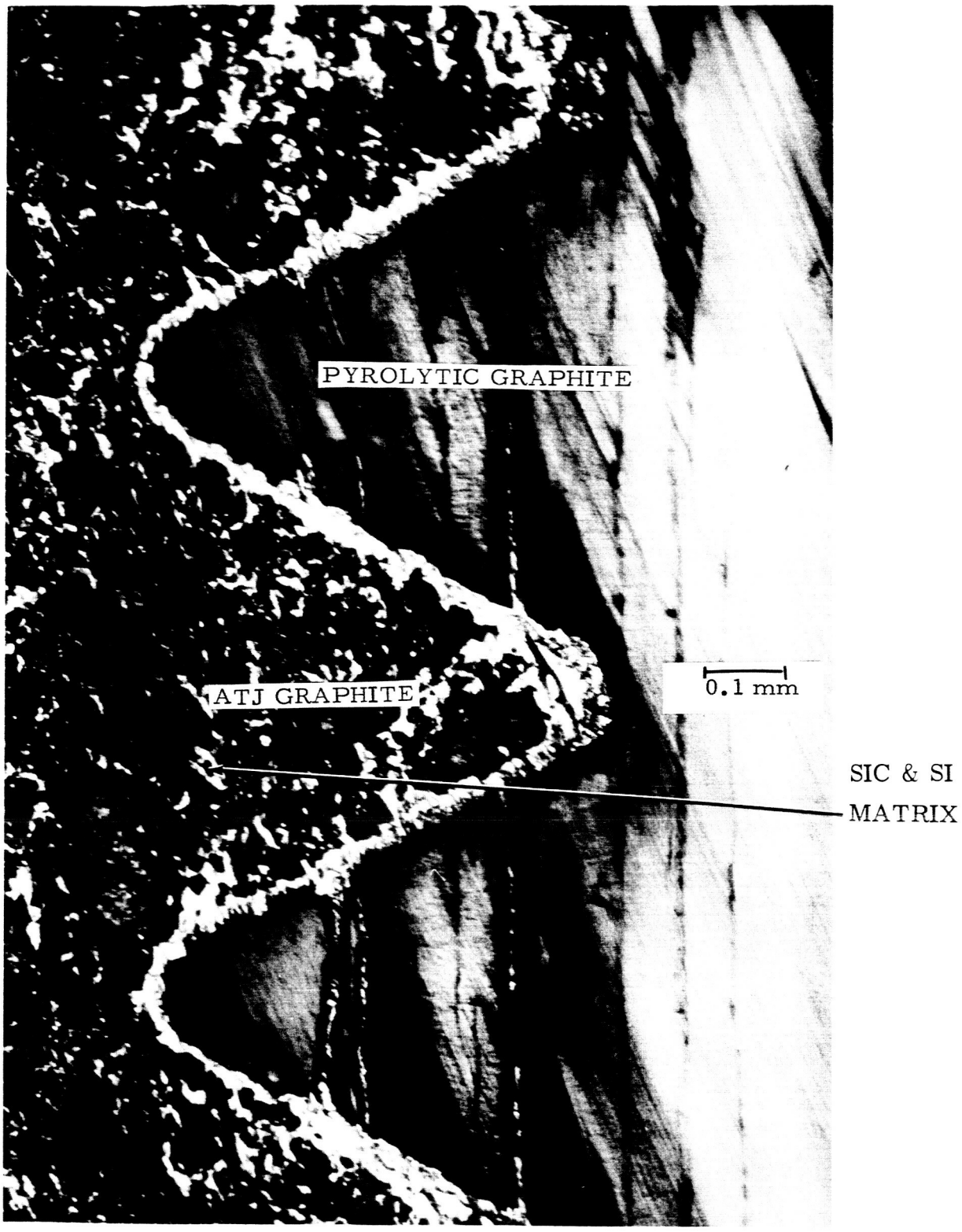

Figure 24. Joining Experiment of Pyrolytic Graphite to ATJ Graphite in a Silicon Environment

All of these experiments (sealing and joining) were conducted at relatively moderate temperatures (1400-1500^{o}C). Some of the reactions considered were known to occur at higher temperatures and it was assumed that they would also occur at lower rates at somewhat reduced temperatures.

All test samples were heated in graphite crucibles in an induction furnace under an initial pressure of less than 10^{-5} mm Hg. Because of degassing during heating and the generation of gaseous reaction products, pressure varied considerably during the course of an experiment. No mechanical pressure was applied to these samples other than their own weight.

1. Pyrolytic Graphite to Itself

   a. Silicon Carbide Bond

   Bonding was not found to occur when a composite consisting of powdered silicon or a mixture of powdered silicon and graphite was sandwiched between two pieces of pyrolytic graphite, and was vacuum heated (above 1500^{o}C) for one hour. However, in both of the above cases a silicon carbide layer was found to have been formed on the pyrolytic graphite surfaces. Some mechanical pressure might have helped to induce a better bond.

   b. Titanium Carbide Bond

   Slight bonding of pyrolytic graphite to itself occurred when powdered titanium hydride was reacted between a pair of pyrolytic graphite surfaces at 1500^{o}C for one hour in vacuum. When the mild bond was broken, a mottled porous "metallic" layer was observed at the interface. Small islands of pyrolytic graphite were found to adhere tenaciously to the "bonding layer." Again, mechanical pressure might have helped.

2. Pyrolytic Graphite to Boron Nitride

   a. Boron Carbide Bond

   Boron carbide can be formed by reacting boron nitride with graphite at about 2400^{o}C (Ref. 17).

Extremely weak or no bonding at all was found when pyrolytic graphite in intimate contact with boron nitride was vacuum heated for one hour at about 1600°C. X-ray diffraction examination of the dark mottled boron nitride surface after the test revealed the presence of carbon and boron carbide.

b. Titanium Diboride Bond

It had been hoped that titanium diboride could be used to bond PG-BN since it had shown excellent resistance to molten silicon attack.

Boron carbide reacts with titanium carbide to form titanium diboride and graphite (Ref. 18). It was reasoned that a titanium diboride bond would be formed when boron carbide, which results from the reaction between boron nitride and graphite at relatively low temperatures, is reacted with titanium carbide.

A bonding experiment was run in which titanium carbide powder was placed within a cylindrical cavity in ATJ graphite and capped with a tightly fitted boron nitride plug. After heating for one hour at about 1450°C in vacuum, it was found that the boron nitride plug could not be removed from the crucible. Sectioning revealed the formation of a grayish bonding layer between the boron nitride and ATJ graphite. The bonding layer was not identified. No bonding between graphite and boron nitride was found where the titanium carbide layer was sufficiently thick to prevent contact between C and BN.

3. Boron Nitride to Itself

It was reported earlier that although titanium carbide failed in a compatibility screening test with molten silicon, a thin tenacious metallic coating was found on the boron nitiride crucible used for this test. X-ray diffraction indicated that this coating contained titanium diboride and titanium nitride and other unidentifiable

components. This reaction might be considered for bonding BN to BN. However, time and equipment were not available for continued BN-BN bonding experiments.

3.3 Summary of Silicon Containment Materials Studies

There are good indications from 100-hour molten silicon containment tests that boron nitride and properly oriented pyrolytic graphite have potential for meeting both the thermal (Ref. 19) and long-time compatibility requirements for TES containers where silicon is the TES medium.

For solar, thermionic, space-power generation, life requirements of one year are anticipated. Therefore molten silicon compatibility tests of at least 10,000 to 15,000 hours should be made. However, before long-time compatibility tests can be made, it would be necessary to provide sealed containers of BN, PG or combinations of the two to prevent silicon loss during a long-time test.

In order of their importance the following tasks should be completed to definitely prove the suitability of BN and PG for long-time molten silicon containment for solar, thermionic, space-power generation applications:

(a) Provide hermetically sealed silicon containers of BN, PG or combinations of the two which will require development of sealing techniques. Obviously, seals employed must be compatible with molten silicon. Vapor or pyrolytic deposition techniques for BN and PG should be investigated for the possibility of providing sealed containers by deposition on preformed silicon ingots. This technique might also be used to seal a silicon container which is closed but not tight (threaded joints, flanges, etc.).

(b) Test sealed containers filled with silicon for 1000 hours and longer at 1500^{o}C in vacuum, with thermal cycling through the melting point.

(c) Develop joining techniques for mating the sealed TES container (filled with silicon) to the cathode of a thermionic converter.

Note: A rather comprehensive report on "The Joining of Pyrolytic Graphite" was very recently published by H. Rauch of the Space Sciences Laboratory and S. Foldes of the Flight Propulsion Laboratory. The work on this program was done under Contract No. NORD 17017 and could provide the ground work for any future effort in the sealing of pyrolytic graphite and in the mating of PG to refractory metals.

4. ALTERNATE THERMAL ENERGY STORAGE MATERIALS STUDIES

4. ALTERNATE THERMAL ENERGY STORAGE MATERIALS STUDIES

4.1 Discussion

Characteristics required of thermal energy storage material for use in the 1600 to 2100°K range limit the mechanism or properties which may be useful. H. W. Wilson et al (Ref. 20) came to the conclusion that reversible chemical reactions (wherein all products and reactants are liquids or solids) were not feasible for the intended mission. He also thought, however, that peritectic reactions did indicate promise and might be considered. The most promising method concluded by Wilson was the use of latent heat of fusion of certain selected compounds. A number of tables prepared from a literature survey and analysis are also presented in Wilson's report.

In the search for suitable materials in this effort it was found that only the oxides had melting points and heats of fusion of interest. The melting points of the stable oxides far exceeded the temperature range of interest but upon closer examination compounds and eutectic mixtures of the so-called refractory oxides as binary or ternary systems could meet most requirements. The basic objectives were to find oxide systems which: (1) exhibited congruent melting points in the temperature range of interest, (2) had heats of fusion at least 100 wh/lb, and (3) were compatible with one or more of the refractory metals. Wetting characteristics and volume changes on freezing also had to be determined, and necessary preparation and handling techniques had to be developed.

Table IV lists the single oxides with melting points between 1600 and 2100°K for which heat of fusion data were available. None of these compounds have heats of fusion approaching that of silicon (420 cal/g) and of the three having values in excess of 100 cal/g the two iron oxides could not be contained in refractory metals based on thermodynamic considerations. On a weight basis, MnO heat of fusion was not of great interest. This latter oxide could be used in binary or ternary mixtures with other oxides.

Table IV

THE HEATS OF FUSION OF OXIDES MELTING IN THE 1600°K TO 2100°K RANGE (21)

Oxide	Melting Point (°K)	Heat of Fusion (cal/g)
CuO	1720	35
FeO	1650	110
Fe_3O_4	1870	140
MnO	2060	183
Mn_3O_4	1830	Unknown
Cb_2O_5	1785	92
SiO_2 (Quartz)	1880	34
SnO_2	1900	75
WO_3	1740	60

In undertaking this study, it became apparent early that heat of fusion data for refractory oxide mixtures were virtually nonexistent. It was, therefore, necessary to rely upon the available basic data for each individual oxide as a starting point. In selecting the group of oxides to be considered, the overriding criterion was thermodynamic stability relative to refractory metals. High heats of fusion are desirable although it was felt that a high density might compensate, in part, in view of the importance of volumetric heat content to the ultimate application.

With these facts in mind, Table V was compiled from the existing data. The relative thermodynamic stability of these oxides compared with those of the refractory metals is presented in Figure 25. It was apparent that molybdenum and tungsten offered potential as container materials for all these oxides although tantalum and columbium also appeared to be compatible with the most stable oxides listed. However, it must be recognized that a favorable free-energy relationship, while the only means of predicting possible compatibility, is no assurance that reaction will not take place. In the case of tantalum and columbium, for instance, extensive solubility of oxygen base metal may result in a significant decomposition of oxide. In addition, free-energy relationships give no indication of the solubilities of various system components in one another.

While there are other oxides which could be included in the list presented in Table V, necessary basic data to warrant their consideration are not available. Also, since heat of fusion on a weight basis had to be high for space application, it was believed reasonable to eliminate most heavy-metal oxides.

The application considered of these thermal storage materials required a congruent melting point, and it was necessary therefore to restrict the mixtures to compositions representing a eutectic or a compound. The ceramic literature was used to establish the existence of the compositions and melting points of suitable mixtures from available phase diagrams of the oxides and these are listed in Table VI.

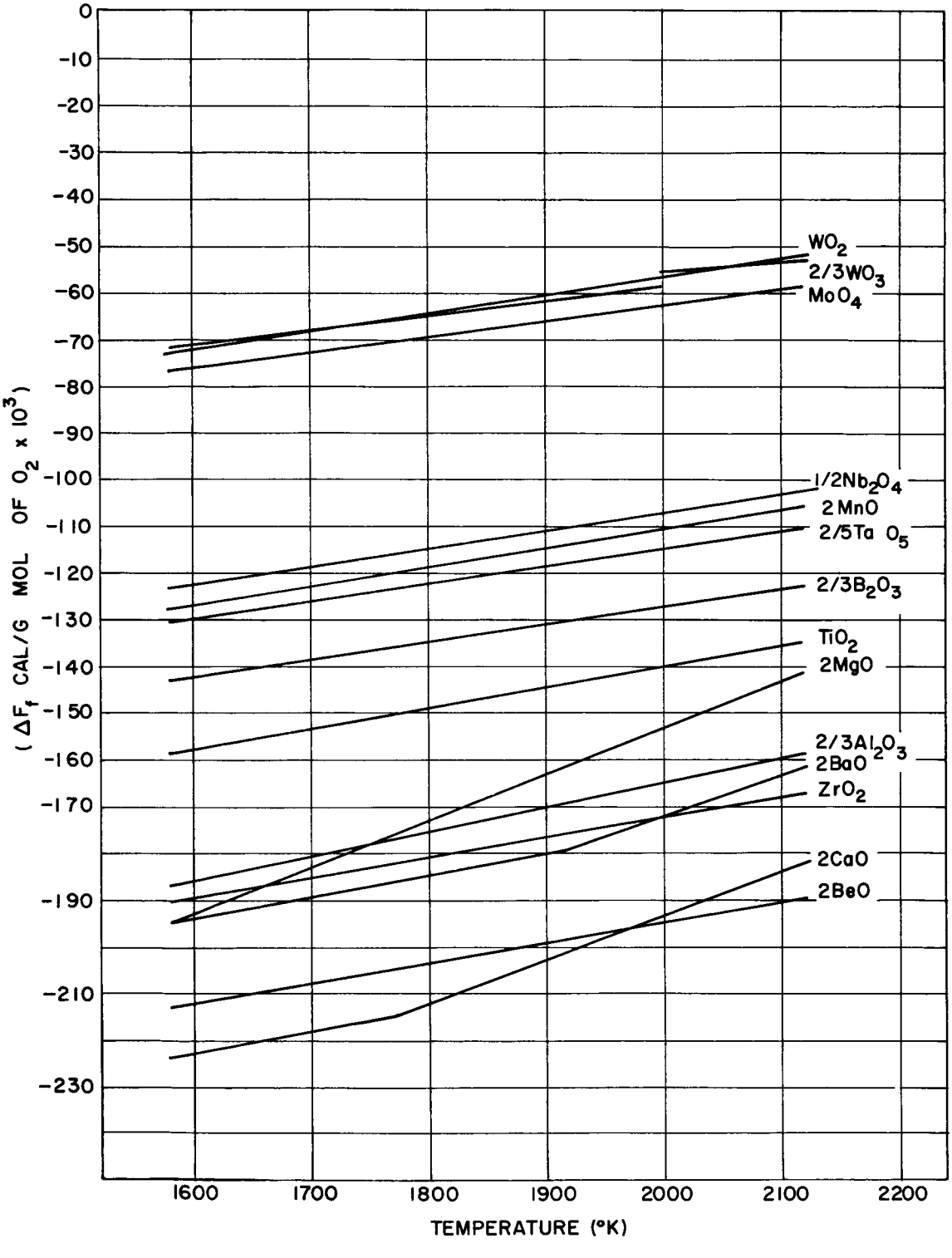

Figure 25. The Standard Free Energies of Formation of the Oxides Per Gram Mol Of O_2 (Gas)

Table V

PHYSICAL PROPERTIES OF OXIDES

Oxide	Molecular Weight (g)	(21)* M. P. (°K)	(22) Density (g/cc)	ΔH_f (cal/gm-mol)	(21) (cal/g)	S (eu/mol)	(eu/g)	(23) K @1670°K (cal. sec^{-1}. cm^{-2}. cm. $°C^{-1}$)	(22) Crystal Structure
Al_2O_3	101.96	2303	3.97	26,000[16]	255.0	11.3	0.11	0.0131[15]	Hex
BaO	153.36	2198	5.72	13,800[16]	90.0	6.3	0.04		Cubic
BeO	25.01	2803	3.01	17,000[16]	679.7	6.1	0.24	0.0362[15]	Hex
B_2O_3	69.64	723	1.85	5,500[16]	79.0	7.6	0.11		Glass
CaO	56.08	2873	3.32	19,000[16]	338.8	6.6	0.12	0.0174[15]	Cubic
MgO	40.32	3073	3.65	18,500[16]	458.8	6.0	0.15	0.0144[15]	Cubic
MnO	70.93	2058	5.40	13,000[16]	183.2	6.3	0.09		Cubic
TiO_2	79.90	2113	4.25	15,500[16]	193.9	7.3	0.09	0.0079[15]	Tet
ZrO_2	123.32	2950	5.56	20,800[22]	168.7	7.1	0.06	0.0058[15]	Monoclinic

*Denotes References

Table VI

PROPERTIES OF OXIDE MIXTURES SURVEYED (CALCULATED H_f VALUES)

Composition	Weight(%)*	M. P. (°K)	ΔH_f (calculated) cal/g	(wh/lb)	Density g/cc	lb/in^3	Form	Figure No. In reference 31
B_2O_3-3MgO	36.5B;63.5	1635	225	119	3.000	.108	Compound	80
3BeO-2CaO	40.1;59.9D	1635	273	144	3.192	.115	Compound	32
$3Al_2O_3$-6CaO-MgO	44.8A;49.3;5.9E	1720	208	110	3.631	.131	Eutectic	276
3BeO-B_2B_3 (predicted from ref. 32)	51.9C;48.1B	1723	307	162	2.446	.088	Compound	
3CaO-$B_2)_3$	29.3B;70.7D	1723	200	106	2.900	.105	Compound	44
5CaO-$3Al_2O_3$	52.2A;47.8D	1730	180	95	3.659	.132	Compound	43, 1020
Al_2O_3-3MgO-$4TiO_2$	18A;60F;22E	1840	198	104	4.069	.147	Eutectic	1120
2BeO-Al_2O_3-$2TiO_2$	16.0C;32.7A;51.3F	1842	273	144	3.958	.143	Eutectic	259
3BeO-Al_2O_3-$2TiO_2$	22.3C;30.7A;47.4F	1845	248	131	3.890	.141	Eutectic	259
4MgO-ZrO_2	56.7E;43.3G	1845	200	106	4.477	.162	Eutectic	147, 88
2BeO-Al_2O_3-$4TiO_2$	10.6C;21.6A;67.8F	1850	267	141	4.057	.147	Eutectic	259
BeO-$Al_2O_3TiO_2$	12.1C;49.3A;38.6F	1850	220	116	3.961	.143	Eutectic	259
MgO-$3ZrO_2$	9.8E;90.2G	1870	124	65	5.372	.194	Eutectic	147, 88
CaO-Al_2O_3	64.5A;35.5D*	1870	210	111	2.730	.099	Eutectic	264
$4TiO_2$-$3ZrO_2$	45F;55.G	1873	137	72	4.971	.180	Eutectic	140
4BeO-$4TiO_2$-ZrO_2	18.4C;58.9F;22.7G	1880	225	119	4.317	.156	Eutectic	264
2BeO-TiO_2-ZrO_2	19.8C;31.6F;48.6G	1900	200	106	4.581	.166	Solid Sol'n	264
MgO-TiO_2	33.5E;66.5F	1900	219	116	4.049	.146	Compound	86
4BeO-4MgO-Al_2O_3	27.5C;28.1A;44.4E	1910	350	185	3.561	.129	Eutectic	255
MgO-$2TiO_2$	20.2E;79.8F	1920	190	100	4.129	.149	Compound	86
5BeO-4MgO-$3ZrO_2$	19.1C;24.6E;56.3G	1940	225	119	4.604	.166	Eutectic	257
2BeO-$3TiO_2$	17.3C;82.7F	1940	229	121	4.034	.146	Eutectic	38
Al_2O_3-$5TiO_2$	20.3A;79.7F	1975	198	104	4.193	.151	Eutectic	120
2MgO-TiO_2	50.2E;49.8F	2000	234	123	3.949	.143	Compound	86
4BeO-Al_2O_3-MgO	34.5C;47.0A;18.5E	2020	348	184	3.572	.129	Compound	255
2BeO-$5Al_2O_3$-$2TiO_2$	7.0C;70.8A;22.2F	2025	233	123	3.965	.143	Compound	259
3BeO-2MgO	48.2C;51.8E	2120	415	219	3.195	.115	Eutectic	32

*Note:

A - Al_2O_3 C - BeO E - MgO G - ZrO_2

B - B_2O_3 D - CaO F - TiO_2

On a weight basis, beryllium oxide offers the highest heat of fusion of the oxides for which data are available. This is followed in decreasing order by magnesium oxide, calcium oxide, and aluminum oxide. Utilizing all four oxides mentioned, there are six possible binary system combinations, BeO-Al_2O_3, BeO-MgO, BeO-CaO, MgO-CaO, MgO-Al_2O_3, and CaO-Al_2O_3. The BeO-Al_2O_3 [24, 25] system as reported contains three eutectics and two compounds all melting in the 2100°K to 2200°K range. In the BeO-MgO system, a eutectic has been reported at about 35 mol percent MgO with the eutectic temperature indicated as being about 2130°K[25, 26]. Since this combination appears to offer the potential of a very high heat of fusion, it was considered worthy of consideration in spite of the apparently high melting point. A eutectic was reported in the BeO-CaO system at about 40 mol percent CaO with the melting point at 1600°K[25] or 1620°K[27]. This mixture was of interest. The CaO-MgO system has one eutectic with a melting point of about 2570°K[25, 28] while the MgO-Al_2O_3 system has no mixture with a congruent melting point below 2300°K[10, 8]. Of the six binary systems, the CaO-Al_2O_3 system has apparently received the most detailed attention, [29, 25] and there are three congruent melting point compounds as well as four associated eutectics existing with melting points between 1600 and 2100°K in this system.

Of the six possible binary systems of the four most promising oxides, only two had potential for application. It then became necessary to consider ternary mixtures. It was in this search that the limitations and general unreliability of the desired data became most apparent. The properties required for thermal storage applications are, in general, not those sought in the usual ceramic research programs. As a consequence, the relatively low melting point compositions, in general, have not received detailed attention. Table VI lists the various binary and ternary mixtures of the basic oxides with melting points of interest which could be located in the literature. In most cases the molecular ratios presented are those representing mixtures found to have depressed and essentially congruent melting points. These mixtures are not necessarily the exact eutectic or compound compositions.

In order to attempt an evaluation of these materials on the basis of their potential heat of fusion, a series of calculations which led to the values listed in Table VI was undertaken. A basic assumption made is the additive nature of entropies of fusion. This has been found applicable in the case of binary eutectics in metallic systems. Intermetallic compounds and eutectics formed from two compounds have been shown by Wagner[30] to require certain corrections. Since necessary data involved in these corrections were not available for ceramic oxide systems, each mixture has been treated as a simple eutectic of the basic oxides. The results were found to be indicative of the magnitude of the heat of fusion which could be expected.

As an example of this calculation, the $3MgO\text{-}B_2O_3$ mixture is used with pertinent values taken from Tables V and VI. The entropy of fusion is, by definition, the heat of fusion divided by the melting point in ^{o}K. As given in Table V this value for MgO is 6.0 eu/mol and for B_2O_3, 7.6 eu/mol. For $3MgO\text{-}B_2O_3$ with a melting point of $1635^{o}K$, the heat of fusion was calculated as follows:

$$3 \times 6.0\ (MgO) + 7.6\ (B_2O_3) = \frac{X}{1635^{o}K}$$

$$x = 25.6 \times 1635 = 43,000\ cal/mol$$

The molecular weight of the mixture is

$$3 \times 4 \times 40.32 + 69.64 = 109.6\ g$$

so the calculated heat of fusion on a weight basis is

$$\frac{42,000\ cal/mol}{190.6\ g/mol} = 210\ cal/g\ or,$$

$$\frac{210\ cal/g \times 454\ g/lb}{860\ cal/watt\text{-}hr} = 111\ watt\text{-}hrs/lb$$

Since it was a basic objective of the program to provide a spectrum of thermal storage materials with melting points which would provide a choice of converter operating temperatures, oxide mixtures with melting points at approximately 100-degree intervals were selected from Table VI for experimental evaluation.

4.2 Experimental Effort

4.2.1 Preliminary Investigations

While the heat of fusion is a fundamental consideration in evaluating a potential thermal energy storage material, of parallel importance is compatibility with suitable container materials. Obviously, the determination of heat of fusion also required a suitable capsule material. A primary advantage anticipated for the oxides was use of refractory metals for containment.

Initial exploratory compatibility efforts were successfully conducted with the calcia-alumina mixtures using molybdenum as the container material. However, oxide preparation difficulties were found in that the hydroscopic nature of CaO interfered with obtaining the required stoichiometeric composition of the charge as initially weighed. For this reason, calcium carbonate was used as the source for calcia. The correct proportions of the carbonate and alumina were intimately mixed and the CO_2 driven off by heating the mixture in an alumina crucible in air to approximately $1550^{o}K$ for one hour.

After transferring this material to a molybdenum crucible and heating under vacuum, it was found that the mixture melted at essentially the predicted melting point. In the course of these preliminary investigations, the calcia-alumina mixtures $5CaO\text{-}3Al_2O_3$, $CaO\text{-}Al_2O_3$, and $3CaO\text{-}5Al_2O_3$ exhibited congruent melting points. In the molten state they wetted molybdenum and gave evidence of little volume change on freezing. The volume change was slightly positive in the first case and slightly negative in the other two.

A similar study was undertaken with the $MgO\text{-}TiO_2$ mixtures. In this case, however, it was found that extensive attack of molybdenum occurred at the liquid level interface in vacuum. This was attributed to dissociation of TiO_2 to TiO and oxygen. The latter element evidently reacted with molybdenum to form the volatile MoO_3 allowing the reaction to proceed with the continuous erosion of the molybdenum crucible wall. It was apparent that if TiO_2 was to be a component in a TES material, it would be necessary to carry out tests in a sealed system to prevent escape of volatile reaction products.

The necessity for employing sealed capsules was further emphasized since highly toxic BeO was present in many mixtures of interest. The toxic nature of BeO required careful handling throughout. Hot pressing was used in order to minimize handling of BeO as well as to ensure charging the maximum volume of oxide mixture into a capsule. This process involves the intimate mixing of basic oxide powders in their stoichiometric proportions and charging the mixture into a graphite die having a cavity of the desired dimensions. A hydraulic press was used with die and charge heated to approximately 90 percent of the reported melting point. The compacting pressure used was 2000 psi. It was found that maintaining these conditions for approximately 30 minutes was sufficient to reach a density usually better than 90 percent of the theoretical value.

Cold pressing techniques were considered; however, the lower densities attainable (60-80%) would have produced bodies which would shrink considerably on fusion. Remote handling techniques of these materials as liquids would certainly be more desirable and eventually such techniques might need to be developed. Voids in any thermal storage container will be, in all likelihood, a detriment to the system.

Another phenomena was also observed while heating in open cups in vacuum furnaces: evidently high surface tension of some of these mixtures resulted in considerable "creeping" of the melt up container walls. Pouring and casting in this case would then be quite difficult. For this reason and the others mentioned previously, hot pressing was utilized for the most part to prepare oxide specimens for study. (The chemical analyses of the raw materials used in preparing the heat of fusion specimens are listed in Table VII.)

4.2.2 Heat of Fusion Studies

Capsules for use in the heat of fusion investigation were fabricated from one-inch diameter unalloyed molydenum rod which had been arc melted, extruded, and swaged. The capsule dimensions were 7/8 inch O.D. 11/16 inch I.D. and two inches long. The oxide slugs were hot pressed to a diameter of 5/8 inch

Table VII

RAW MATERIAL, SOURCE AND IMPURITY LEVELS

Oxide	Grade	Supplier	Impurities (ppm, greater than 10)
Al_2O_3	A	Linde	C-1780, Pb-100, P-100, S-33, Fe-20, Na-80, Si-30
B_2O_3	Commercial	Borax Corp. of America	SO_4-100, Ca-50, all others <10.
BeO	UOX	Brush Beryllium	Al-100, Cu-20, Fe-40, Pb-20, Mg-100, Mn-20, Mo-100, Ni-20, Si-100, Na-150, C-1000, F-500, P-100, S-300
$CaCO_3$	ACS	Matheson, Coleman & Bell	Ba-50, Cl-10, Pb-10, Fe-30, Mg-200, HCl+NH_4OH-150, NO_3-50, K-100, Na-1000, SO_4-100, Sr-1000, NH_4-30
MgO	SL	Mallinckrodt	F-37, Cl-31, P-26, C-1170, Al-30, Be-50, Ca-300, Fe-30, Na-500, Si-100, Sn-20, Zn-20
TiO_2	Ti Pure	Dupont	2% impurities consisting of Fe, Mg, Pb, Si, Sr, V, W, Sb as oxides
ZrO_2	XP	Reactive Metals	Al-10, Fe-475, Na-15, Si-20, C-140, S-15, P-25, N-15

(Analyzed by GE, ANP)

with lengths adjusted according to the predicted heat of fusion so that the heat capacity of the entire assembly did not exceed the capacity of the calorimeter. After loading, the capsule was sealed under vacuum using a 30-kv electron beam welder. A total of eighteen oxide mixtures representing a range of melting points were encapsulated for study on the basis of predicted heats of fusion.

4.2.2.1 Enthalpy Measurements

Enthalpy determinations were made at various temperatures using the "drop" method in an adiabatic water calorimeter. Figure 26 is a photograph of the furnace and calorimeter. The furnace is a 25 kilowatt resistance-heated vertical carbon-tube furnace (Hevi-Duty Electric Company Model C-218). The heated zone in the furnace was 18 inches long and two inches in diameter. An inert atmosphere in the furnace was maintained using argon flow (approximately 10 cubic feet per hour).

The calorimeter was an oxygen bomb-type calorimeter (Parr Instrument Company Series 1200 adiabatic calorimeter) which was modified to accept a drop tube. The lower part of the drop tube, which was beneath the surface of the water in the calorimeter proper, was finned copper tubing. Three radiation gates, two between the furnace and calorimeter and one within the calorimeter, prevented radiant heat transfer between the furnace and calorimeter.

The sample temperature was measured using an optical pyrometer sighted on a blackbody hole in the capsule through a sight port in the side of the furnace. The pyrometer was calibrated against a standard tungsten ribbon lamp. The transmission of the quartz window through which the black body hole was observed was independently measured with a spectrophotometer and appropriate corrections were made to the indicated temperature.

The oxide compositions were encapsulated in molybdenum as described previously, and an empty capsule was used to calibrate the calorimeter. In this way, from a single series of "drops" at different temperatures with the empty capsule, both the calorimeter constant and radiation losses as a function of temperature were obtained under the same conditions used for actual measurements.

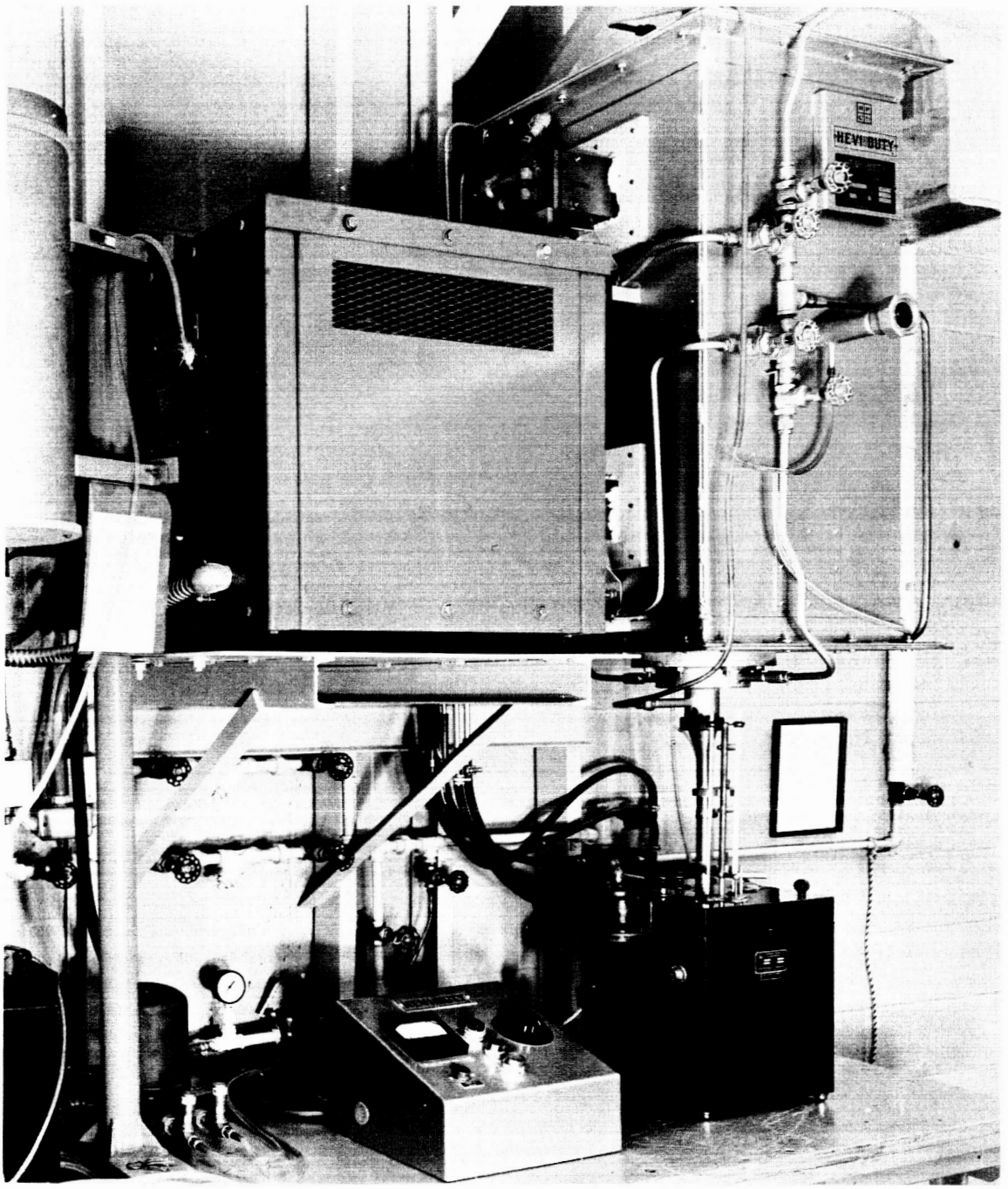

Figure 26. Heat of Fusion Calorimeter

The following procedure was used for this calibration. It was assumed that only the radiation loss from the capsule during the time of fall in the unheated zone was important. With this assumption, the enthalpy change (ΔH) of the capsule plus contents between the initial temperature in the furnace and the final temperature of calorimeter plus capsule may be written:

$$\Delta H = K \Delta T_c + kT_k^4$$

where K is the calorimeter constant (the heat in calories necessary to increase the calorimeter temperature by one degree), ΔT_c is the change in temperature of the calorimeter, k is a constant having the dimensions Cal per ^oK, and T_k is the absolute temperature (^oK). Four drops with the empty capsule were made between 1470^o and 1920^oK.

With these data, a plot of $\Delta H/\Delta T_c$ versus $T_k^4/\Delta T_c$ was made, and K and k were obtained from the intercept and slope respectively. The enthalpy values for molybdenum were taken from Reference 33. For these measurements (as well as for all the measurements reported here), 2500 ml. of distilled water were used in the calorimeter.

From this procedure the values K = 2759.6 cal per ^oC and $k = 1.90 \times 10^{-11}$ cal per $^oK^4$ were obtained. It should be noted that the constant k is the product of total emissivity of molybdenum, the capsule area, the time during which radiation loss occurs, and the Stefan-Boltzmann constant. Assuming the total emissivity of molybdenum to be 0.3 over this temperature range, the value of k given above corresponds to a time of 1.2 sec during which radiation loss occurs. The calculated free fall time is 0.25 sec in the unheated zone between the furnace and top of the calorimeter. This comparison indicates that radiation losses are considerably reduced in the system with provisions made for the capsule to drop directly to the bottom of the calorimeter.

In actual oxide enthalpy measurements, the enthalpy change of oxide from the high temperature T to the reference temperature (298^oK), $H_T - H_{298}$ in cal per g, was calculated from the following expression:

$$H_T - H_{298} = \frac{1}{M_{ox}} \left[K + kT_k^4 - M_m (H_T - H_{298})_m + C_{pm} M_m (T_f - 298) + C_{pox} M_{ox} (T_f - 298) \right]$$

where: M_{ox} = mass of oxide composition (g)

K = calorimeter constant (2579.6 cal per ^{o}K)

ΔT_c = change in calorimeter temperature (^{o}K)

M_m = mass of molybdenum capsule (g)

$(H_T - H_{298})_m$ = enthalpy change of molybdenum (cal per g)

C_{pm} = specific heat of molybdenum at 298^{o}K (.0592 cal per g per ^{o}K)

T_f = final temperature of calorimeter (^{o}K)

C_{pox} = specific heat of oxide composition at 298^{o}K (cal per g per ^{o}K)

The last two terms on the right are small factors which account for the fact that the final temperature of the calorimeter was generally higher than 298^{o}K. C_{pm} was obtained from Reference 33 and C_{pox} was calculated assuming that the specific heat of the composition is equal to the specific heat of the pure oxides in the proper molar proportion. This is certainly a sound assumption considering the small magnitude of the correction. The specific heats of the individual oxides were taken from Reference 34 except for CaO which is from Reference 35. Figures C-1 to C-18 in Appendix C present the enthalpy as a function of temperature as obtained from the various oxide mixtures studied.

The accuracy of the enthalpy measurements was quite difficult to estimate. Several factors such as temperature uniformity of the capsule with the furnace, accuracy of the tabulated molybdenum enthalpy which was used for calibration, assumptions made regarding radiation losses and reproducibility of such losses were unknown. In addition, accuracy of any individual enthalpy measurement will depend on the ratio of oxide enthalpy to total enthalpy of oxide plus capsule.

However, some indication of data accuracy may be obtained by comparing measured enthalpy of the oxide composition in the solid phase with that calculated from the enthalpies of the individual oxides combined in the proper molar proportion.

These of course should be identical if there is no solid solubility or compound formed. The dashed lines in Figures C-1 through C-18 are the calculated solid enthalpies. The enthalpy of the solid for the composition $3CaO-B_2O_3$ is from Reference 35. As can be seen from the curves, the agreement between the calculated and measured values is generally good (within a few percent) except for some compositons containing TiO_2 (which were found to have reacted with molybdenum).

Another indication of data accuracy may be inferred from the fact that melting temperatures obtained from enthalpy measurements are in general agreement with phase diagrams found in Reference 31.

4.2.2.2 Evaluation of Results of the Heat of Fusion Studies

The overall results obtained from heat of fusion studies are presented in Table VIII. It can be seen that in order to satisfactorily cover the desired range of melting points it was necessary to include several TiO_2 containing mixtures. This was done in spite of the early indications of incompatibility of such mixtures with molybdenum. It was hoped that in a sealed system, equilibrium would be established early and no further reaction would occur. The results obtained with these mixtures, however, were somewhat disappointing. The $2BeO-5Al_2O_3-2TiO_2$ mixture, for instance, came through the capsule after only a short time above the melting point (1960°K). This effect was noted in two different capsule systems so that it was not believed to be a function of capsule fabrication. The mechanism of failure in this case is not understood since no evidence of gross capsule-wall attack was noted nor was there evidence of a crack or pinhole. The molten material escape appeared to be a process best described as "weeping."

Similar loss of material was encountered in the case of the $2BeO-3TiO_2$ mixture (M.P. 1930°K). Evidence of some solutioning attack, emphasized at the grain boundaries in this case, is shown by Figure 27 which presents the micro-structure of the molybdenum capsule at the metal-oxide interface.

TABLE VIII. EXPERIMENTALLY DETERMINED PROPERTIES OF SELECTED OXIDE MIXTURES

Composition	M. P. (°K)	Hf (cal/g)	Hf (wh/lb)	(wh/in^3)	Density (as hot-pressed)	Density (cc melted)	Degree of (*) Shrinkage	Reference to figures in App. C
$3MgO-B_2O_3$	1630	180	95	0.611	0.00612	0.00643	Large	C-4
$6CaO-3Al_2O_3-MgO$	1630	78	42	0.261	.00491	.00621	None	C-10
$5CaO-3Al_2O_3$	1650	70	37	0.218		.00589	None	C-8
3BeO-2CaO	1685	221	117	0.714		.00610	Small	C-15
$3BeO-B_2O_3$	1730	72	38	0.162	.00543	.00426	Slight Expansion	
$3CaO-B_2O_3$	1770	130	69	0.447	.00627	.00648	Medium	C-5
$2BeO-TiO_2-ZrO_2$	1880	40	21	0.184	.00921	.00877	Large	C-7
$3BeO-Al_2O_3-2TiO_2$	1883	230	121	0.914		.00755	Large	C-16
$2BeO-Al_2O_3-4TiO_2$	1883	240	127	1.053		.00829	Large	C-14
$CaO-Al_2O_3$	1883	115	61	0.389	.00601	.00638	Small	C-17
$Al_2O_3-3MgO-4TiO_2$	1910	160	85	0.670	.00769	.00788	Medium	C-2
$4BeO-Al_2O_3-4MgO$	1910	340	179	1.162	.00733	.00649	Medium	C-12
$2BeO-3TiO_2$	1930	190	100	0.781		.00781	Large	C-13
$2BeO-5Al_2O_3-2TiO_2$	1960	152	80	0.704	.00793	.00880	Large	C-3
$5BeO-4MgO-3ZrO_2$	1973	215	113	1.066	.00879	.00943	Large	C-18
$4BeO-Al_2O_3-MgO$	2020	360	190	1.357	.00690	.00714	Large	C-6
3BeO-2MgO	2145	500	264	1.859	.00662	.00704	Large	C-9
$4MgO-ZrO_2$	2117				.00847			C-11
Silicon	1693	432	227	1.158		000513	10% Expansion	

(*) Estimated

Large	4-6%
Medium	2-4%
Small	1%

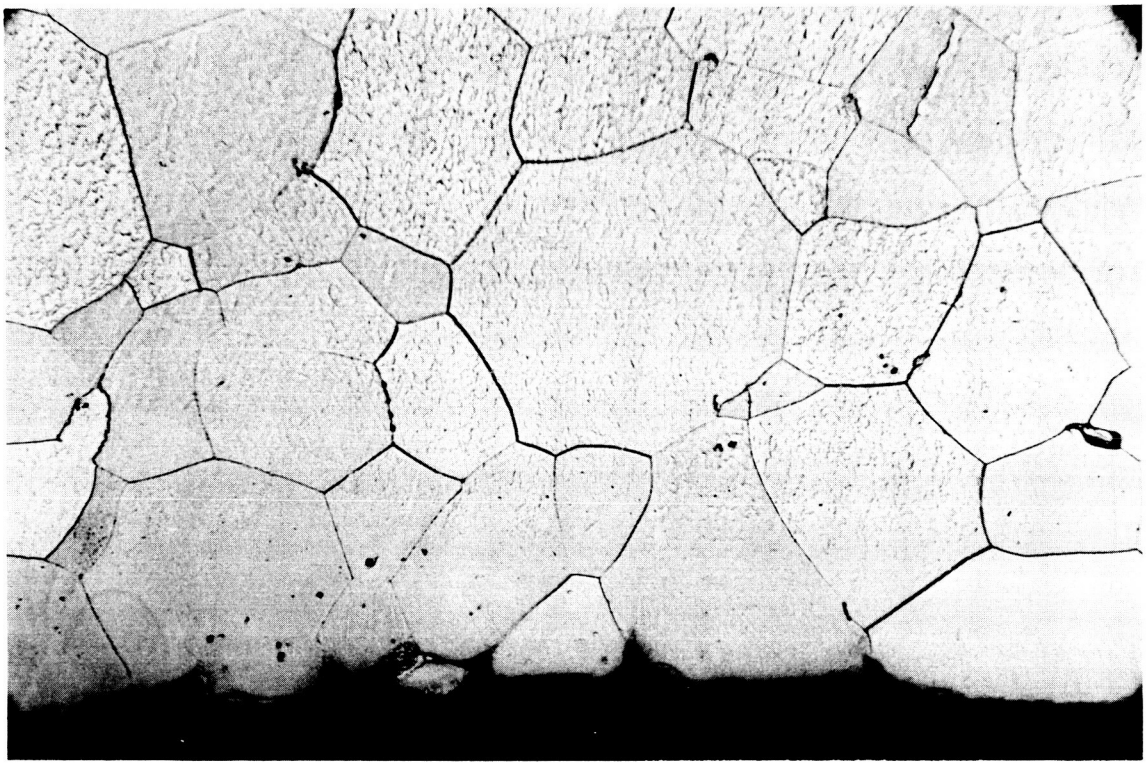

Figure 27. Microstructure of the Molybdenum-Molten $2BeO \cdot 3TiO_2$ Interface

This appeared to be typical of TiO_2 mixtures. The extent of reaction encountered after an equivalent time (approximately 10 hours) at a comparable temperature between molybdenum and the molten $4MgO\text{-}4BeO\text{-}Al_2O_3$ mixture (M.P. 1910°K) is shown in Figure 28 which is characteristic of mixtures without TiO_2.

The extent of crucible attack was evaluated in the heat of fusion samples by an analysis of the oxide for molybdenum. The results are listed in the following table.

Table IX

Mo Content of Various Oxide Mixtures After Heat of Fusion Determinations

Mixture	Mo Content w/o
$4MgO \cdot 5BeO \cdot 3ZrO_2$	0.09
$4MgO \cdot 4BeO \cdot Al_2O_3$	0.14
$3BeO \cdot Al_2O_3 \cdot 2TiO_2$	0.04
$2BeO \cdot Al_2O_3 \cdot 4TiO_2$	3.48
$3BeO \cdot TiO_2 \cdot ZrO_2$	0.07
$3BeO \cdot 3TiO_2$	5.00
$6CaO \cdot MgO \cdot 3Al_2O_3$	0.76
$3CaO \cdot B_2O_3$	0.08
$3MgO \cdot B_2O_3$	0.28
$CaO \cdot Al_2O_3$	0.11
$3BeO \cdot 2CaO$	0.53
$5CaO \cdot 3Al_2O_3$	0.02
$MgO \cdot 4BeO \cdot Al_2O_3$	0.41
$Al_2O_3 \cdot 3MgO \cdot 4TiO_2$	0.26

It is difficult to establish a trend from these data, although it is apparent that the two mixtures which exhibited the highest molybdenum content were those having the maximum TiO_2, 57 mol percent, and 60 mol percent, respectively.

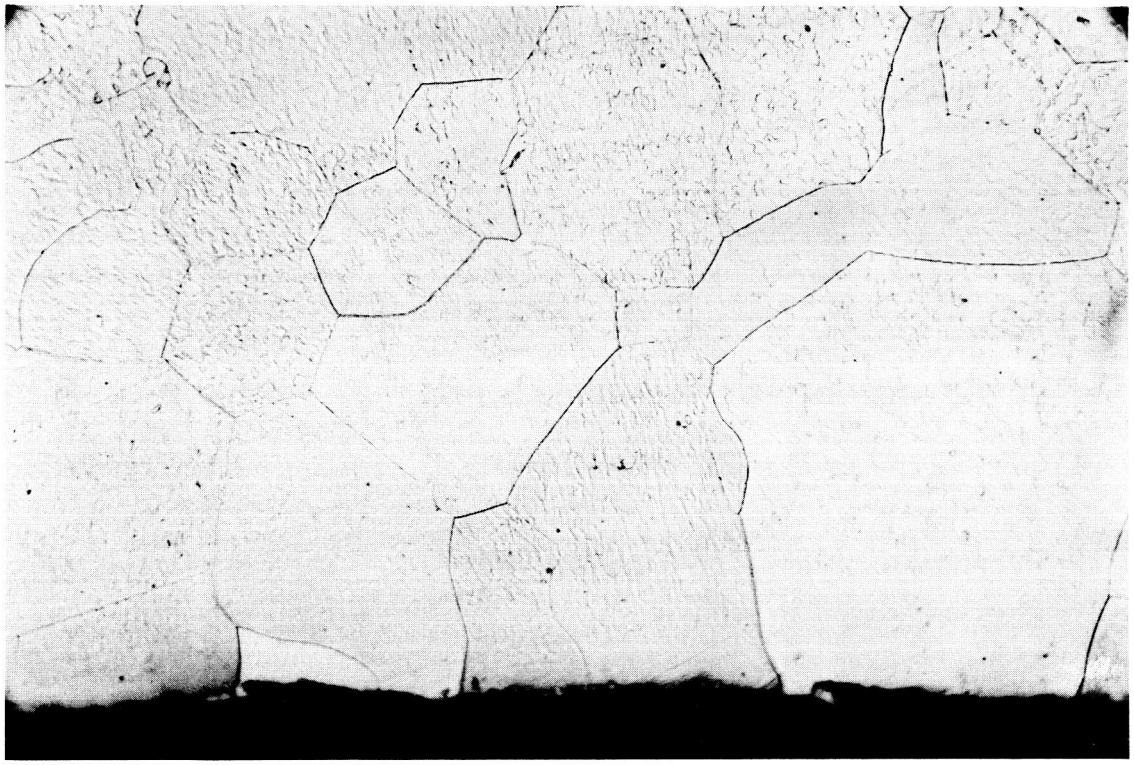

Figure 28. Microstructure of the Molybdenum-Molten $4MgO \cdot 4BeO \cdot Al_2O_3$ Interface

An attempt was made to establish a value for the change in wall thickness of the capsule by direct measurement. It was found, however, that these changes were in general well within the measurement error. A calculation was made for the $2BeO \cdot 3TiO_2$ capsule in which 5.00 w/o molybdenum was found dissolved in the oxide. This represents the removal of 0.0013 inch of Mo from the wall of the capsule. It is apparent that in the other capsules this change in wall thickness would be undetectable in most cases, being of the order of 0.0001 inch.

A microhardness traverse was made on each capsule wall after the heat of fusion run. In no case was a hardness gradient found. The overall hardness in all cases was that expected for recrystallized unalloyed molybdenum. This is sufficient evidence to indicate that no solution of either oxygen or the metallic components of the oxides in the molybdenum resulted from the elevated temperature exposure. This is supported by metallographic evidence of a normal molybdenum structure as indicated by Figures 27 and 28 which are typical of all the capsules. Some inconsistency in grain growth was noted. This was, in general, confined to the surfaces, both internal and external, and could not be correlated with the contained oxide. It is highly probable that the cold work induced by machining the capsule is largely responsible.

With regard to the possibility of compositional changes in the oxide mixtures during processing, this was eliminated on the basis of the consistency of the weights of as charged powders and the resulting hot pressed bodies. The only opportunity for change in the heat of fusion measurements, other than the solution of molybdenum, would be the solution of one or more of the oxide components in the capsule material. As pointed out earlier, this was eliminated on the basis of the absence of any hardness or microstructural change in the capsule wall.

It is apparent that titania containing mixtures are questionable for use as thermal storage materials with molybdenum containers. There is no reason to believe that the other refractory metals will be more satisfactory with the possible exception of tungsten. This is particularly unfortunate since, as can

be seen from Table VI, a large majority of the otherwise attractive mixtures contain this objectionable component. This is particularly true of the mid-region of the temperature range of interest.

The heat of fusion values derived from enthalpy measurements presented in Table VIII include, in four cases ($3BeO-Al_2O_3-2TiO_2$, $4MgO-Al_2O_3-4BeO$, $MgO-Al_2O_3-4BeO$, and $3MgO-Al_2O_3-4TiO_2$), results obtained from mixtures which obviously were not the exact stoichiometric composition of the congruent melting point mixture desired. The fact that so many of the mixtures investigated did indicate the correct compositions is remarkable considering the type of data available for the selection of these compositions. There is definite need for further work in establishing, with greater accuracy, the compositions of the congruent melting mixture in several of the most attractive systems.

The full significance of these oxide mixtures for application as thermal energy storage materials will be shown in the directive systems study in a later section of this report. Apparently, as was predicted over one year ago, mixtures containing both beryllia and magnesia have high heats of fusion. The melting temperatures are high and may be "container materials limited" but continued effort should point the way to reduce these melting temperatures without serious sacrifice of heat of fusion as well as finding metals and alloys which will be useful at the higher temperatures.

Other physical properties of interest which were qualitatively observed indicate that most of the oxides studied wetted refractory metal container walls and show little volume change on freezing (most oxides contracted). Estimates of these volume changes are shown in the table. Upon cooling to room temperature, all of the oxide "castings" were contracted away from the crucible walls and could be easily removed.

In a no-gravity situation, wetting characteristics of these oxides should be an advantage. The high densities of these light-metal oxides would also be considered an advantage. Graphical presentations of weight-to-power and volume-to-power relations are shown in Figures 29 and 30. These graphs show that on either weight or volume bases one can use several oxide mixtures studied in lieu of silicon.

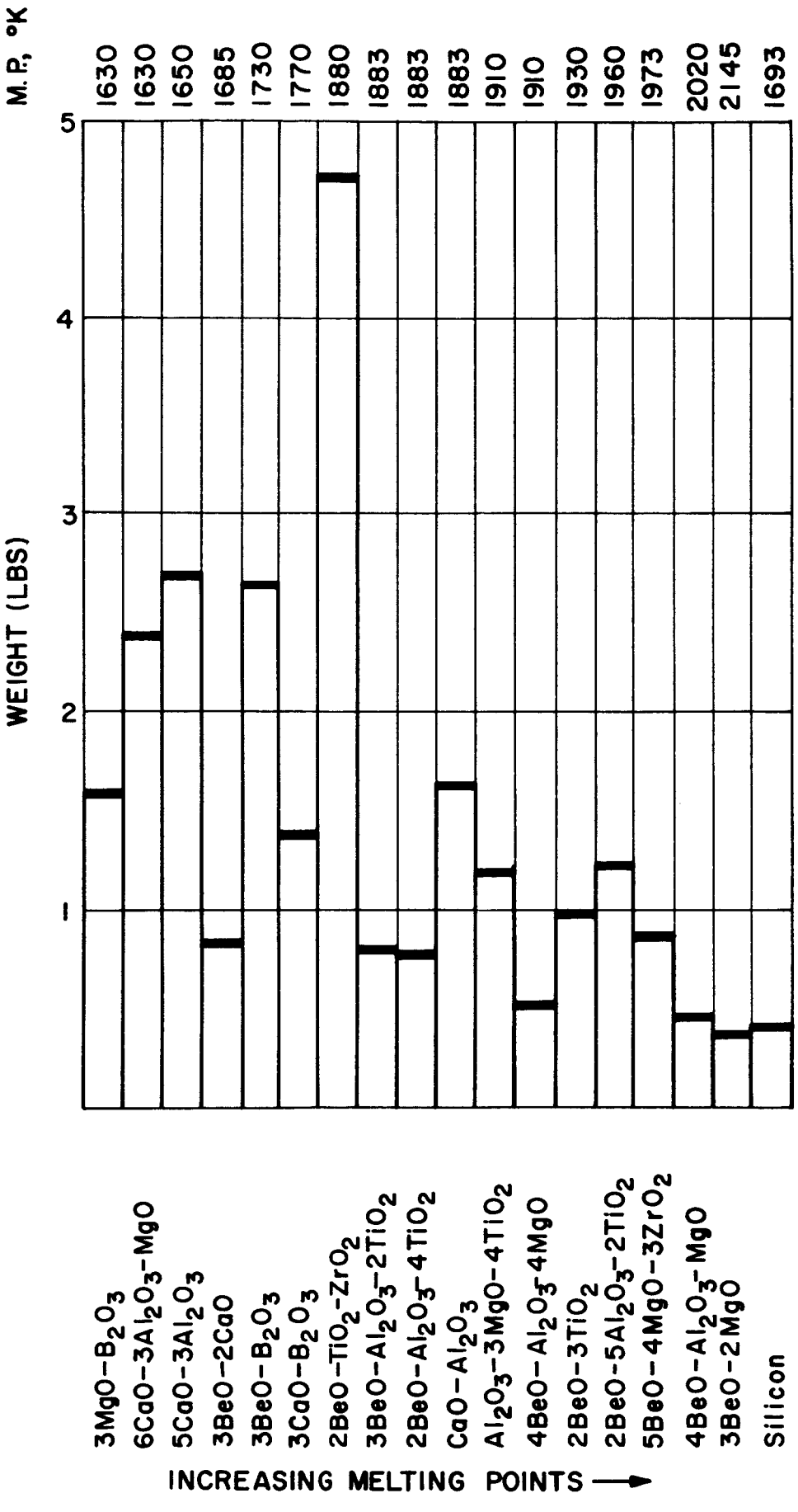

Figure 29. TES Material Required for 100 Watt-Hrs. of Power (Weight)

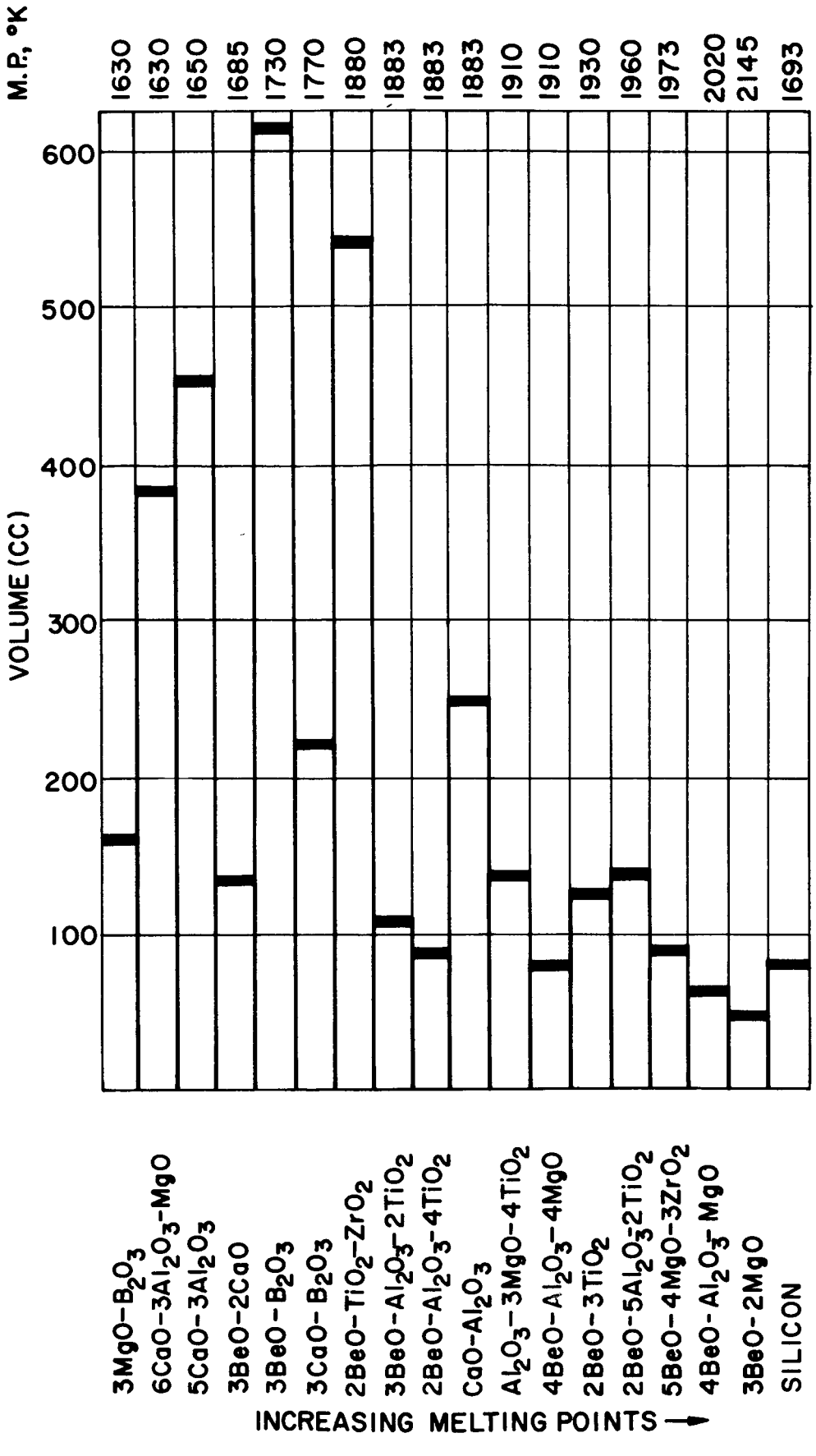

Figure 30. TES Material Required for 100 Watt-Hrs of Power (Volume)

4.2.3 Corrosion Tests

Although heat of fusion determinations did give some information relative to compatibility of selected oxide mixtures with molybdenum, the ultimate application of these materials will require that they co-exist for thousands of hours. For this reason separate longer time compatibility tests were conducted with several of the more favorable oxide mixtures in molybdenum capsules for 500 hours at temperatures approximately 150°K above the oxide melting points.

These studies were made in a vacuum induction furnace using a two-inch diameter tantalum susceptor. Five capsules, 7/8 inch O.D. by one inch long, were prepared for each of two runs in a manner similar to that used in the heat of fusion studies.

In the first run, molybdenum capsules were used alone and in the second run, strips of tantalum and tungsten were inserted inside the molybdenum capsules with the oxide. By virtue of the position of each capsule in the susceptor, it was possible to vary each capsule temperature. The oxides tested and their respective test temperatures are given in Table X.

Since the temperature of each capsule depended on its position in the susceptor, the capsule containing $4MgO\text{-}4BeO\text{-}Al_2O_3$ did not reach the mixture melting temperature. This oxide was retested in the second run (see Table).

In Run No. 1, the capsule which contained $2BeO\text{-}5Al_2O_3 \cdot 2TiO_2$ (M.P. 1960°K) leaked after six hours. This same mixture leaked from its heat of fusion capsule in that study. No evidence could be found in either case as to the cause of failure. The capsule walls were intact with no visible structural change and no sign of chemical reaction. In Run No. 2, $Al_2O_3 \cdot 3MgO \cdot 4TiO_2$ was contained for 274 hours with no sign of attack. However, tantalum was also exposed in this capsule and was completely dissolved. The resulting composition was therefore quite altered and, in turn, may have affected the apparent reactivity of the oxide mixture.

Table X

LONG TERM COMPATIBILITY TESTS

Material	Temperature (°K)	Time (hours)
Run 1		
$4MgO-4BeO-Al_2O_3$(*)	1720	500
$MgO-4BeO-Al_2O_3$	2030	500
$2BeO-5Al_2O_3-2TiO_2$	2050	6 (leaked)
$4MgO-5BeO-3ZrO_2$	2050	500
3BeO-2MgO	1970	500
Run 2 (**)		
$3MgO-B_2O_3$	1800	88 (leaked)
$3CaO-B_2O_3$	1800	88 (leaked)
$4MgO-4BeO-Al_2O_3$	1950	274 (leak noted)
$Al_2O_3-3MgO-4TiO_2$	1950	274
3BeO-2CaO	1870	274 (leaked)

(*) Did not melt
(**) Capsules contained Ta and W specimens

The results are therefore nonconclusive regarding the molybdenum compatibility of oxide mixtures containing titania (TiO_2). It should also be noted that the titania used was only 98 percent pure and the effects of various impurities might be quite serious. The limited nature of this compatibility study did not allow for continued or closure scrutiny of titania mixtures.

The two capsules containing B_2O_3 mixtures in Run 2 leaked after 88 hours. Although it was rather difficult to determine the exact mechanism of capsule failure, it was quite conclusive that attack was not catastrophic. Leaks could have resulted from poor weldments, not unusual in welded molybdenum bar stock. In some cases, the oxide apparently "sweated" through the capsule walls although this was not ascertained. Again, as in the case of the titania mixtures, no conclusive decision could be made regarding molybdenum compatibility with these two oxide mixture types.

The MgO-BeO mixture alone and in combination with Al_2O_3 or ZrO_2 survived at least 274 hours and up to 500 hours, respectively. These mixtures were of most interest (high heat of fusion values) and were observed more closely. Upon sectioning, the $MgO \cdot 4BeO \cdot Al_2O_3$ and $4MgO \cdot 5BeO \cdot 3ZrO_2$ capsules did not show any signs of gross attack. The first mixture and the capsule are shown in Figure 31 where the liquid level interface on the capsule wall is presented.

First of all, by observing the cross section of the wall, it can be noted that practically no erosion took place. The wall is about 100 mils thick. The crystalline metallic mass on the surface of the oxide ingot was identified as molybdenum. These metallic crystals are believed to be either (1) the result of a limited Mo solubility in which the Mo recrystallized from the oxide melt upon solidification, (2) the reaction and subsequent reduction of molybdenum with one or more of the impurities in the oxide, or (3) vaporization and condensation of Mo in oxide voids, or (4) some other phenomena which remains to be uncovered. The fairly large void space in the capsule may have enhanced any possible reactions which could have taken place and which had gaseous reaction products at these temperatures.

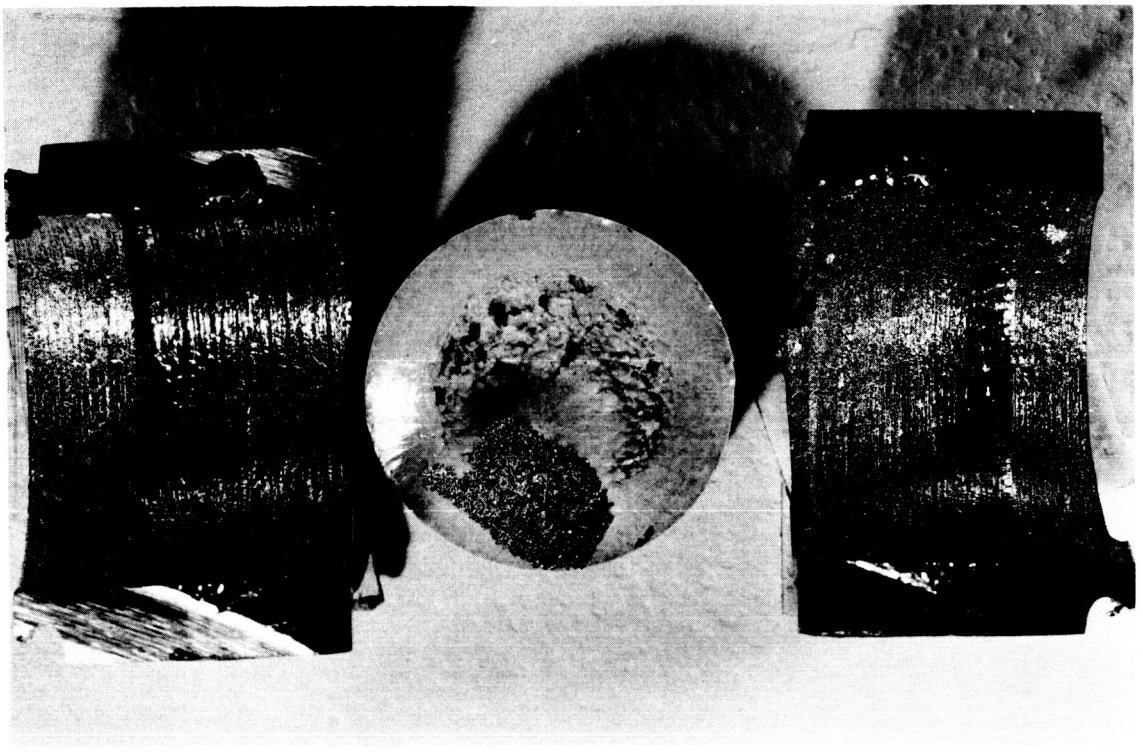

Figure 31. The $MgO \cdot 4BeO \cdot Al_2O_3$ Fused Button and the Contacting Surface of the Molybdenum Container After 500 Hours at 2030°K

The second MgO-BeO combination, $4MgO \cdot 5BeO \cdot 3ZrO_2$, (contained for 500 hours) had essentially the same compatibility characteristics as $MgO \cdot 4BeO \cdot Al_2O_3$. Figure 32 shows the oxide ingot cross sectioned axially. In this case, metallic crystals are shown to be dispersed throughout the oxide as well as on the surface. Reaction of some kind had evidently taken place; however, the mechanism is not known but might be postulated as being a result of reactions similar to those mentioned earlier. Further study of a more quantitative nature is required to fully understand the mechanisms involved.

A more aggravated result was found in the $3BeO \cdot 2MgO$ capsule although having similar identifying characteristics. In this particular case (Figure 33) one can see definite attack at the liquid level interface.

Note that definite etching occurred with a penetration of at least 25 to 50 mils. Some attack had also taken place below the liquid surface and can be noted in Figure 34. This view of the bottom of the ingot shows "bubbles" which have crystals of molybdenum deposited in them. Evidently, these crystals were formed from a vapor phase but the exact mechanism involved is not understood. It is possible that a molybdenum oxide (MoO_3 or lower oxide) could have been formed and gaseous reaction products formed the bubble. The molybdenum oxide was then continuously decomposed by magnesium vapor in the cooler portion of the bubble. For example, at hot interface,

$$xMgO_{vapor} + Mo \longrightarrow MoO_{x\,vapor} + xMg_{vapor}$$

At cooler face inside bubble,

$$MoO_{x\ vapor} + xMg_{vapor} \longrightarrow Mo_{solid} + xMgO$$

The vaporization rate of molybdenum alone would not account for the amount of metal found in the cavity nor would the cavity size, based on vapor pressure of molybdenum at $1970^{o}K$, be an indication of mechanism.

The other possible source producing this effect, of course, would be impurity in either the oxide mixture or container metal itself.

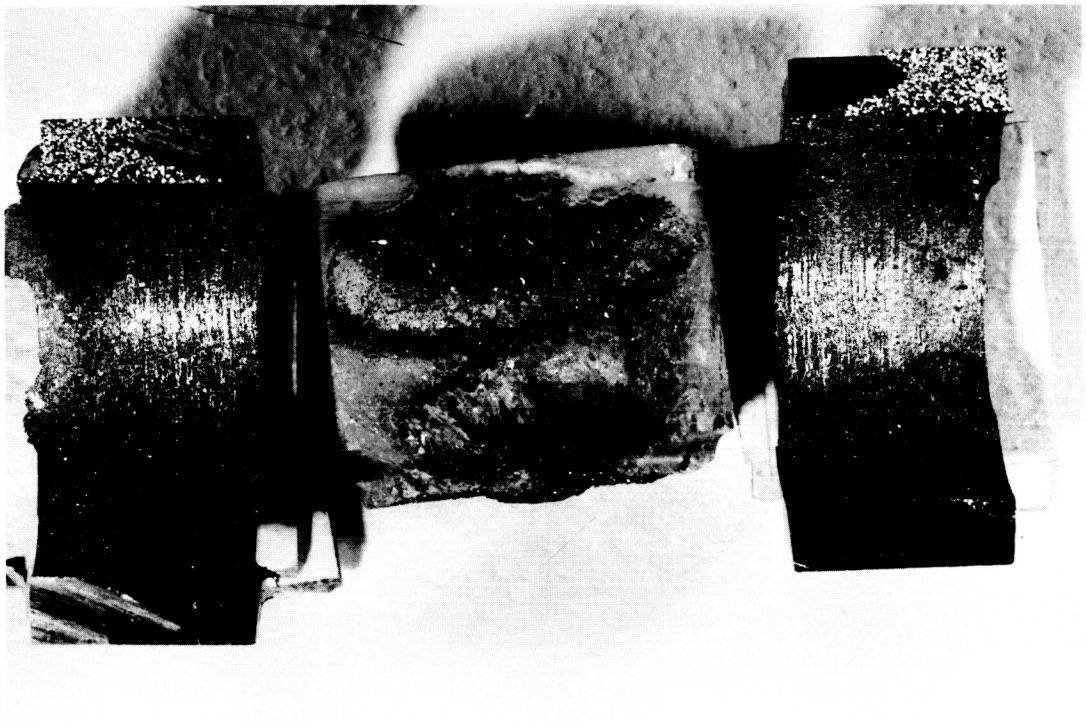

Figure 32. The Axial Cross-Section of the Fused $4MgO \cdot 5BeO \cdot 3ZrO_2$ Button and the Contacting Walls of the Molybdenum Container After 500 Hours at $2050^{\circ}K$

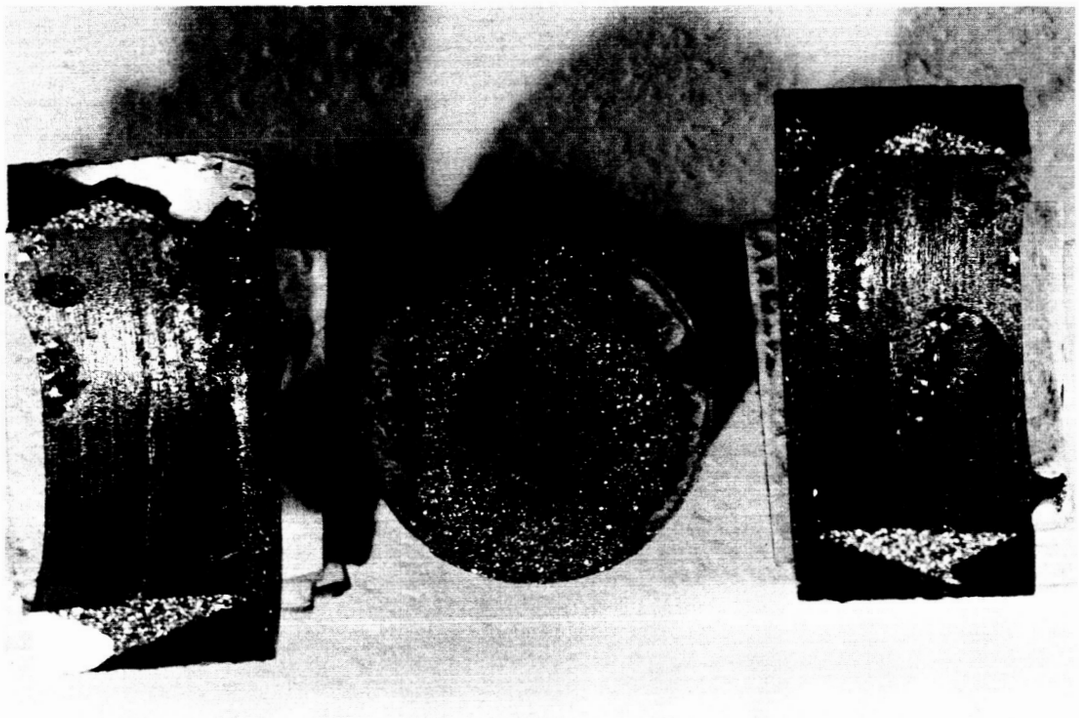

Figure 33. The Top Surface of the 3BeO· 2MgO Button and the Contacting Surfaces of the Molybdenum Container After 500 Hours at 1970°K

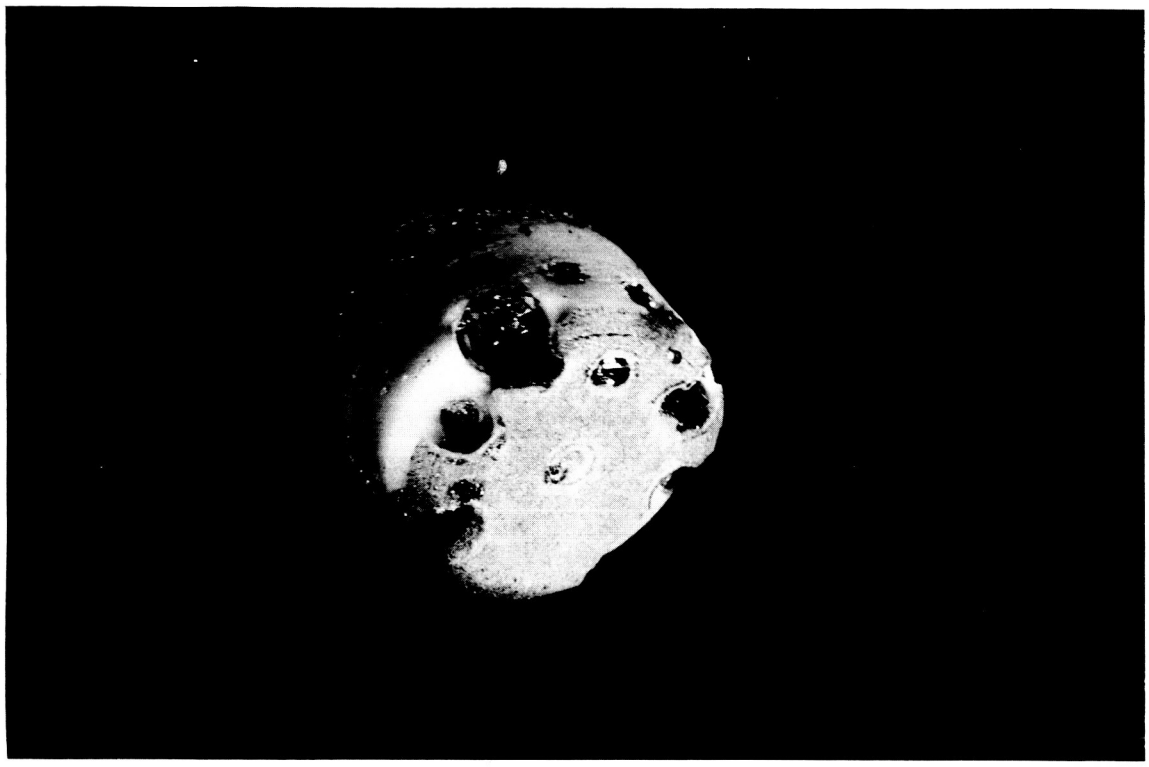

Figure 34. The Bottom of the 3BeO·2MgO Fused Button After 500 Hours at 1970°K

Since the capsules were sealed under vacuum, one might also postulate and comment on the effects of whether capsules were studied in an inert atmosphere (heat of fusion studies) or in vacuum. A bad capsule weld-closure might have different consequences during its exposure at high temperature in each of these situations.

In Run 2, it was possible to identify pinhole failure in the weld of the capsule containing the $4MgO \cdot 4BeO \cdot Al_2O_3$ material. It is apparent that the wetting characteristics and low surface tension of these materials permit them to flow readily through very small faults. It is very possible that such undetected faults existed in the other capsules in this series which failed and could account for failures. Generally, there was no evidence of serious attack of molybdenum.

In Run 2, all tungsten samples remained unaffected indicating an apparent compatibility equivalent or superior to that of molybdenum with these molten oxides. In the case of the tantalum, however, the results were less encouraging. In the two capsules containing borates as well as with $Al_2O_3 \cdot 3MgO \cdot 4TiO_2$, the tantalum had completely disappeared. In the remaining capsules, the tantalum was found to be seriously embrittled indicating oxygen pickup. It appears that in spite of the apparent thermodynamic suitability of tantalum, the oxygen solubility exerts sufficient influence on the general reaction with the molten oxides to make it unattractive as a container material.

Because of the obviously inhomogeneous distribution of molybdenum in the oxide samples after the long term compatibility tests, it was not possible to obtain meaningful results from chemical analysis. A detailed examination of the capsule walls again revealed no significant hardness changes indicating that no contamination of the molybdenum by the oxide components had taken place. Grain growth was, of course, extensive. This, however, would be expected solely from the long time at high temperature treatment of unalloyed molybdenum and is not believed to be related to the presence of molten oxide.

It will be noted that the impurity level of the titania employed is somewhat higher than in the remaining oxides. Consideration has been given to the possibility of corrosion being influenced by these impurities. It is apparent that the

oxides of the impurities present are stable with respect to molybdenum with the possible exception of the lead, strontium and antimony. These oxides are relatively unstable and would reasonably be expected to decompose and the metals volatilize off during the hot pressing operation.

The fact is that of all the oxides employed, only titania is capable of reverting to a lower oxide with the release of oxygen. This fact alone is sufficient to account for the more corrosive nature of the mixtures containing this material. It is believed that in future work the monoxide of titanium could be used to advantage in that this excess oxygen would be removed from the system prior to contact with any metallic container.

Needless to say, the corrosion studies made were of a qualitative nature and were not intended to solve compatibility problems except to point out potential problem areas. The tests have served this purpose admirably. One such problem area involves weldment of molybdenum capsules. The problem of encapsulation will be increased if tungsten has to be used. The use of alloys might also solve many fabrication problems and should be considered in future effort.

4.3 Summary

1. Several oxide systems, particularly those containing BeO and MgO offer congruently melting mixtures whose heats of fusion and melting points lie in the range of interest.

2. The molten oxides, in general, can be contained up to 500 hours in molybdenum and tungsten but not in Ta and Cb.

3. TiO_2-containing mixtures (consistently) appear to react with refractory metal container materials.

4. As a general rule, oxide mixtures of interest wet container metals readily, shrink slightly on freezing and do not require excessively high temperature to melt them initially. There is no sign of supercooling of oxide melts.

5. The oxide mixtures can be hot pressed to densities of the order of 90 to 95 percent of their theoretical density.

6. The data available on BeO-MgO based ternary systems are limited. Since this area is most promising, there is need for further exploratory investigations on the melting points of compounds or eutectics in these systems.

7. Although, in a few instances, containment of selected oxide mixtures with molybdenum and tungsten has been demonstrated up to 500 hours, there is need to expand this area of testing for longer times as well as to determine corrosion reactions and rates over these longer times.

5. DIRECTIVE SYSTEM STUDIES

5. DIRECTIVE SYSTEM STUDIES

5.1 Introduction

A preliminary limited directive system study has been undertaken. The objective was to investigate various design approaches for thermionic-thermal energy storage (TES) systems and to determine the influence of material properties such as heats of fusion, density, thermal conductivities, heat capacities, etc. on orbiting vehicle power supply designs. The immediate advantages of mating thermal storage to thermionic converters are twofold. First, it eliminates alternate energy storage systems such as fuel cells or batteries and, secondly, it should eliminate deleterious effects of temperature cycling on converter life. Without thermal energy storage, the converters would cycle from operating temperatures to some point well below operating temperatures depending upon the heat lost from the cavity during the dark phase. This temperature drop would have to be overcome as the system re-entered sunlight in its orbit. The use of thermal energy storage would necessarily minimize this temperature cycling.

Because of a scarcity of physical property and life data, it would be difficult to presently design an optimized system. However, a few simple configurations have been analyzed using the modular concept of separate containers for each converter. Collector-absorber and converter systems have been studied quite extensively in other programs. Converter efficiencies have been shown to increase with increasing cathode temperature (to a limit). However, converter life and collector-absorber efficiency decrease with increasing temperature. A prime requirement, therefore, is that the temperature gradient from the absorber wall through to the cathode surface be as small as possible at the highest tolerable cathode temperature.

This study describes an approximate method for calculating the performance of a solar thermionic electric power system with attendant thermal storage. Estimates of specific weight have been made using this method and conservative

assumptions of efficiency and weight. Specific system weights of 75 pounds per kilowatt at high cathode temperatures appear possible for an earth orbit of 35 minutes dark, 55 minutes light, including the weights of collector, support structure, generator, thermal storage container and thermal storage material. No weight has been included for orientation. The specific system weights calculated compare very favorably to anticipated weights of 256 pounds per kilowatt for future (possibly optimistic) photovoltaic and battery power supply systems.

Figures 35 and 36 show curves of converter efficiency and collector-absorber efficiency as functions of cathode temperatures. Figure 37 is a curve of system efficiency versus temperature drop between the absorber wall and cathode surface. It is significant to note that temperature gradients of the order of 300 to 400^{o}C result in an overall system performance decrease of only 10 percent for a fixed cathode temperature. However, from a materials consideration, an upper temperature limitation is placed on the absorber wall.

The thermal gradient might be minimized two ways:

a. Geometrically design the thermal storage container for a minimum length in the direction of heat flux.
b. Select thermal storage materials that have high thermal conductivities, heats of fusion, and density.

Systems A, B, and C of Figure 38 illustrate three configurations studied. Analysis of each configurations leads to the following equations for temperature drop from the absorber wall to the cathode surface:

System A

$$\Delta T = \frac{P_d}{\eta} \left\{ \left[1 + \frac{t_d}{t_1} \right] \left[\frac{t}{k} + \frac{P_d t_d}{\eta H_f \rho k_s} \right] + \frac{t}{k} \right\} \qquad (1)$$

System B

$$\Delta T = \frac{P_d}{\eta \alpha_1} \left\{ \left[1 + \frac{t_d}{t_1} \right] \left[\frac{t}{k} + \frac{3 P_d t_d}{\eta H_f \rho k_s (\alpha_1 + \alpha_1^{1/2} + 1)} \right] + \frac{t \alpha_1}{k} \right\} \qquad (2)$$

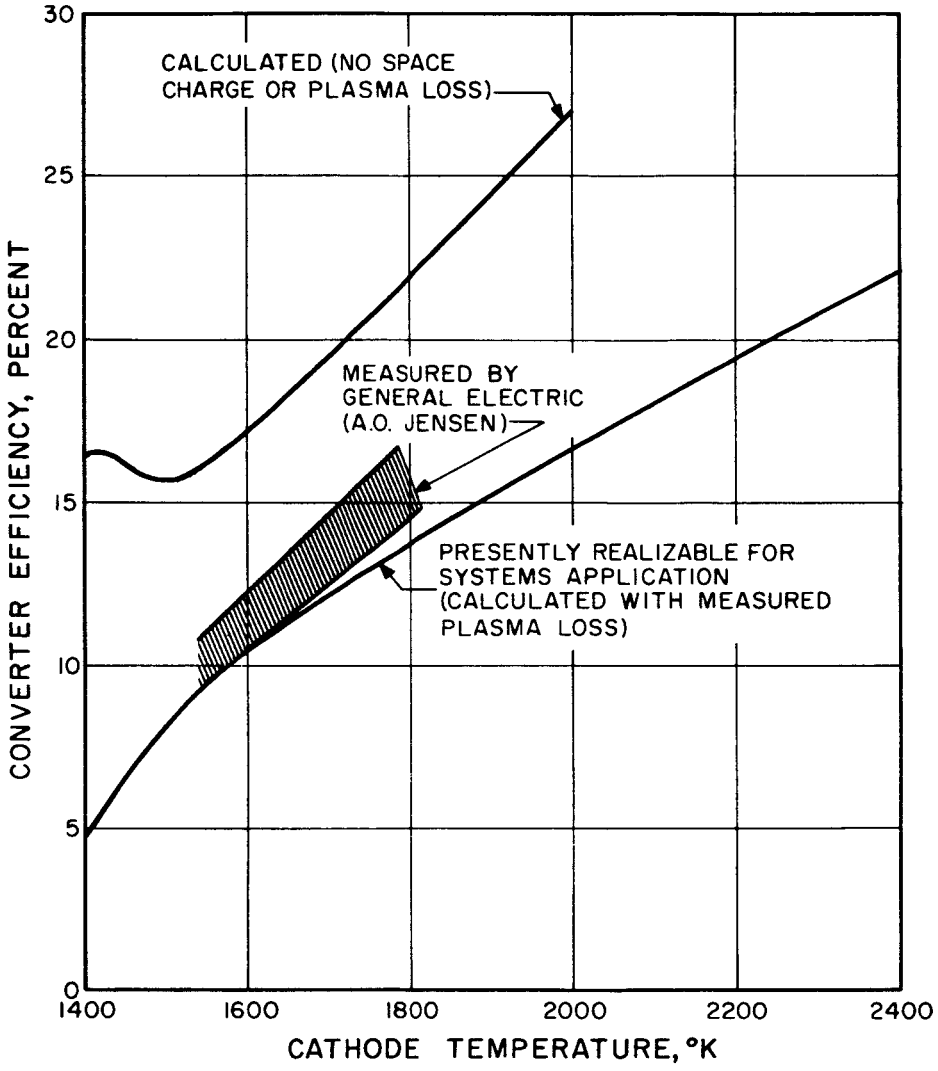
CALCULATED (NO SPACE CHARGE OR PLASMA LOSS)
MEASURED BY GENERAL ELECTRIC (A.O. JENSEN)
PRESENTLY REALIZABLE FOR SYSTEMS APPLICATION (CALCULATED WITH MEASURED PLASMA LOSS)
CONVERTER EFFICIENCY, PERCENT
CATHODE TEMPERATURE, °K
0
5
10
15
20
25
30
1400
1600
1800
2000
2200
2400

Figure 35

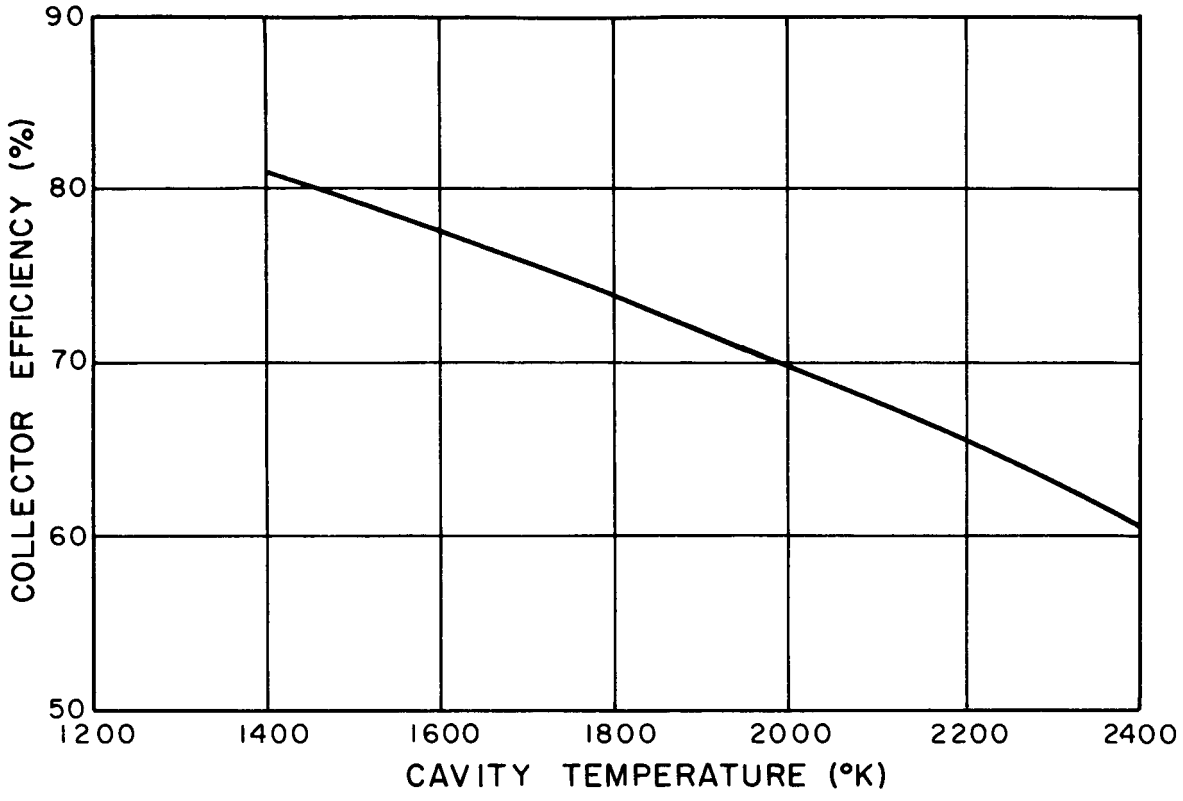

Figure 36. Collector-Absorber Efficiency Versus Absorber Cavity Temperature, ^{o}K

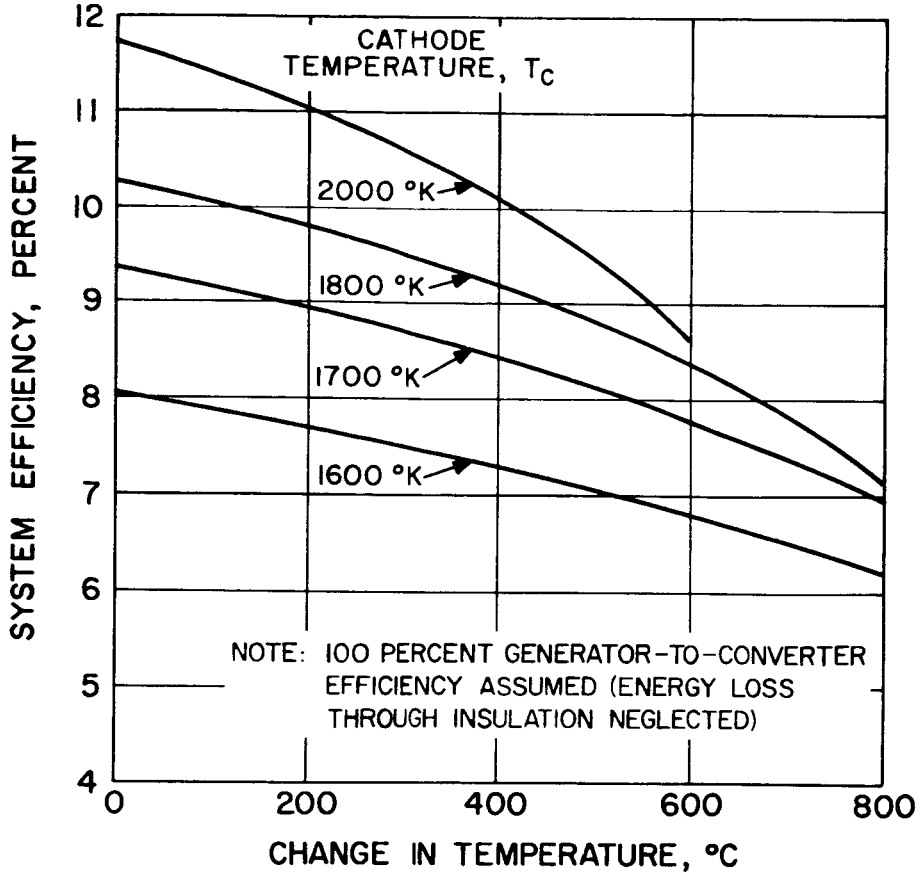

Figure 37. System Efficiency Versus Temperature Drop Between Absorber Wall and Cathode

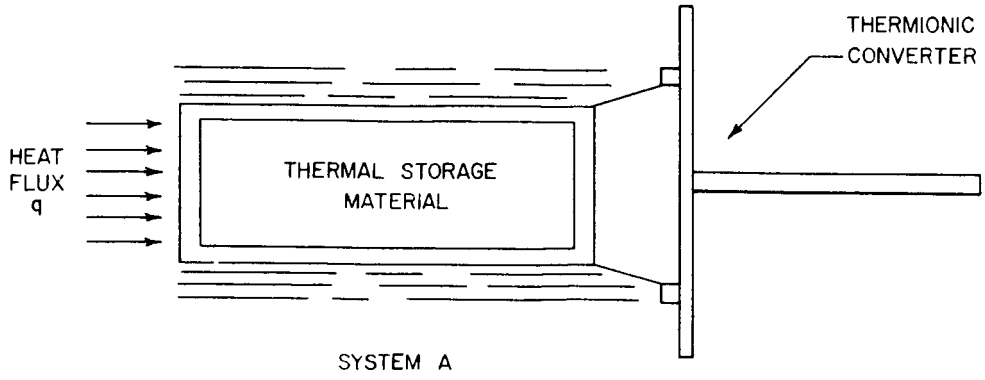

SYSTEM A

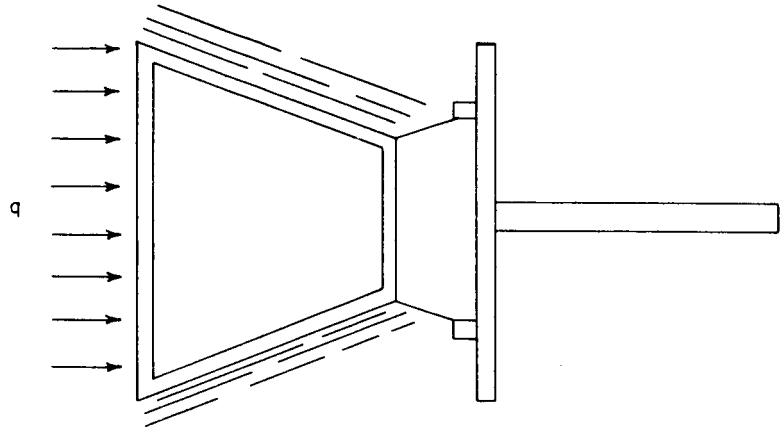

SYSTEM B

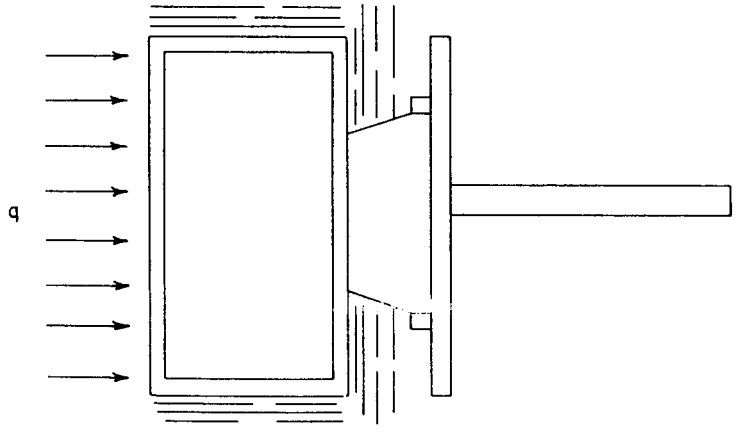

SYSTEM C

Figure 38. Three Geometries Used to Evaluate Thermal Gradients in Converter-TES Unit

System C

$$\Delta T = \frac{P_d}{\eta \alpha_1} \left\{ \left[1 + \frac{t_d}{t_1} \right] \left[\frac{t}{k} + \frac{P_d t_d}{\eta \alpha_1 H_f \rho k_s} \right] + \frac{t}{k} \right\} \qquad (3)$$

where

P_d = converter output power density, electrical watts per sq cm

η = converter efficiency

t_d = dark time portion of orbit, hours

t_1 = light time portion of orbit, hours

t = container wall thickness, cm

k = container thermal conductivity, watt-cm per cm^2-^oC

α_1 = ratio of absorber surface area to cathode surface area

H_f = heat of fusion of TES material, watt-hr per lb

ρ = density of TES material, lb per cm^3

k_s = thermal conductivity of solid TES material, watt-cm per cm^2-^oC

T_c = converter cathode temperature, ^oK.

The above equations represent that point in the satellite orbit where the satellite is just leaving the dark portion and is entering sunlight.

It is assumed that:

a. The TES container is ideally insulated except for areas of heat flux transfer.

b. The contact resistances between the TES material and container inner walls and cathode to container wall were assumed zero. This effect is small in relation to the other temperature drops in the binary eutectic-refractory metal systems, but may be of significant value in systems where the TES material does not wet the container, e.g., silicon and BN.

From Equations (1), (2), and (3) the parameters which have most affect on temperature drop and feasibility of thermal storage systems are:

a. $H_f k_s \rho$ = Product of heat of fusion, density and thermal conductivity

b. t/k = Container wall thickness/Container thermal conductivity

c. P_d/η = Converter electrical power output density/Converter efficiency

d. α_1 = Area of absorber surfaces/Area of cathode surface

e. t_d/t_1 = Dark-time portion of orbit/Light-time portion of orbit

A most critical parameter is a. above. This term should be as large as possible. For System A, assuming an allowable ΔT of $50^{o}C$, the parameter $H_f \rho k_s$ should equal approximately 4 watts^2-hour/cm^4-^{o}C. The anticipated values of $H_f \rho k_s$ for thermal storage materials are uncertain, but are expected to be in the range of 0.2 to 1. Therefore it is concluded that area ratio configurations and/or better thermal conductivity will be required to minimize ΔT. For example, the t/k parameter (b. above) should be as small as possible. Values ranging from 0.06 to 25 could exist. Using typical values representing best estimates of physical property data as shown in Table XI, sample calculation of temperature drops for configurations A, B, and C were made and are tabulated in Table XII. Systems B and C typify generator configurations as now envisioned where absorber area is made equal to fin area required to radiate heat flux passing through the converter at a fixed temperature.

It can be seen from Table XII that, for a silicon-PG system, t/k accounts for 95 percent of the temperature drop, or approximately $200^{o}C$. Note that these results (Table XII) are based on simple geometries and conservative material parameters mainly for orientation purposes. It is obvious that much more data need to be obtained, but these calculations do indicate that a wide variety of successful solutions do exist.

A series of systems parameters and their effects are discussed in the following sections along with system operational theories and derivations of equations used to calculate specific system weights.

TABLE XI. PHYSICAL PROPERTY DATA

Material Properties - Estimated						
Parameter	Unit	Silicon	CaO:BeO	BN	PG	Molybdenum
H_f	watts	207	175			
ρ	pounds/cm^3	5.13×10^{-3}	7.72×10^{-3}			
k	watts/cm ^{o}C	0.8	0.117	0.25	0.01	1
t	cm			0.254	0.254	0.0635

Converter Characteristics

T_c	$P_{d/\eta}$	α_1
1400	14.2	5.2
1600	21.5	7.4
1700	27.0	9.0
1800	34.5	11.2
2000	55.0	17.0

NOTE: The thermal conductivities of pyrolytic graphite and BN are directionally oriented and the values used above represent the lower values. In the case of the PG the k value is better by a factor of 10 along the planes, and in BN, k improves by a factor of two.

TABLE XII. TEMPERATURE DROPS FOR VARIOUS MATERIALS AND SYSTEMS

System	T_c(° K)	TES Material	Container Material	T_{cw}	T_m	T_t
A	1400	CaO. BeO	Molybdenum	2.3	1220	1222
B	1700	CaO. BeO	Molybdenum	2.0	110	112
C	1700	CaO. BeO	Molybdenum	1.0	53	54
B	1700	Silicon	BN	32.0 **	21	53
C	1700	Silicon	BN	8.0 **	10	18
C	1700	Silicon	PG	198 **	10	208

NOTE: T_{cw}= $T_{container\ wall}$ T_m=$T_{material}$ T_t=T_{total}

* 300 mile circular orbit.

** Using lower k factors where heat flux is perpendicular to the crystal or pressing planes.

5.2 Discussion of Equations and Derivations

5.2.1 Cavity Temperature Increase Effect

At the instant the solar thermionic power system emerges from the earth's shadow, the freezing interface will have arrived at the thermal storage container wall opposite the converter cathode. As solar energy impinges on this absorber wall, energy will be needed to begin melting thermal storage material and energy must also be supplied to the cathode from the melting interface as the satellite continues on its orbit through the sunlight. As sufficient energy is supplied, the melting interface will eventually advance to the cathode and should arrive just as the satellite leaves sunlight. At this instant, the temperature at the energy-absorbing surface will have reached a maximum to drive energy through the thermal storage material to melt the interface material as well as supply sufficient energy to the converter. The total amount of energy required will determine the cavity temperature reached (maximum) as the solar powered system goes into the dark. For the calculations here, the cavity temperature was assumed to be at this maximum temperature continuously which is a conservative assumption. The equation which expresses this maximum temperature is as follows:

$$\Delta T = T_a - T_m = \left(\frac{P_d}{\eta\alpha}\right)^2 \left(\frac{t_d}{H_f \rho k}\right) \left(\frac{td}{t_1} + 1\right) \left(\frac{\eta_{conv}}{\eta_{gen}}\right)^2 \qquad (4)$$

It is evident that the ΔT is a linear positive function of the $H_f \rho K$ product. This equation derivation stems from Equations (1), (2) and (3) but also includes the generator efficiency.

5.2.2 Cathode Temperature Decrease Effect

As the satellite goes into the shadow the freezing interface will begin to move toward the absorber wall. A thermal gradient will exist from the moving freezing interface to the cathode, and (when the satellite has completed the dark portion of its orbit) the temperature at the cathode will have decreased

a certain amount below the thermal storage material melting point. This degradation of the cathode temperature causes the generator efficiency to decrease because of lower converter efficiency at lower temperatures.

The equation which expresses this cathode temperature drop can be expressed as follows:

$$\Delta T = T_m - T_c = \left(\frac{P_d}{\eta \alpha}\right)^2 \left(\frac{t_d}{H_f \rho k}\right)\left(\frac{\eta_{conv}}{\eta_{gen}}\right)^2 \quad (5)$$

The importance of $H_f \rho K$ product is again evident since it sets ΔT between cathode and absorber wall. For analysis, the cathode temperature (T_c) was assumed to be at this lower temperature through the entire cycle. This, of course, is also a pessimistic assumption because the cathode temperature will actually cycle between the TES material melting point and this lower temperature.

5.2.3 Calculation of the Collector Specific Weight

The collector specific weight was assumed to be 0.3 of a pound per square foot and it is expressed by the equation:

$$S.W._{coll.} = \left(lb/ft^2/\eta_s q_s\right)\left(\frac{t_l + t_d}{t_e}\right)(1000) \quad (6)$$

where N_s is system efficiency and

9_s is solar flux intensity and

t_e is

It is evident that specific weight of the collector is a function of solar intensity and system efficiency. With increasing system efficiency, specific weight of the collector becomes correspondingly lower. System efficiency and specific weight will also depend on the orbit but this parameter is set at 90 minutes (55 min. light, 35 min. dark) in this analysis.

5.2.4 Generator Specific Weight

The generator specific weight is computed by using the following equation:

$$\frac{\text{lb/cm}^2 \text{ of converter}}{P_d \text{ in watts/cm}^2} \times \frac{1000 \text{ watts}}{\text{K.W.}} = \frac{166}{P_d} \tag{7}$$

This specific weight was calculated by totaling all the weights of a 5 sided cube generator proposed for a Mariner B application. The weight of a square centimeter of converter structure had been calculated from known converters available. The generator specific weight is inversely proportional to the power density passing through a square centimeter of cathode. This assumption is felt to be conservative since the converter assumed for the above proposal was a production converter which was not optimized on a specific weight basis and had an extremely heavy anode slug to allow better cooling of the anode structure.

5.2.5 Thermal Storage Specific Weight

The specific weight of the thermal storage material is computed using the following equation:

$$\text{S.W.}_{\text{T.S.}} = \frac{t_d}{\eta_g H_f} \tag{8}$$

It is evident that dark cycle time is very important, since this sets the weight of TES material required. The specific weight of TES is inversely proportional to generator efficiency (M_g) and heat of fusion product.

5.2.6 Generator Support Structure

The collector structure and generator support weight is assumed to be a certain percentage of the collector specific weight and is based on the weight calculated for the Mariner B application which assumed beryllium support arms, doubling as electrical leads and a 5 foot diameter collector.

The equation is:

$$\text{S.W.}_{\text{structure}} = 0.28 \, (\text{S.W.}_{\text{collector}}) \tag{9}$$

5.2.7 Thermal Storage Container Weight

The thermal storage container weight was assumed to be a certain fraction of the specific weight of the thermal storage material and is equal to the following equation:

$$S.W._{T.S.\ Container} = 0.24\ (S.W._{T.S.})$$

The numbers in the equation were determined by assuming that the thermal storage material could be contained by a 20-mil wall of molybdenum. This assumption may be somewhat optimistic since life versus wall thickness is still uncertain.

5.3 Discussion of Results

In order to obtain generator efficiency as a function of thermal storage melting temperature, generator efficiency as a function of cathode temperature is required. This is shown as the upper curve in Figure 39. At each cathode temperature a certain thermal thru-put energy is required and if the $H_f \rho K$ product is known, the resultant ΔT through the TES material can be obtained from equation (5). Thus the thermal storage melting temperature and generator efficiency can be related and curves prepared for various $H_f \rho K$ products. These are illustrated in Figure 39 and Figure 40. The $H_f \rho$ K products were those calculated (with K assumptions) for the materials listed in Table VIII (p. 69). It is quite evident that the best material is the binary eutectic 3BeO·2MgO since its $H_f \rho$ K product is large thereby resulting in a small ΔT and preventing generator efficiency degradation.

From the plot of solar collector efficiency versus cavity temperature (Figure 36, page 91) the cavity temperature ΔT increase as a function of melting point an $H_f \rho K$ product can be obtained. This value multiplied by the generator efficiency taken from figures 39 or 40 give system efficiency as a function of melting temperature and $H_f \rho K$ product. These curves are shown in Figure 41 and 42. Again beryllia-magnesia binary material appears to be superior. The upper curve shows the effect of no $\Delta T (H_f \rho K = \infty)$, and is the theoretical maximum efficiency which could be attained with a system if no temperature degradation effects occur.

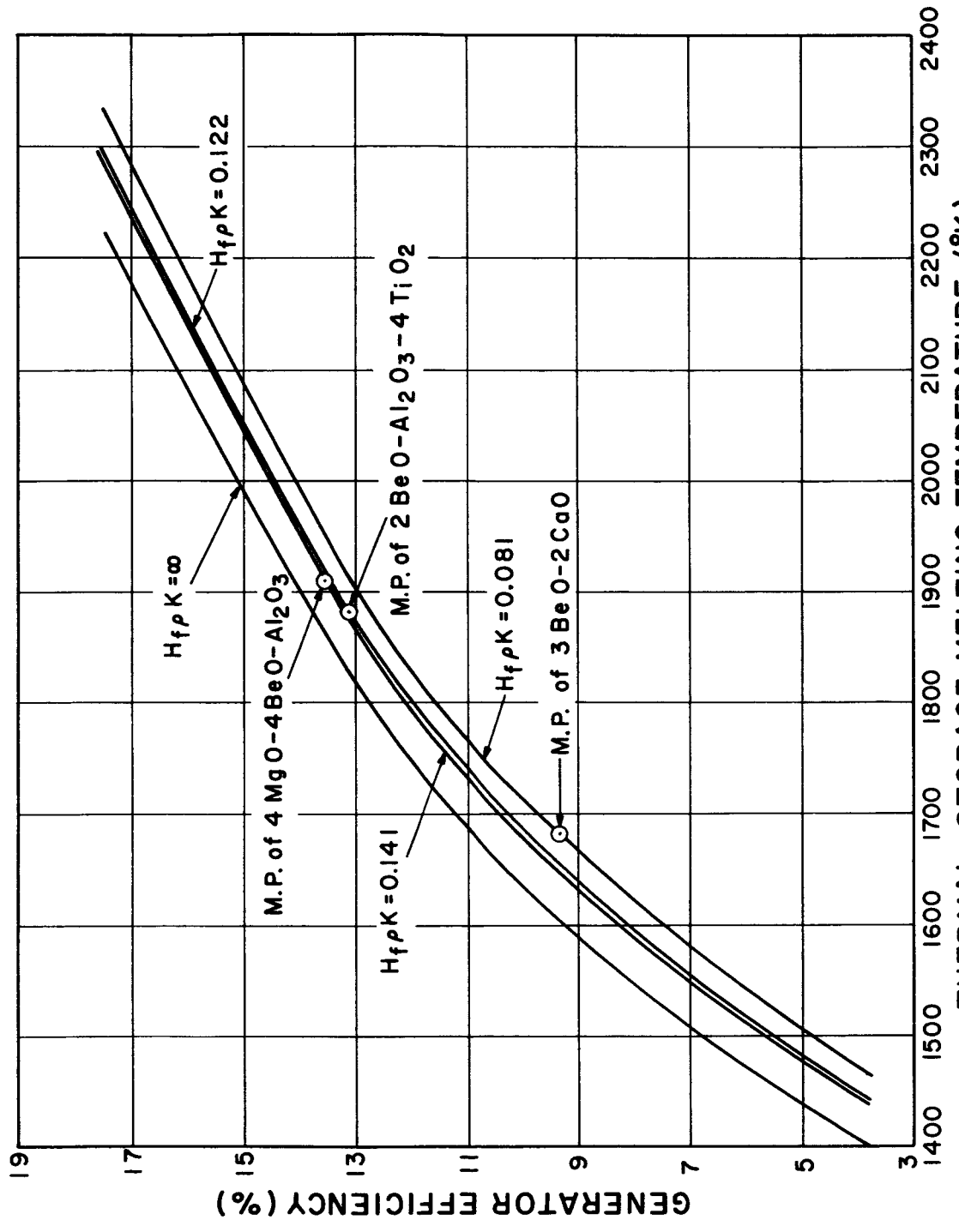

Figure 39. Generator Efficiency vs. Melting Temperature of Thermal Storage Material

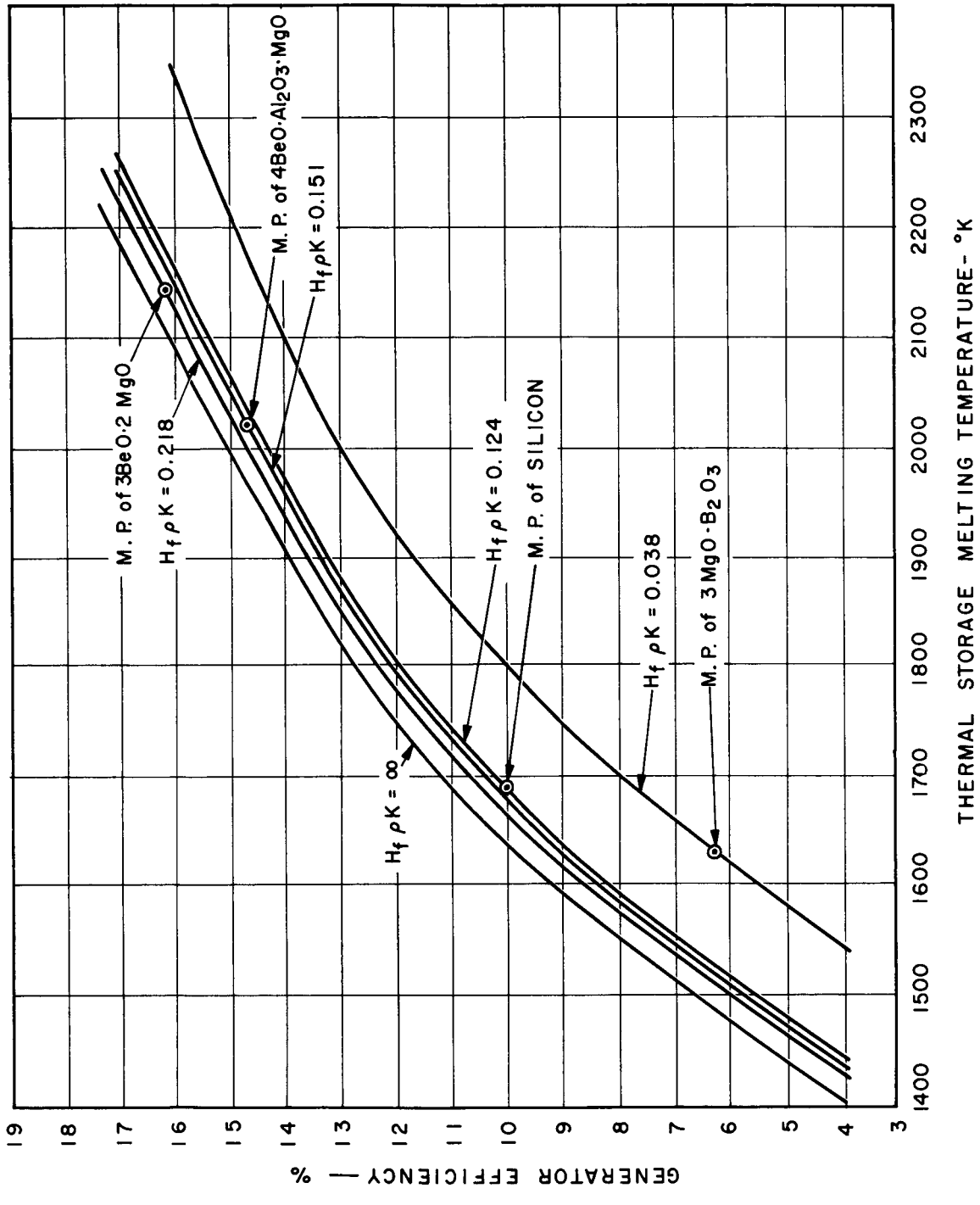

Figure 40. Generator Efficiency vs. Melting Temperature of Thermal Storage Material

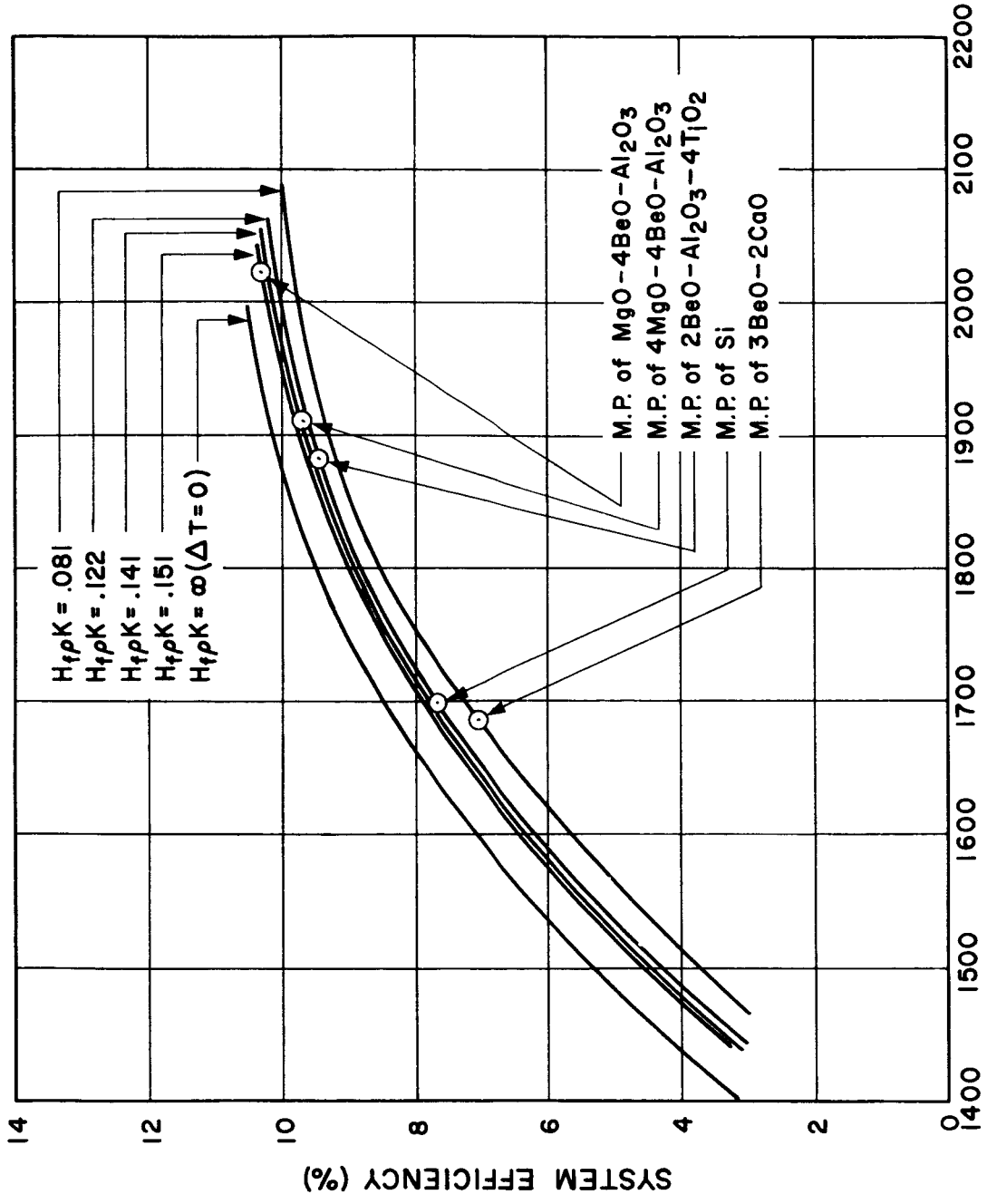

Figure 41. System Efficiency vs. Thermal Storage Melting Temperature

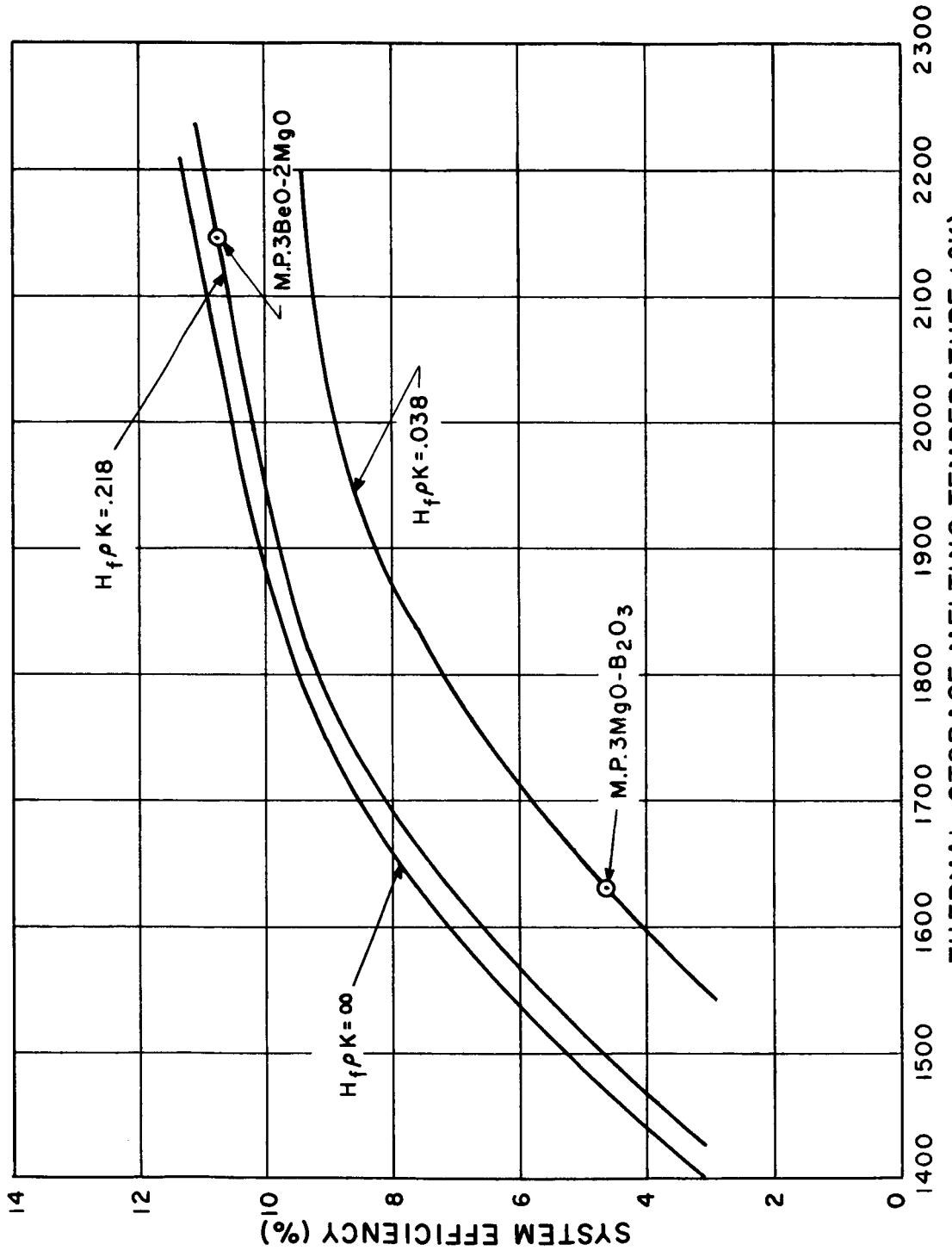

Figure 42. System Efficiency vs. Thermal Storage Material Melting Temperature

In Figure 43, collector and generator support structure as a function of system efficiency is plotted along with system efficiencies which were obtained from Figures 41 and 42 for the various oxide mixtures. This defines collector and generator support structure specific weights for the various oxide mixtures considered.

To obtain the generator and thermal storage specific weight equations (7) and (8) above were used. The plot of the generator specific weight is shown as a function of generator efficiency in Figure 44. This generator specific weight would be that which would be obtained independent of thermal storage. The thermal storage material specific weight is a function of the generator efficiency and heat of fusion and these are also shown plotted in Figure 44. The generator specific weight plus thermal storage material specific weight can be obtained from this graph for the various oxides. The total system specific weight can be attained by summing all of the component specific weights; shown in Figure 45 and 46.

The system specific weights versus the thermal storage melting point are shown in Figure 45. Since specific weight is a function of $H_f \rho K$ product, thermal storage melting point, generator efficiency, collector efficiency and heat of fusion, all of these variables will tend to cause a scattering of the data. However, it is quite evident that effects of increased heats of fusion and increased melting temperature have improved the system considerably. The lightest system being that with the highest melting point but here, of course, also the one with the highest heat of fusion. In Figure 46 in which the total system weight is plotted as function of the heat of fusion, this effect is again illustrated. The heat of fusion and melting point of beryllia-magnesia-binary is highest, therefore providing the lowest specific system weight of all materials used in these calculations.

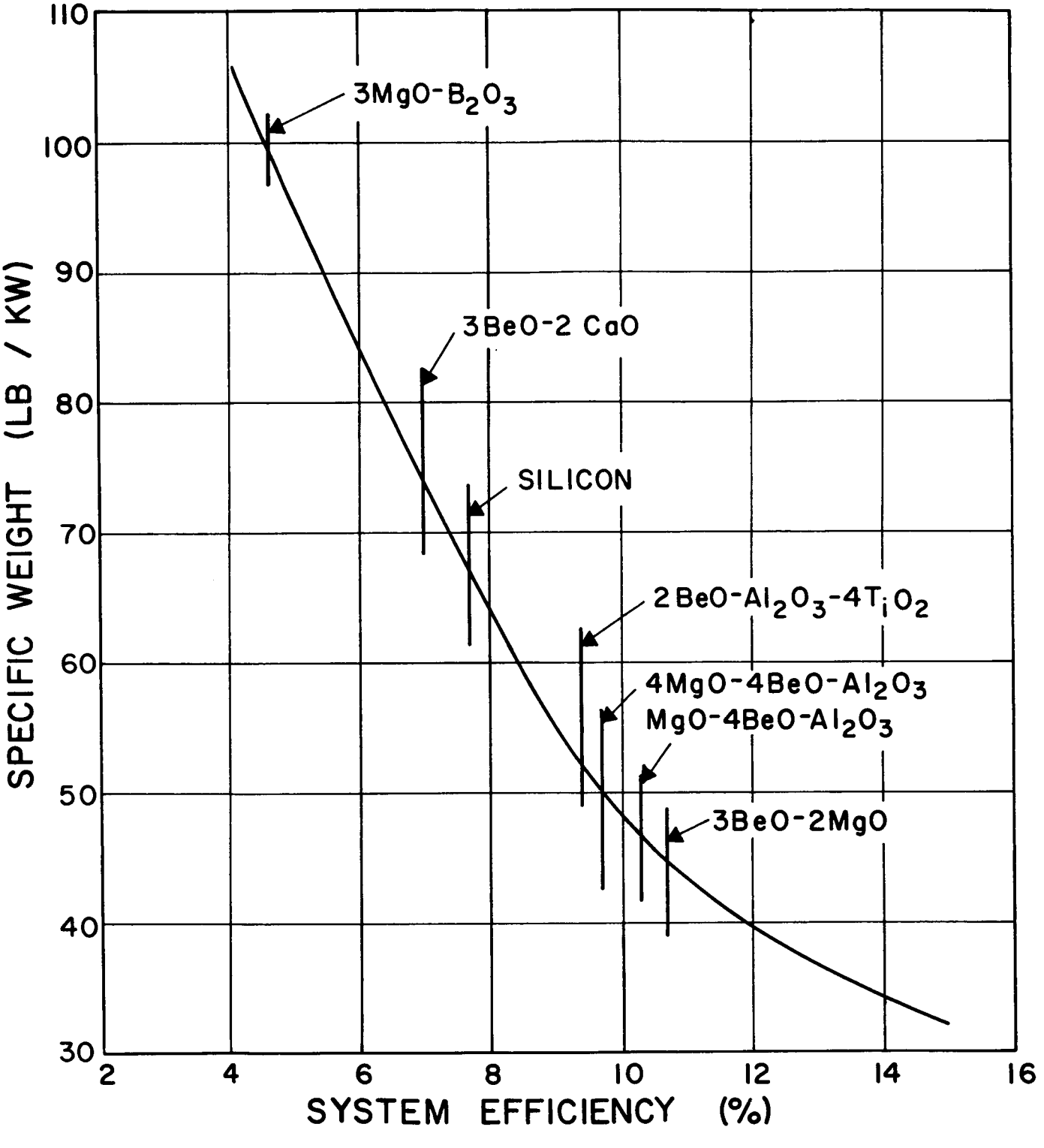

Figure 43. Collector and Generator Support Structure Specific Weight vs. System Efficiency

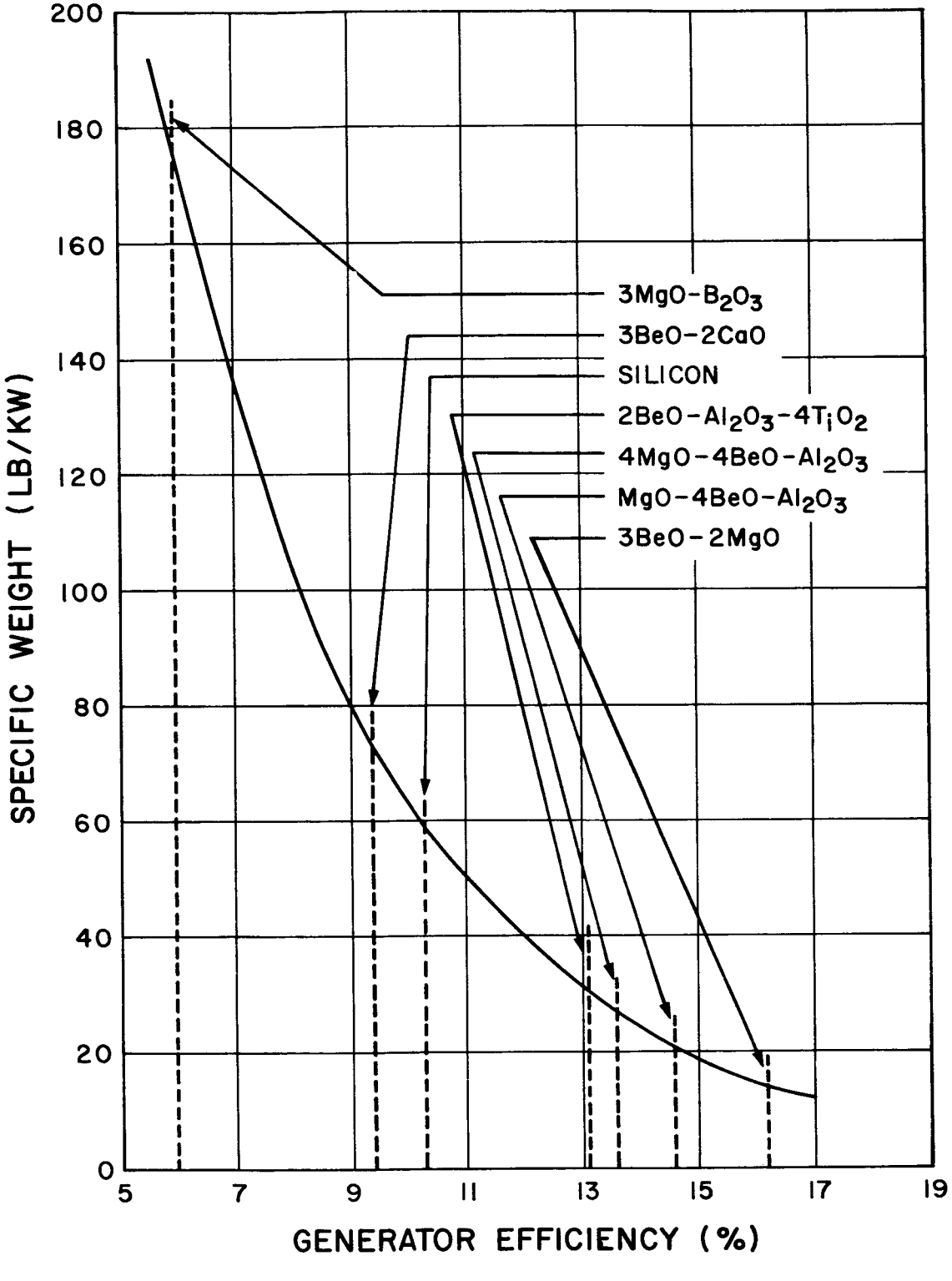

Figure 44. Thermal Storage Material and Generator Specific Weight vs. Generator Efficiency

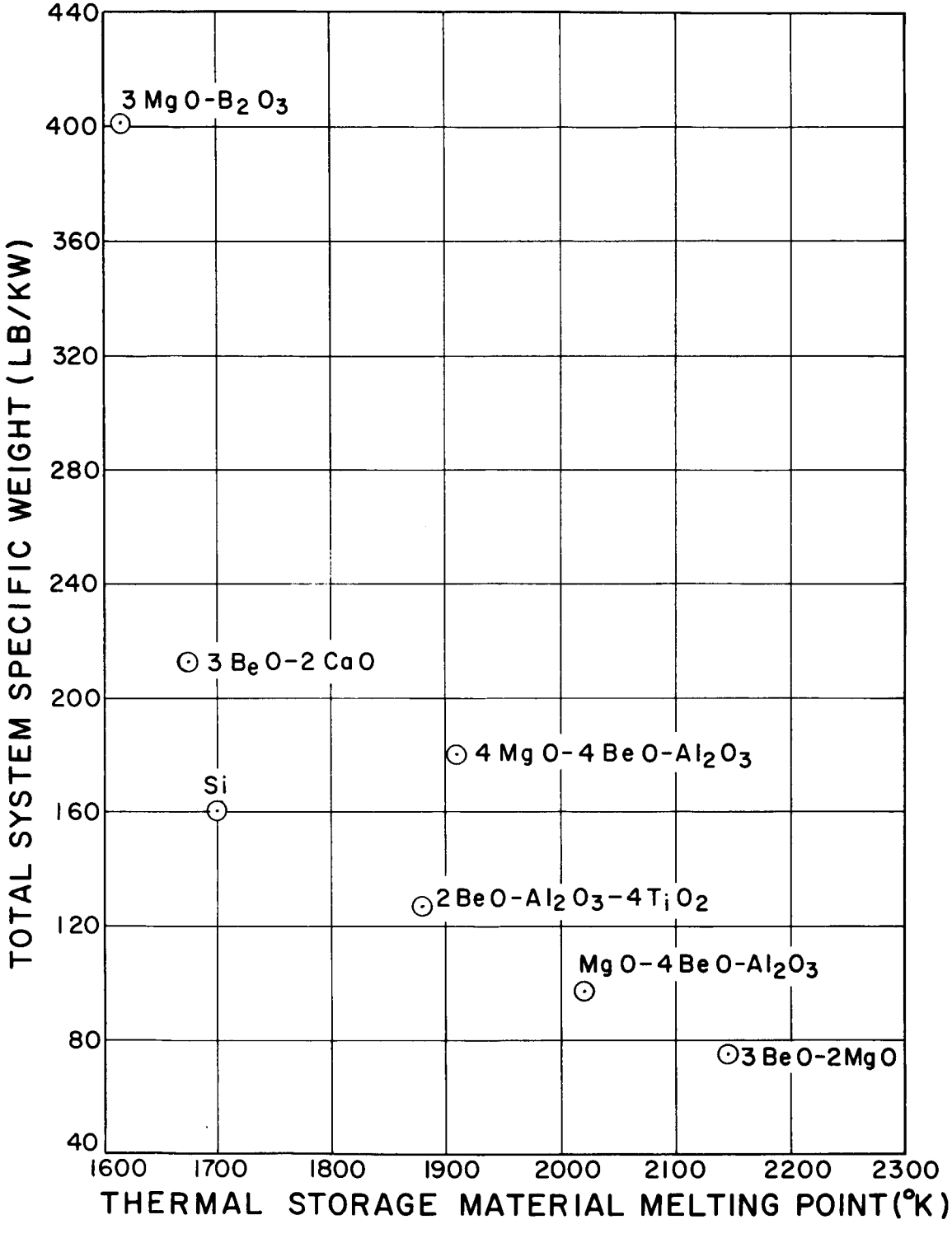

Figure 45. System Specific Weight vs. Thermal Storage Material Melting Point

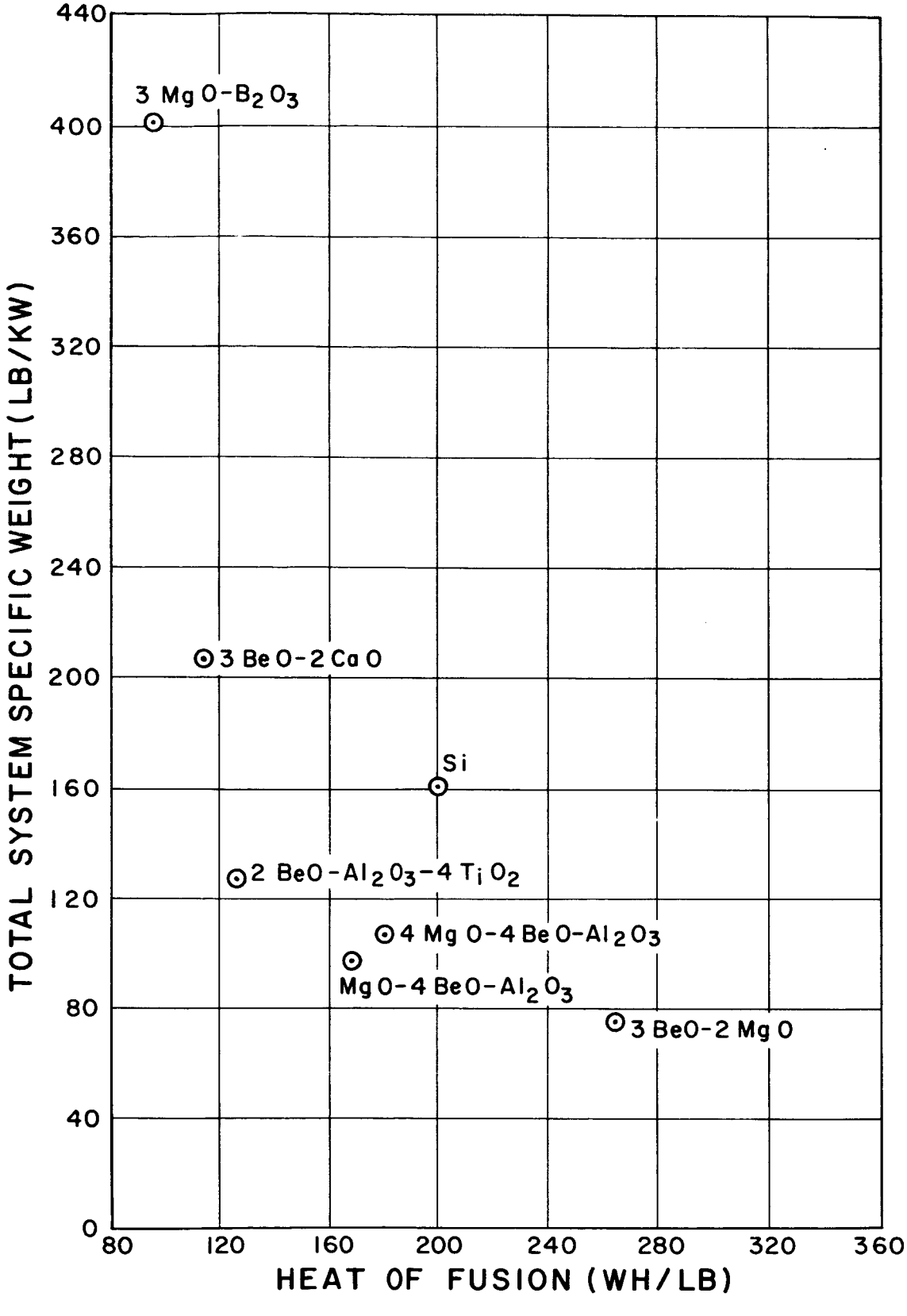

Figure 46. System Specific Weight vs. Thermal Storage Material Heat of Fusion

To compare thermionic conversion systems on a specific weight basis with a photovoltaic converter system, D. L. Kerr, General Electric Company, MSVD, calculated the specific weight of photovoltaic systems based on the following assumptions:

1. Paddle structure - 0.3 lb per square foot.
   Weight of cells, bond, glass, and wire - 0.45 lb per square foot.
   Total solar cell array weight - 139.3 lb.
2. Battery weight - 58.3 lb and battery capacity of 10 watt hours per lb.
3. Cell area per array area - 0.83.
4. Taper charge.
5. Development of rechargeable silver cadmium or silver zinc batteries.
6. The secondary fuel cell remotely possible.
7. Charge control - 49 lb per kilowatt.
8. 35 - minute dark, 65 - minute light cycle.
9. Total system of 256 lb per kilowatt.

If a charge control (of 59 lb) is necessary for the solar thermionic system, the comparable photovoltaic system specific weight would be item 9 minus item 7 or 197 lb per kilowatt. The comparative solar thermionic specific weight is 75 lb per kilowatt. (At present, using essentially current state of the art photovoltaic systems, the specific weight would be 857 lb per kilowatt.)

6. DISCUSSION OF OVERALL TEST RESULTS AND CONCLUSIONS

6. DISCUSSION OF OVERALL TEST RESULTS AND CONCLUSIONS

From a systems standpoint in this particular application, the most important parameters are reliable life and best efficiency. Life on the order of one year will probably be a requirement in this case, and required operating temperatures immediately impose a materials restriction of major proportions. Because of this restriction, the refractory metals and their alloys are the only metals which could be used and so-called ceramic materials represent the second choice. The available technology in these materials classes is scarce and is especially limited for use in a vacuum environment.

From the experimental effort reported, it is apparent that materials have been uncovered which have potential application as high temperature thermal energy storage media. The ceramic oxide mixtures studied meet most of the specific requirements for applied use in solar thermionic electrical power systems. The oxide TES materials have useful heats of fusion and high densities. They are compatible to an attractive degree with the same metals used in converter fabrication. These oxides also have good wetting characteristics and apparently do not have large density change on passing through the liquid-solid phase. They also exhibit sharp, congruent melting points and show no signs of super-cooling. The oxides would also have negligible vapor pressure over a wide temperature range.

Although the enumerated advantages are somewhat imposing, there are several disadvantages of these materials. First, in all likelihood these oxide mixtures will have rather low thermal conductivities at temperatures immediately above and below the melting points. Poor thermal conductance implies undesirable thermal flux impedances which will produce large temperature gradients. Essentially, the problem then becomes one of knowing or learning how to extract stored energy efficiently and how to utilize the heat available from liquid-solid phase change.

Another problem area (a direct result of large temperature gradients) will be long-time (order of months and years) compatibility with container materials.

Signs of reaction at temperatures in the 2000°K area have been noted and one might expect limited life. The exact causes of some of these reactions have not been fully evaluated in this effort, but one might expect that, at these high temperatures, reaction rates could be grossly affected with small increases in temperature. For example, molybdenum vapor pressure begins to be of concern at 2000°K (10^{-6} mmHg) and higher. The effects of materials impurities are unknown and would most certainly be another factor to consider.

Another potential problem area, which has only been touched on, involves the no-gravity situation in space. This problem might best be relegated to some future study under actual conditions; however, it should be expected that wetting, viscosity, and surface tension will determine the extent of no-gravity effects on the overall thermal storage principle.

The use of silicon as a thermal storage medium has attractive advantages from the stand-point of thermal properties of silicon itself. The container materials in this case, however, do pose additional problems in compatibility, fabrication, sealing, and joining. These latter problems are not believed to be insurmountable, but there might be a detrimental amount of development work required for the application considered.

One very important factor which also precludes the use of silicon for thermal storage is the restriction to a single operating temperature. With this inflexible restriction to the lower end of the operating range of present-day thermionic converters, it is suggested that all follow-on effort should be concentrated on the oxides or other materials offering a spectrum of operating temperatures.

As an aside, the particular silicon containment materials show interesting facets of use with regard to thermal flux patterns. Pyrolytic graphite and boron nitride show a direction-orientation effect on thermal flow and one might conjecture that flux patterns could be shaped to suit the requirements of particular integral thermal storage-converter geometries. For this reason, it would probably be easier to more effectively utilize the thermal energy stored in silicon than might be in the oxide TES materials.

The thermal impedances and flux patterns in an oxide system might be alleviated through judicious use of conducting fins of suitable geometry. The additional weight penalty imposed would require consideration but would probably not impose serious detrimental effects.

In general summary, the experimental effort in thermal energy storage research and development should be deemed successful. The work was mainly of an exploratory nature in an area involving relatively new techniques in high temperature technology, exotic materials, and unique application. The containment of molten silicon should be considered an achievement. The discovery of an application for eutectic oxide mixtures involved and the amount of data developed on melting point, composition, and heat of fusion are also worthwhile achievements. The limited compatibility studies were of a screening nature but these have shown feasibility of longer life containment.

In conclusion, the achievements accomplished can be tabulated as follows:

1. At least several oxide systems, particularly those containing BeO-MgO, have been shown to have congruent melting temperatures with useful heats of fusion.

2. These oxides show good to excellent compatibility with molybdenum and tungsten at temperatures at least 100^{o}K above their melting points for 500 hours, tantalum was solubilized.

3. It has been shown that these oxide mixtures wet container metals.

4. There is very little density change on freezing of oxide mixtures compared with silicon ($\sim$10 percent by volume).

5. The oxide mixtures can be mechanically mixed together and hot sinter-pressed to 95 percent of their theoretical densities.

6. It has been found that boron nitride and pyrolytic graphite will contain molten silicon in vacuum for better than 100 hours.

7. Silicon was found to wet pyrolytic graphite and also form an impervious layer of SiC. Silicon did not wet BN or titanium diboride.

8. The directive system study shows that several oxide mixtures are better than silicon in this application by virtue of their melting temperatures and heats of fusion.

9. The directive system study indicates that a total system weight of 100 lbs/kilowatt is not too optimistic for a solar-integral thermal storage-thermionic converter power system.

10. The program, both experimental and theoretical, points to a definite need for continued study of these TES materials, e.g.; the experimental determination of thermal conductance represents a major problem area.

11. It has also been shown that corrosion rate data of the oxides in metal should be obtained for periods to five or ten thousand hours or better to indicate life capability.

12. If silicon were still to be considered for thermal storage application, there is a definite need for continued study of containment materials especially in the area of fabrication, sealing, and joining.

7. RECOMMENDATIONS

7. RECOMMENDATIONS

The thermal energy storage research and development program has resulted in a number of attractive materials. These storage materials have melting temperatures and heats of fusion which are of practical interest and can be contained.

The next effort should be threefold:

1. The generation of practical design data especially in heat-transfer categories.
2. Long-period life testing of container vessels under cycling conditions.
3. A continuation of the search for even more attractive TES materials.

Item 1 above will require test module designs, testing fixtures and procedures, and finally, test-result evaluation. Item 2 will simply involve continuation of life and cycling test programs of systems incorporating chosen materials. Item 3 requires that studies be continued for alternate TES materials having the useful characteristics desired for this application.

Specific problems will be: design and fabrication of the test fixture (for use in item 1) as well as its high-temperature, high-vacuum operation; design and development of temperature sensing elements, heat shielding, and heat source for use in this fixture. A vacuum chamber large enough to contain the test fixture will also be required. Straight-forward slab-type heat-transfer studies will be difficult under these conditions regardless of how simply the experimental effort can be defined. The approaches essentially do demand simplicity and ingenuity to ensure data which can be readily interpreted and accurately reproduced. Advanced heat-transfer studies utilizing more complex configurations should certainly be more easily undertaken after the more basic studies have proven the worth of the testing fixture itself.

Studies for even better TES materials should be included since the program described in this report has been essentially a screening effort in this area. Using the materials suggested in this report, more refined and exact determinations of properties and compositions should also be made.

8. REFERENCES AND BIBLIOGRAPHY

8. REFERENCES AND BIBLIOGRAPHY

8.1 References

1. Brewer, L., Paper 3. "Chemistry and Metallurgy of Miscellaneous Materials: Thermodynamics," McGraw-Hill, New York, N. Y. (1950).

2. Rossini, F. D., et al., "Selected Values of Chemical Thermodynamic Properties," U.S. Dept. of Commerce, National Bureau of Standards (February 1, 1952).

3. Konigsberger, J., Weiss, J., J. Ann. Physik (4), 35, 16 (1911).

4. Glassner, A., "The Thermochemical Properties of the Oxides, Fluorides, and Chlorides to 2500^{o}K," ANL-5750, Atomic Energy Commission (1959).

5. Berezhnoi, A. S., "Silicon and Its Binary Systems," Academy of Sciences of the Ukrainian SSR, Kiev (1958), translated by Consultants Bureau, New York (1960).

6. Osborn, C. J., J. Metals, 188, 600-607 (1950).

7. Shockley, W., "Preparation of Semiconductor Materials," Quarterly Report No. 1, Shockley Semiconductor Laboratory, Contract NObsr-72706 (1734F).

8. Scaff, J. H., Theuerer, H. C., Schumacker, E. E., J. Metals 185, 383-388 (1949).

9. Torry, H. C., Whitmor, C. A., "Crystal Rectifiers," McGraw-Hill, Inc., New York, N. Y., 308-313 (1948).

10. Tucker, N. P., J. Iron Steel Inst., (London), 412-416 (1927).

11. Seitz, F., "Compounds of Silicon and Germanium," PB 2628.

12. Seitz, F., "The Electrical Conductivity of Silicon and Germanium," PB 2619.

13. Johnson, W. R., Hansen, M., W.A.D.C. Report No. 6383 (June 1951).

14. Runyan, W. R., Texas Instruments, private communication to M. Lapides, September 1960.

15. Garcia, W. M. - "Molten Silicon Containment," G. E. - FPLD Technical Information Series R60FPD342, May 23, 1960.

16. Brewer, L. to Kirtchik, H. - Private communication, May 9, 1960.

17. Campbell, I. E., "High Temperature Technology," John Wiley & Sons, Inc., N. Y. 118, 1956.

18. Nelson, J. A., Wilmore, G. A., Womeldorph, R. C., J. Electrochem. Soc., 98, 465-473 (1951).

19. Batutis, E. F., "Thermal Energy Storage, Research and Development Program," Interim Report, 6 December 1960 to 1 May 1961, Contract No. NAS 5-826.

20. Wilson, H. et al, ASD Technical Report 61-187, Contract AF33(616)-7224, June 30, 1961.

21. Elliott, J. F. and Gleiser, M. - "Thermodynamic for Steelmaking," Addison Wesley Publishing Company, Reading, Mass., 1960.

22. "Handbook of Chemistry and Physics," 42nd Edition, Chemical Rubber Publishing Company, Cleveland, Ohio, 1960.

23. Campbell, I. E. (ed) - "High Temperature Technology," John Wiley & Sons, Inc., New York, 1956.

24. Lang, S. M., Fillmore, C. L., and Maxwell, L. H., J. Res. Natl. Bur. Standards (U.S.) 48 (4) 301, (1952).

25. v. Wartenburg, H., Reusch, H. J., and Saran, E. - Z. anorg. u. Allegem. Chem., 230, 275, (1937).

26. v. Wartenburg, H., and Prophet, - Z. anorg. u. Allegem. Chem., 208, 378, (1932).

27. Doney, L. M., and Taylor, - Metallurgy Division Annual Report, pp. 185-96, ORNL 2988, September 30, 1960.

28. Rankin, G. A. and Merwin, H. E. - J. Am. Ceram. Soc., 38, 571, (1961).

29. Rankin, G. A. and Wright, F. E. - Amer. J. Sci. 4th Series, 39, 11, (1915).

30. Wagner, C. - "Thermodynamics of Phase Diagrams of Binary Systems Involving Compounds," Acta Metallurgia, Vol. 6, May 1958.

31. Levin, E. M., McMurdie, H. F., and Hall, F. P. - "Phase Diagrams for Ceramists," Part I (1956) Part II (1959), Amer. Ceram. Soc., Columbus, Ohio.

32. Rose, D. E. - Project No. 7021, Contract AF 33(616)-6545 (AD235443), New York State Univ., College of Ceramics, Alfred, Aug. 1, 1960.

33. Stull, D. R. and Sinke, G. C. - "Thermodynamic Properties of the Elements," Amer. Ceram. Soc., Washington, D.C. (1960).

34. JANAF Interium Thermochemical Tables, Dow Chemical Co., Midland, Michigan (1960).

35. Kubaschewski, O. and Evans, E. - "Metallurgical Thermochemistry" Pergamon Press, New York (1958).

8.2 Supplementary Bibliography

1. Samsonov, G. V. and Slokovnikova, F. A. - Fix. Metal. i. Metalloved. Akad. Nauk S.S.S.R., 5, 565-6 (1957).

A report of work on the diffusion of silicon; into the transition elements Ti, Cb, Ta, Cr, Mo, W, Fe, Co, and Ni. Diffusion layer depth measured and activation energies calculated.

2. Samsonov, G. V. and Koval'chenko - Inzhener - Fiz. Zhur. Akad. Nauk Belorus S.S.S.R. No. 3, 62-7, 1954.

Activation energies and constants for the change in the diffusion coefficients for silicon in Ti, Fe, Ta and Mo with temperature are tabulated.

3. Geller, R. F., Yavorsky, P. J., Stierman, B. L., and Creamin, A. S. - J. Res. Natl. Bur. Standards (U.S.) 36, 277, (1946).

Summary studies of the $MgO-BeO-Al_2O_3$, $CaO-BeO-Al_2O_3$, and $BeO-Al_2O_3-ZrO_2$ systems. Low melting point mixtures are located.

4. Lang, S. M., Maxwell, L. H., and Geller, R. F. - J. Res. Natl. Bur. Standards (U.S.) 43, 429, (1949).

$MgO-BeO-ZrO_2$ system reported with approximate location of eutectic mixtures.

5. Lang, S. M., Roth, R. S., and Fillmore, C. L. - J. Res. Natl. Bur. Standards (U.S.) 53, 201 (1954).

Eutectic compositions in the $BeO-TiO_2-ZrO_2$ system are reported. Indicates that no low melting mixtures of BeO and CeO exist.

6. Johnson, P. D. - J. Amer. Ceram. Soc. 33, 168 (1950).

Reports the temperatures of which the first evidence of reaction was noted between BeO, MgO and ZrO_2 and Mo and W.

APPENDIX A

APPENDIX A

Apparatus

In general the vacuum furnaces were conventional equipment. Figures A-1 and A-2 are photographs of the systems used.

The following brief description covers an all metal vacuum bell-jar furnace system (Figures A-2 and A-3). This furnace was used for most of the work on the program; that is, for screening studies and longer life tests.

A water-cooled vacuum bell-jar was mounted on a commercial vacuum console (Consolidated, Type PS-40A). The heating element within the bell-jar was a centrally located, slotted graphite cylinder with a working volume about 2 inches in diameter and about 1-5/8 inches deep. These elements were obtained from the Speer Carbon Company.

The heating element was mounted on water-cooled brass electrodes. The electrodes were connected to a 10:1 voltage stepdown transformer with 1/2 inch diameter copper rods. All water, power and thermocouple leads to the heating area were passed through Conax vacuum fittings in a copper ring. Figure A-3 shows the component parts of this heating system.

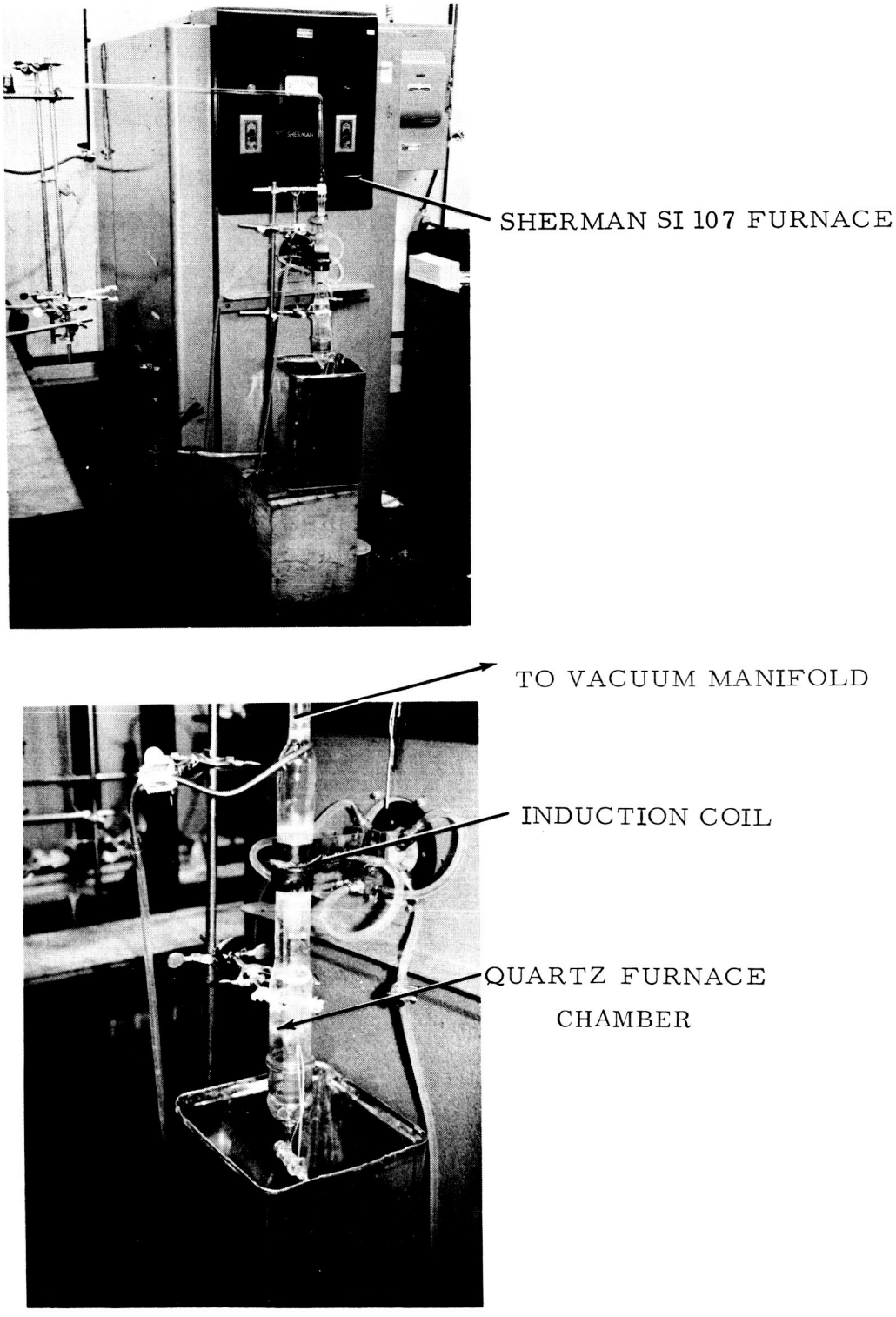

Figure A-1. Glass, Induction Heated Vacuum Furnace

CONSOLIDATED TYPE

PS-40A VACUUM CONSOLE

VIEWING PORTS

METAL BELL JAR

Figure A-2. Metal, Resistance Heated Vacuum Furnace

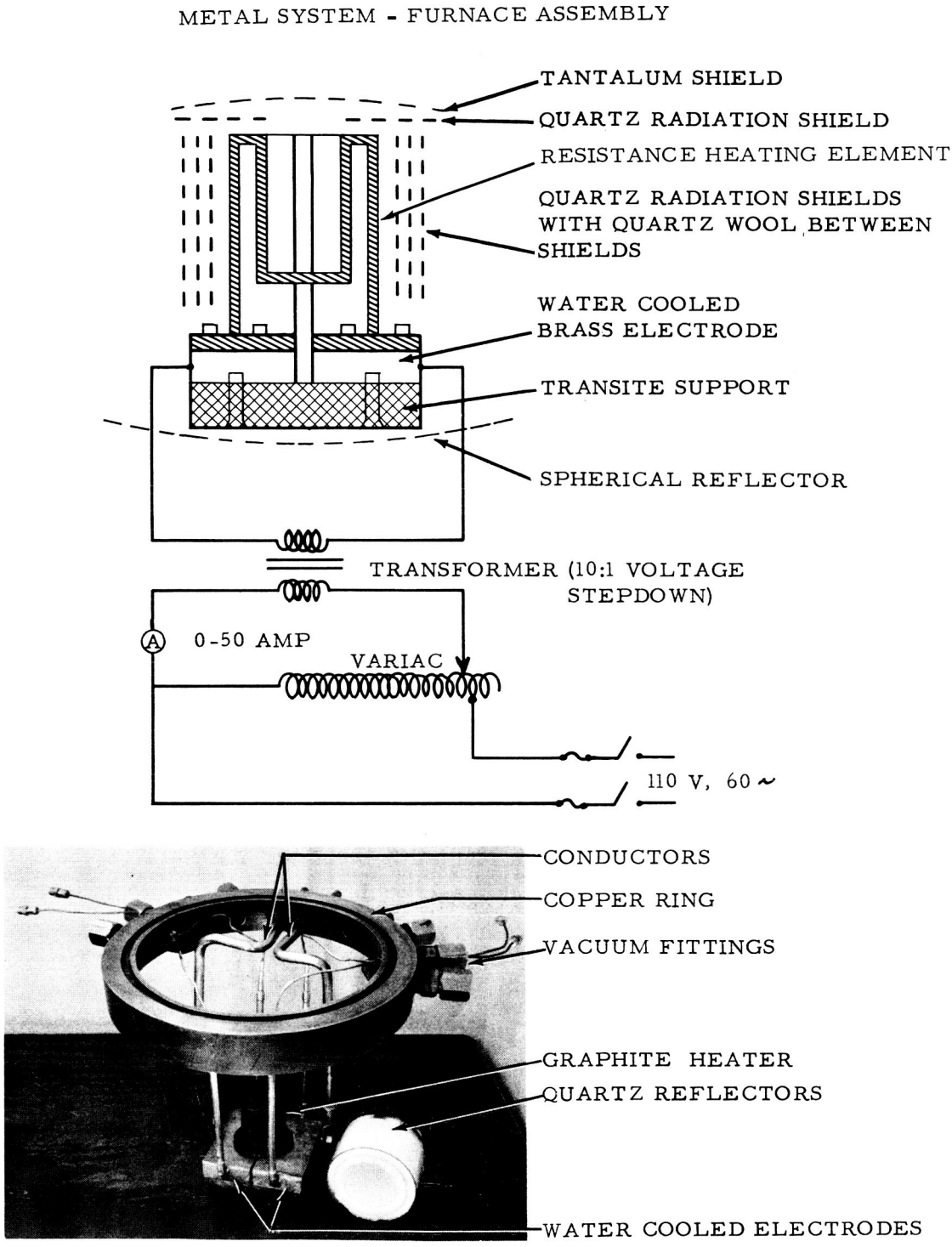

Figure A-3. Metal System - Furnace Assembly

APPENDIX B

Appendix B

Some Selected Physical Properties of Pyrolytic Graphite and Boron Nitride

PROPERTY	PYROLYTIC GRAPHITE (General Electric) "a"-direction	PYROLYTIC GRAPHITE (General Electric) "c"-direction	BORON NITRIDE (National Carbon Co.) direction *1	BORON NITRIDE (National Carbon Co.) direction *2	BORON NITRIDE (Carborundum Co.) direction *1	BORON NITRIDE (Carborundum Co.) direction *2
Density (gm/cm^3)	2.16-2.22		2.05-2.15		2.10	
Sublimation Temp. (^oC)	3652-3697		2700		----	
Vapor Pressure (mm Hg)	1.0 @ 3586 ^oC		< 0.5 @ 1580 ^oC < 5.0 @ 2000 ^oC		----	
Oxidation in Air	better than commercial graphite		very slight to 700 ^oC slight to 1000 ^oC		excellent to 700 ^oC	
Machinability	very poor		excellent		excellent	
Electrical Resistivity (ohm-cm)	@ 24 ^oC 4.7×10^{-4}	5.0×10^{-1}	1×10^{13} @ 24 ^oC 5×10^{8} @ 480 ^oC 1×10^{7} @ 1000 ^oC 2×10^{3} @ 1500 ^oC 1×10^{2} @ 2000 ^oC		1.7×10^{13} @ 24 ^oC 2.31×10^{10} @ 482 ^oC 3.05×10^{4} @ 982 ^oC	
	@ 600 ^oC 3.5×10^{-4}	3.0×10^{-1}				
	@ 800 ^oC 3.8×10^{-4}	2.3×10^{-1}				
Thermal Conductivity ($watt/cm^2/^oC/cm$)	@ 20 ^oC 3.6-4.2	0.025	@ 24 ^oC 0.346	0.173	@ 300 ^oC 0.287	0.154
	@ 1000 ^oC 1.05-1.25	0.012			@ 700 ^oC 0.270	0.133
					@ 980 ^oC 0.267	0.124
Coefficient of Thermal Expansion ($in/in/^oC$)	(24 ^oC to 1000 ^oC) 1.3×10^{-6}	22×10^{-6}	(24 ^oC to 1000 ^oC) 3.6×10^{-6}	9.9×10^{-6}	(24 ^oC to 1000 ^oC) 0.774×10^{-6}	7.51×10^{-6}
Compressive Strength (psi)	@ 24 ^oC 1.4×10^{4}	$5.4\text{-}8.2 \times 10^{4}$	2.7×10^{4} @ 24 ^oC 1×10^{3} @ 750 ^oC 5×10^{2} @ 1000 ^oC		@ 24 ^oC 3.4×10^{4}	4.5×10^{4}
Tensile Strength (psi)	1.4×10^{4} @ 24 ^oC $5\text{-}6 \times 10^{4}$ > 2500 ^oC	1.5×10^{4} (24 ^oC-982 ^oC)	3×10^{3} @ 24 ^oC 1×10^{3} @ 750 ^oC 5×10^{2} @ 1000 ^oC			

*direction 1 = direction perpendicular to pressing direction.
*direction 2 = direction parallel to pressing direction.

APPENDIX C

APPENDIX C

The experimental data presented in these graphs resulted from enthalpy measurements made during the heat of fusion studies.

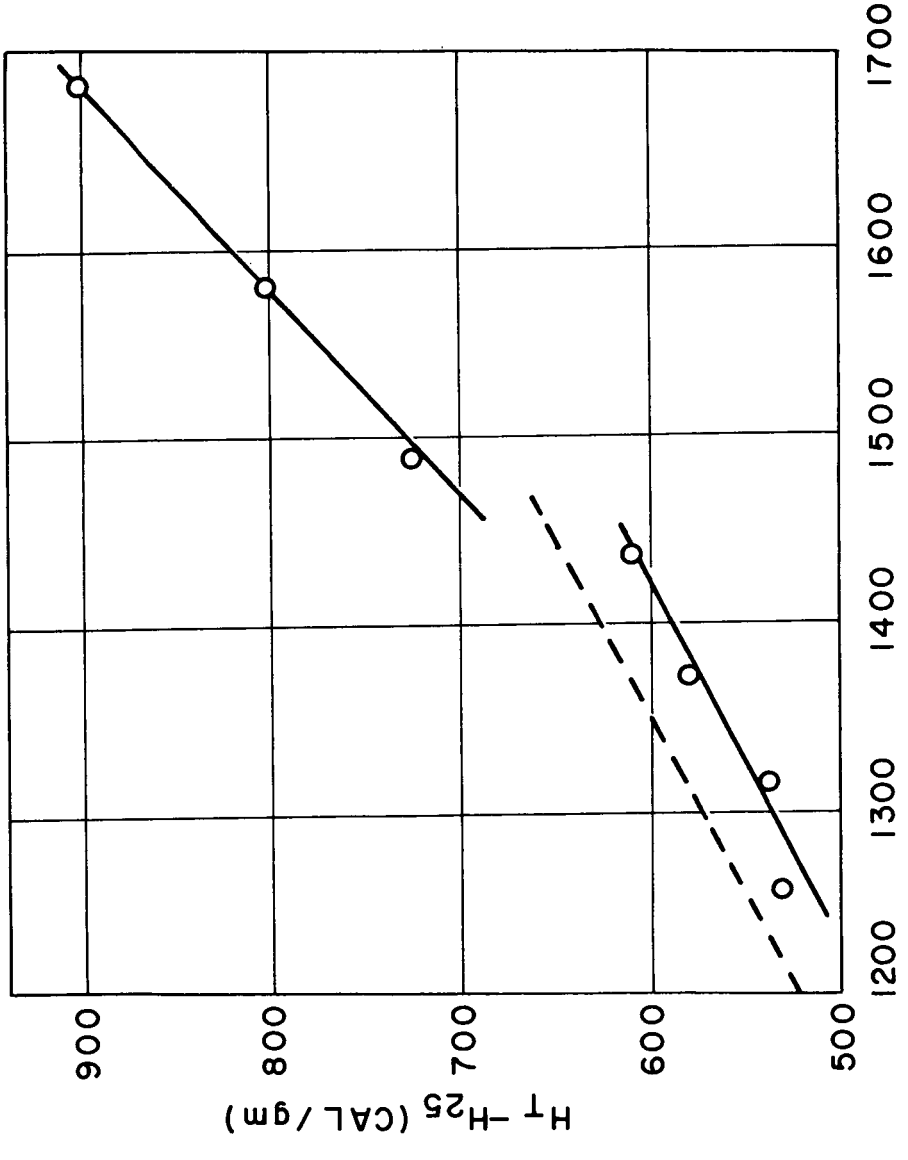

Figure C-1. Experimental Enthalpy Data for $3BeO \cdot B_2O_3$

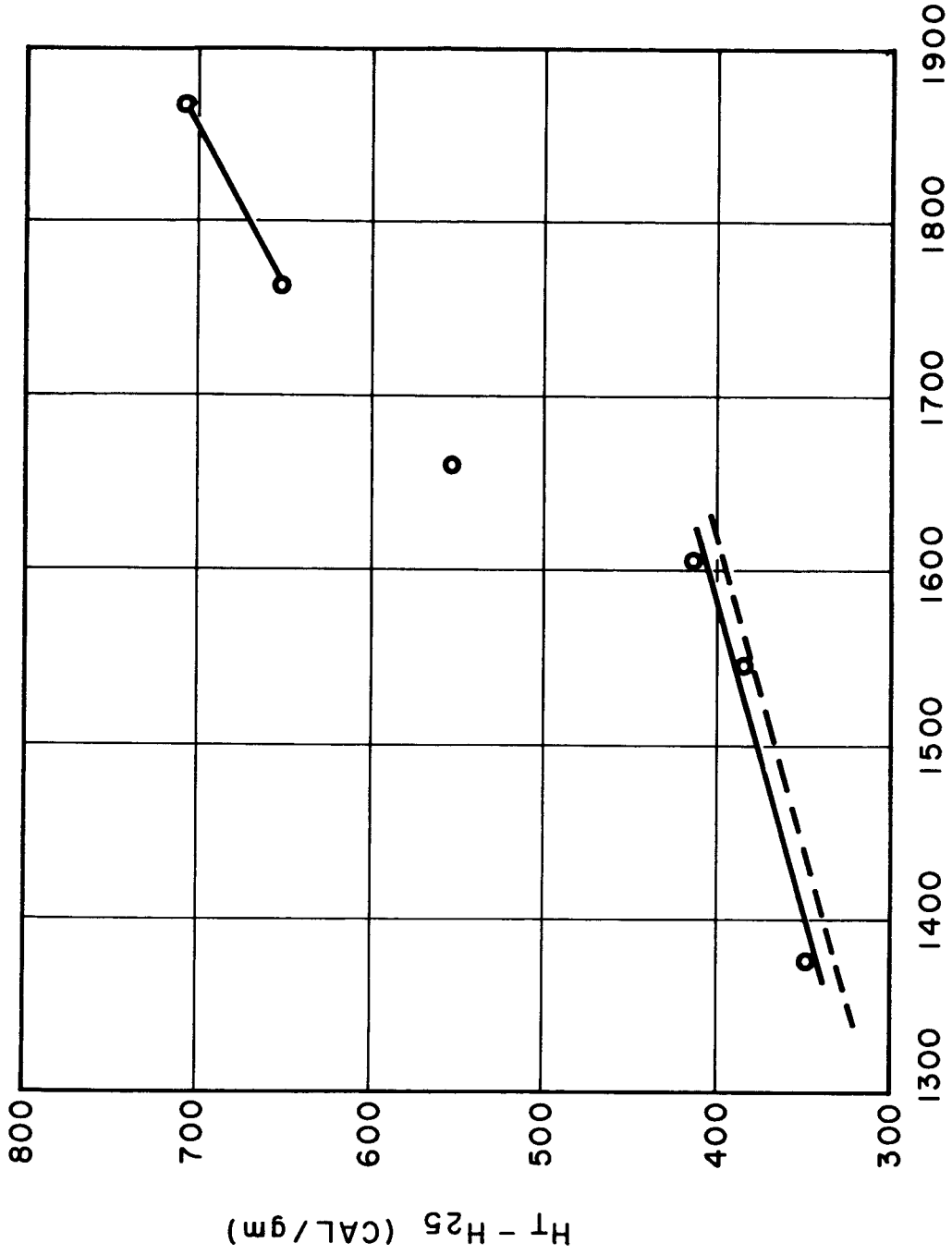

Figure C-2. Experimental Enthalpy Data for $Al_2O_3 \cdot 3MgO \cdot 4TiO_2$

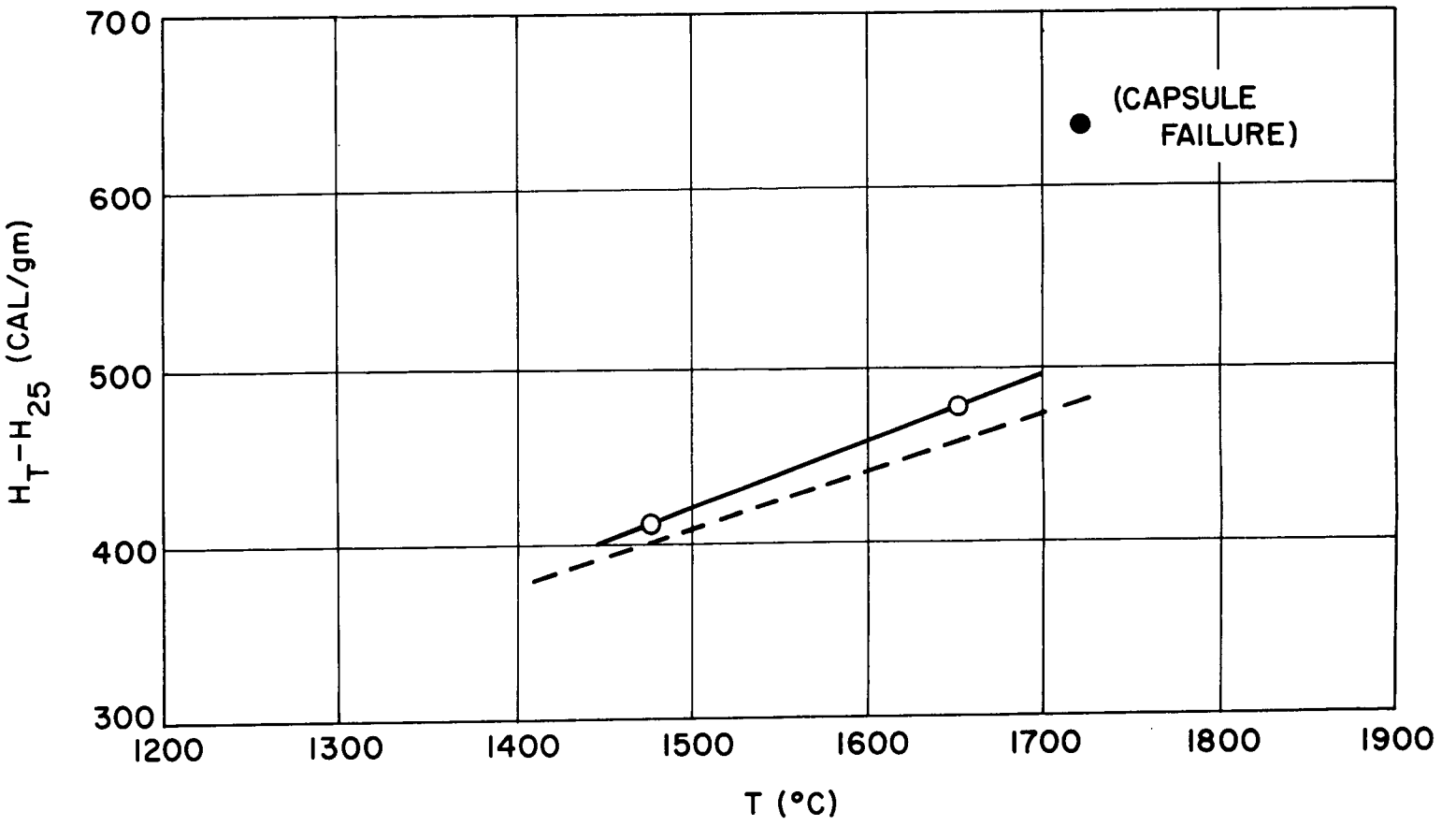

Figure C-3. Experimental Enthalpy Data for $2BeO \cdot 5Al_2O_3 \cdot 2TiO_2$

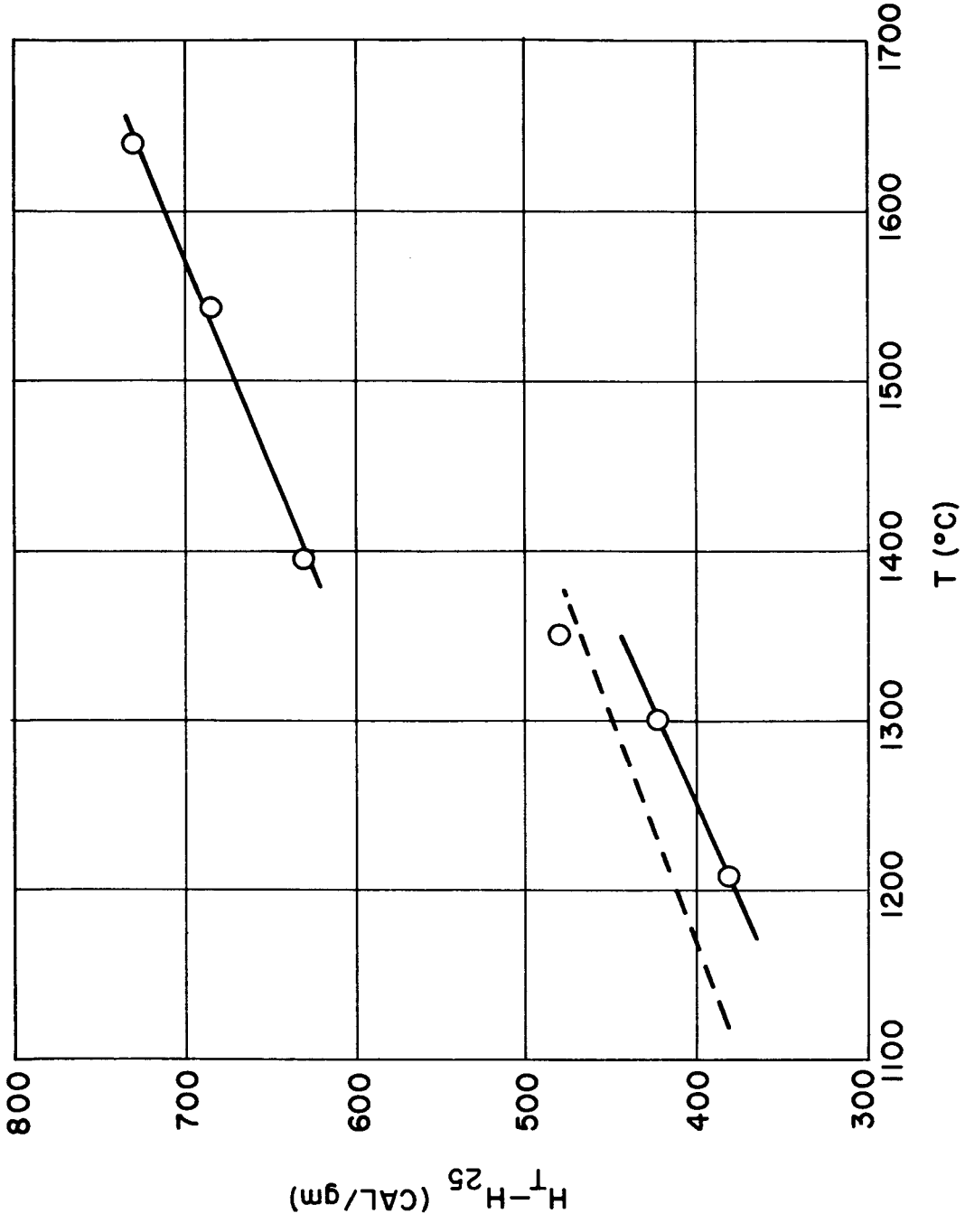

Figure C-4. Experimental Enthalpy Data for $3MgO \cdot B_2O_3$

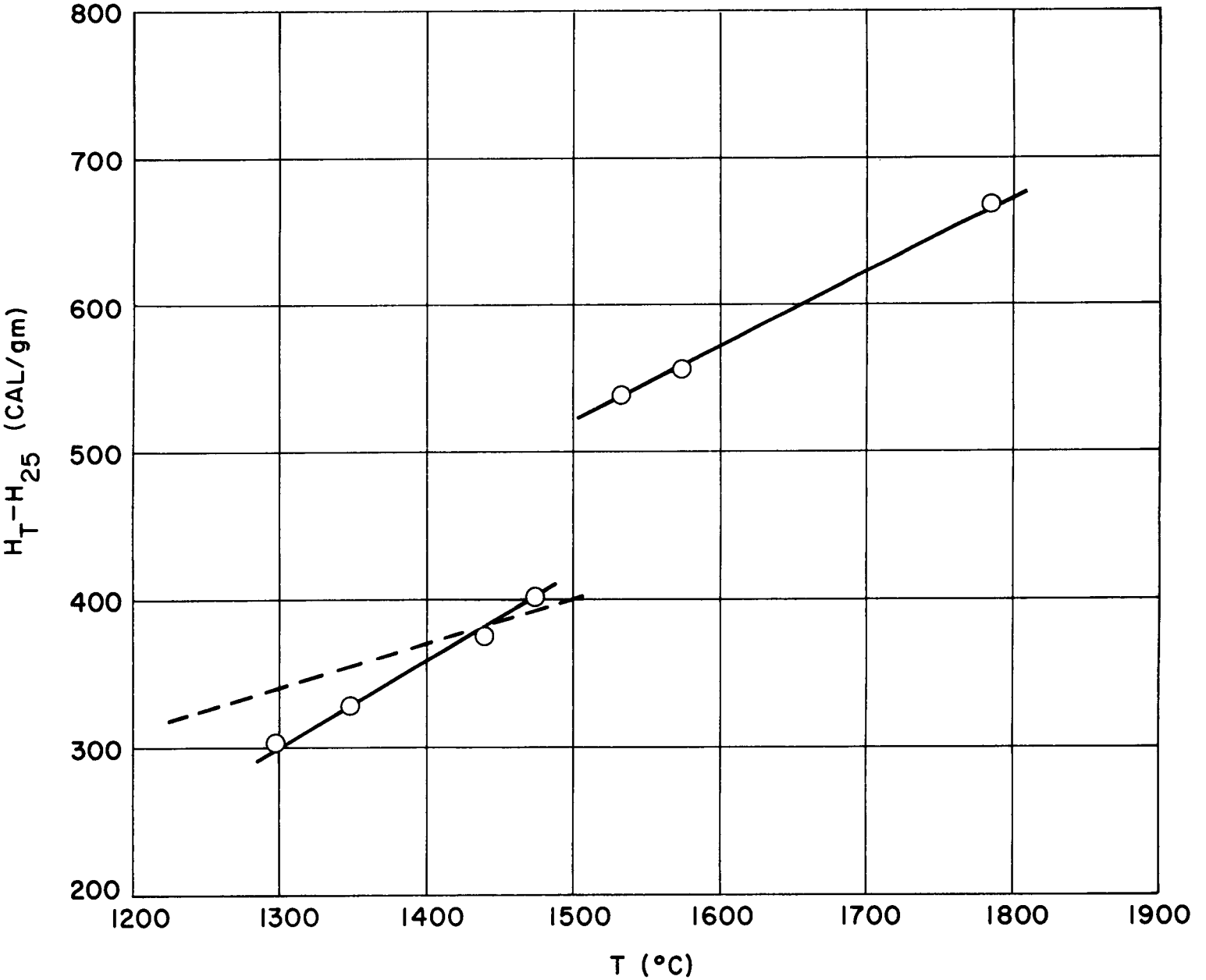

Figure C-5. Experimental Enthalpy Data for $3CaO \cdot B_2O_3$

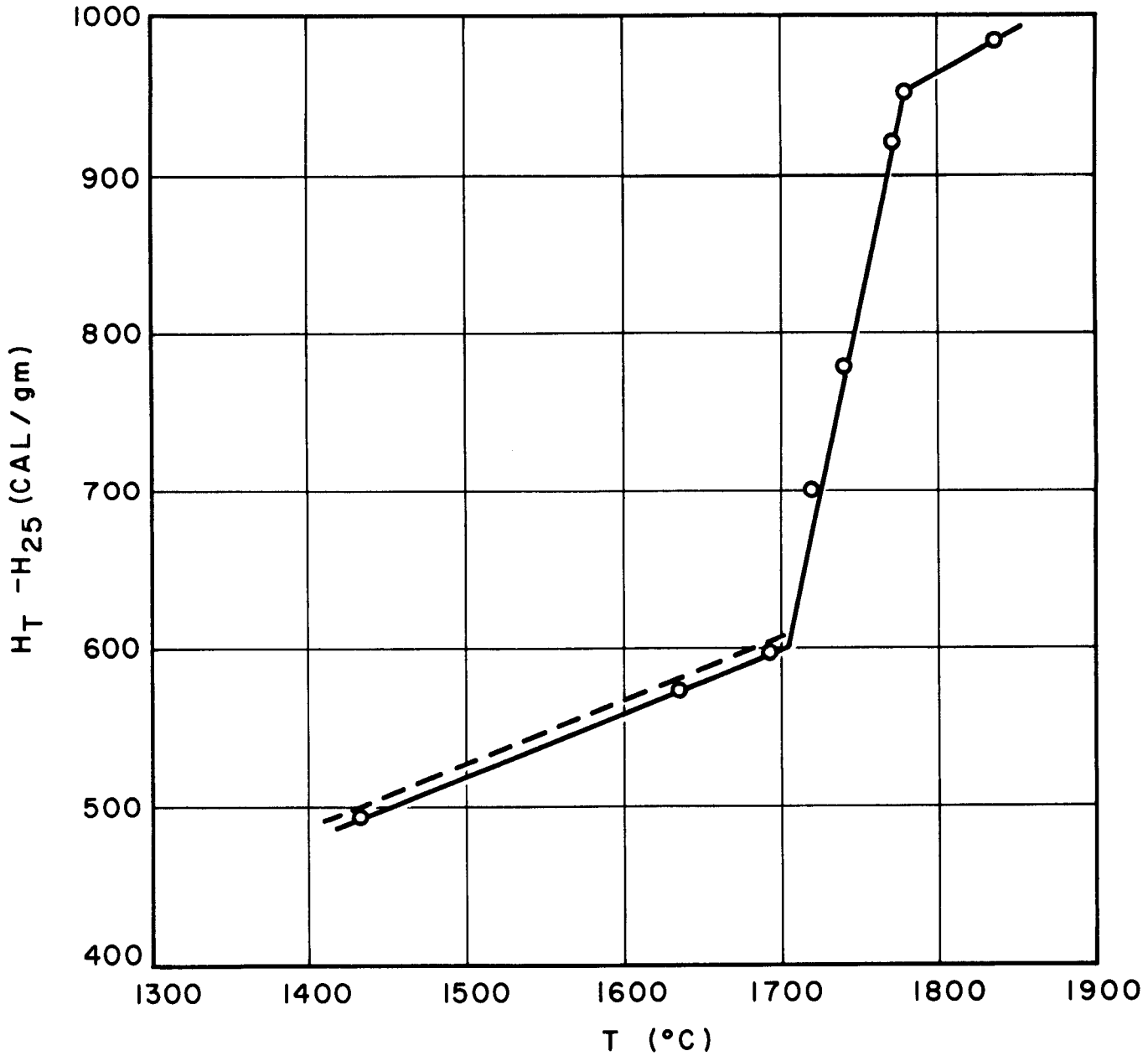

Figure C-6. Experimental Enthalpy Data for $4BeO \cdot Al_2O_3 \cdot MgO$

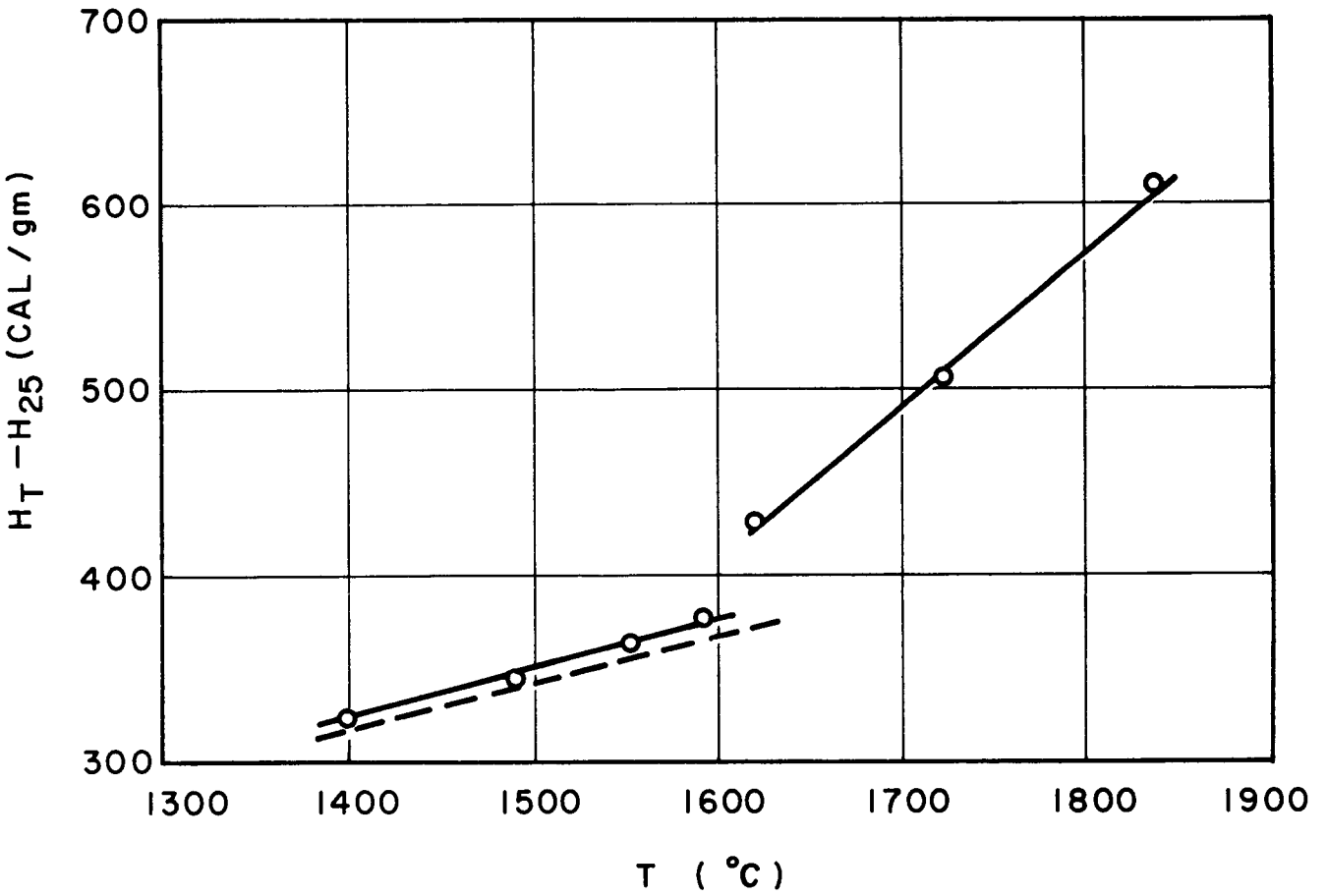

Figure C-7. Experimental Enthalpy Data for $2BeO \cdot TiO_2 \cdot ZrO_2$

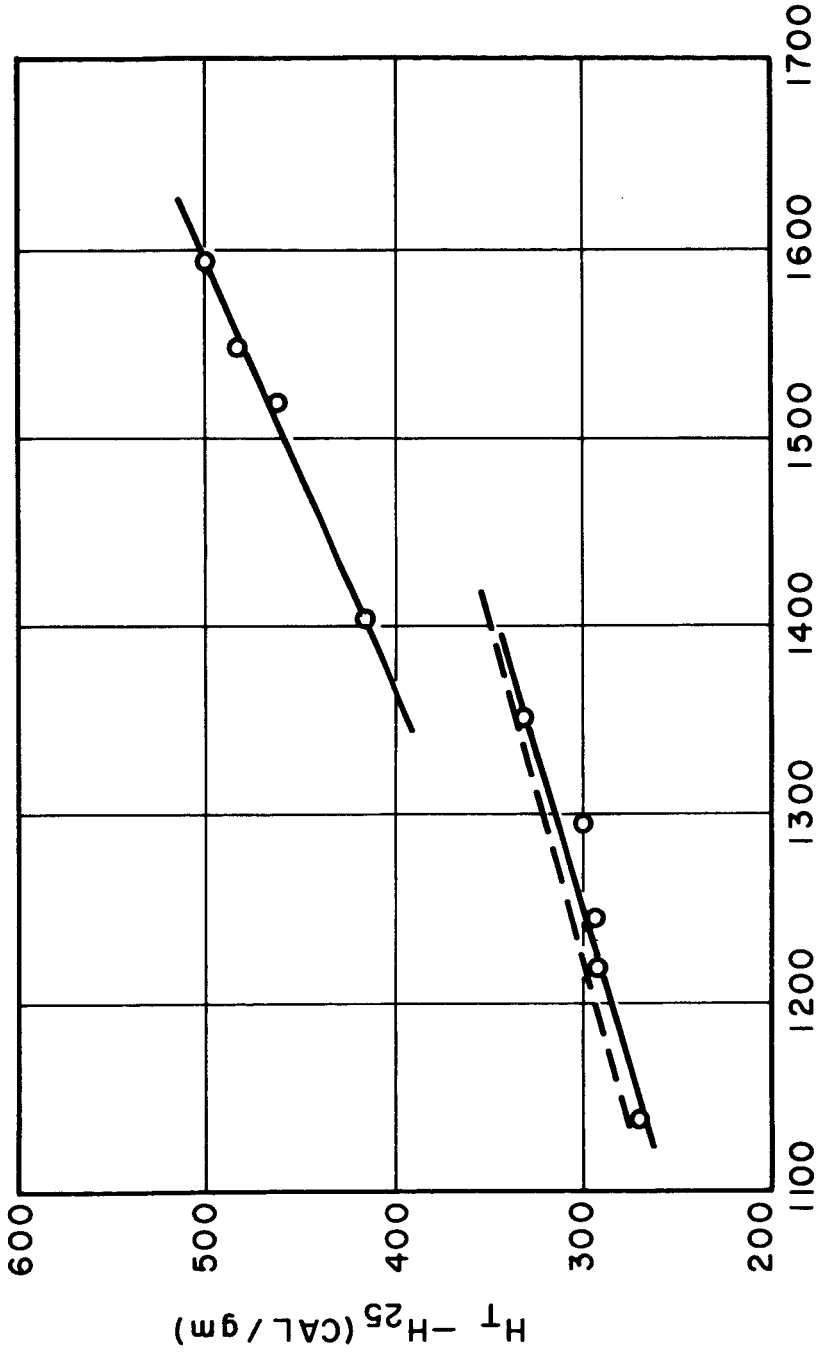

Figure C-8. Experimental Enthalpy Data for $5CaO \cdot 3Al_2O_3$

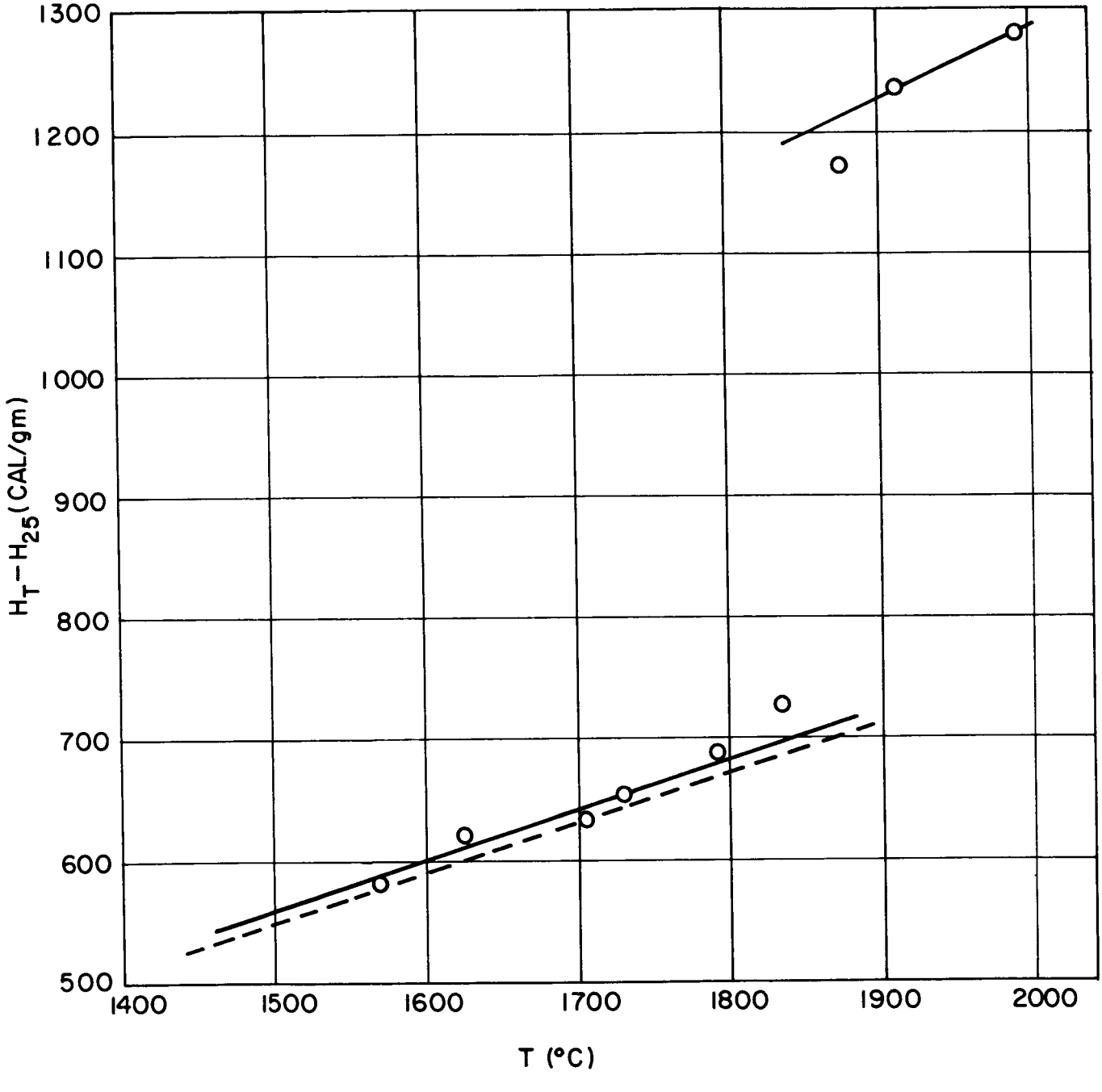

Figure C-9. Experimental Enthalpy Data for 3BeO·2MgO

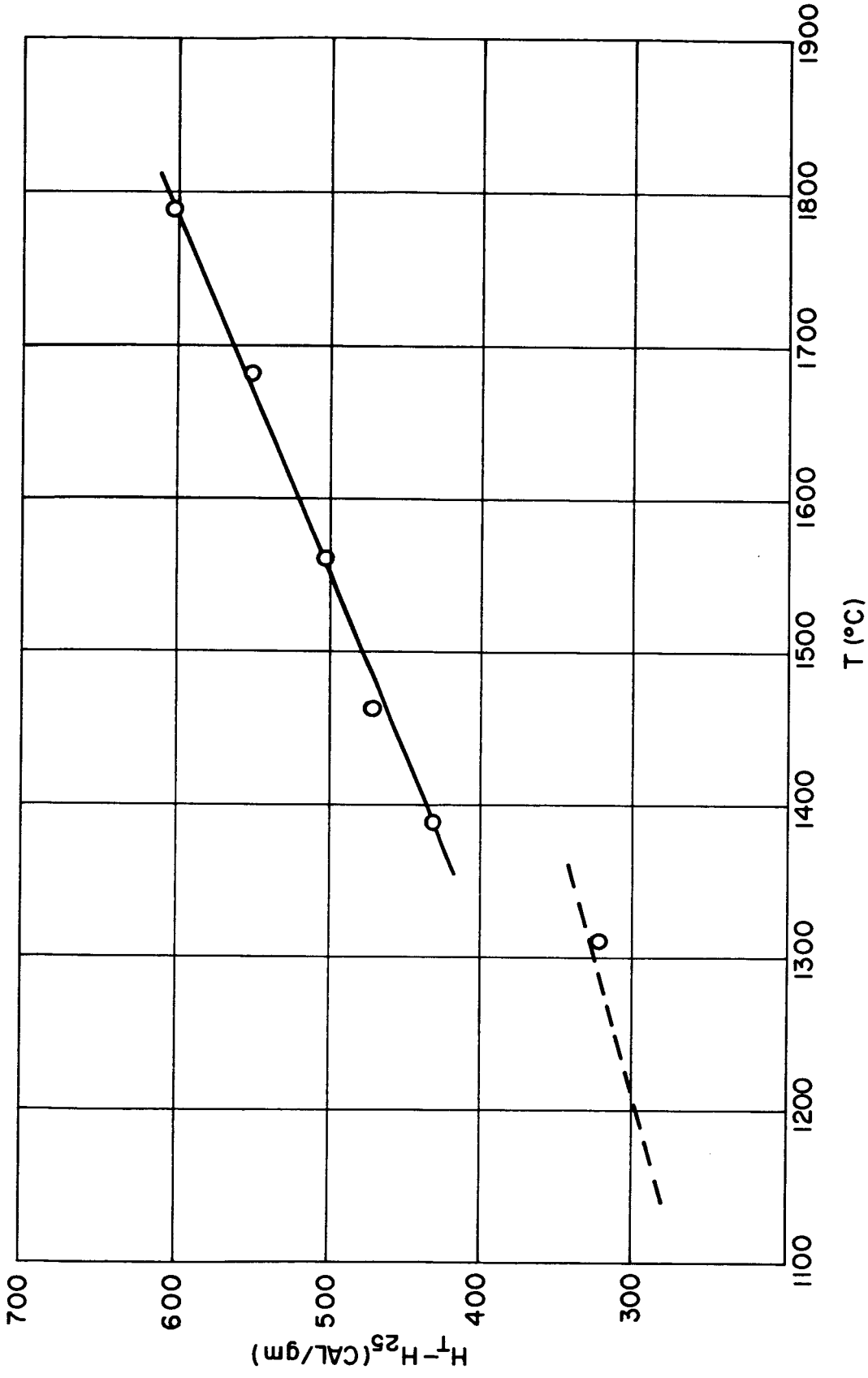

Figure C-10. Experimental Enthalpy Data for $6CaO \cdot 3Al_2O_3 \cdot MgO$

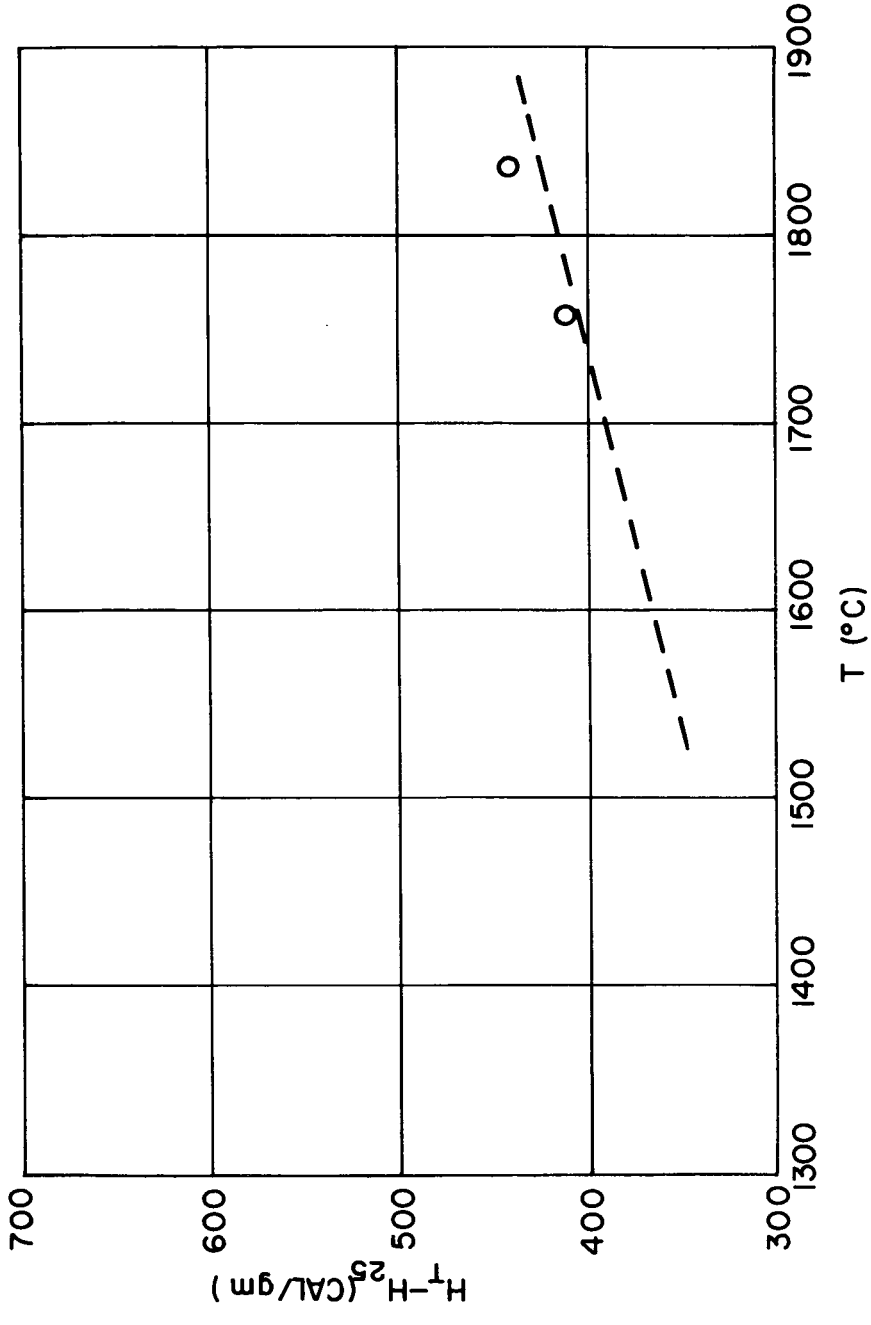

Figure C-11. Experimental Enthalpy Data for $4MgO \cdot ZrO_2$

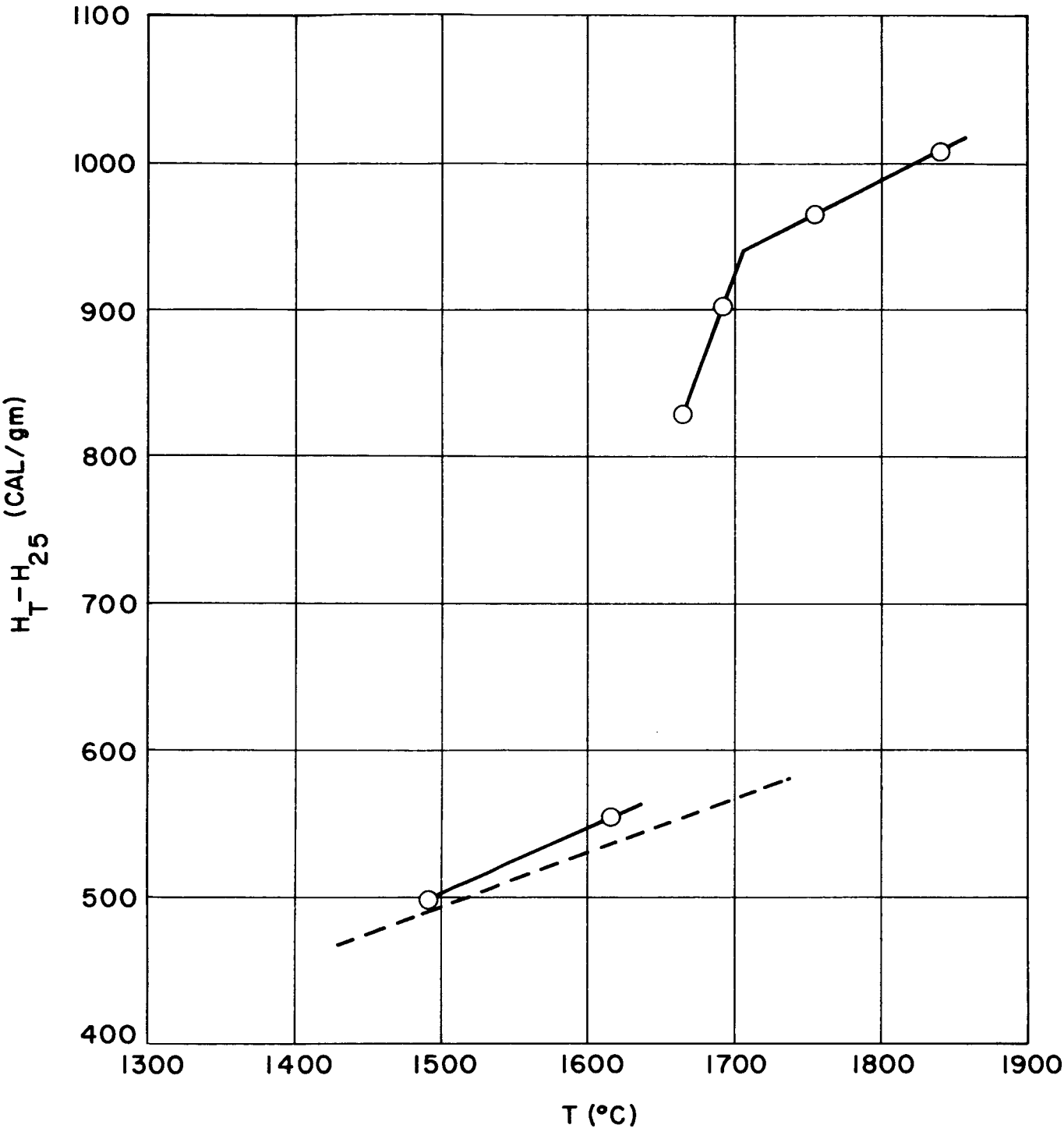

Figure C-12. Experimental Enthalpy Data for $4BeO \cdot Al_2O_3 \cdot 4MgO$

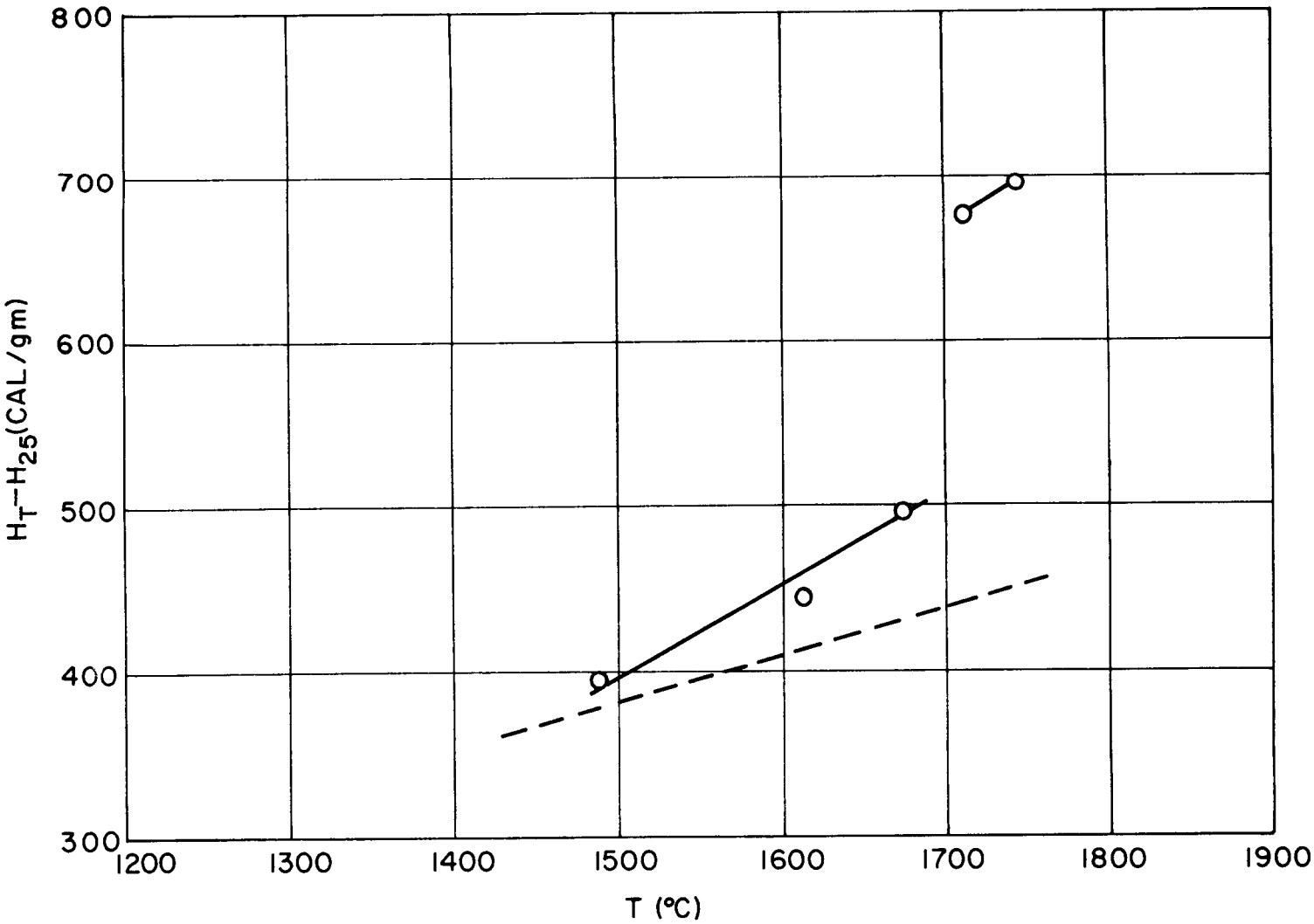

Figure C-13. Experimental Enthalpy Data for $2BeO \cdot 3TiO_2$

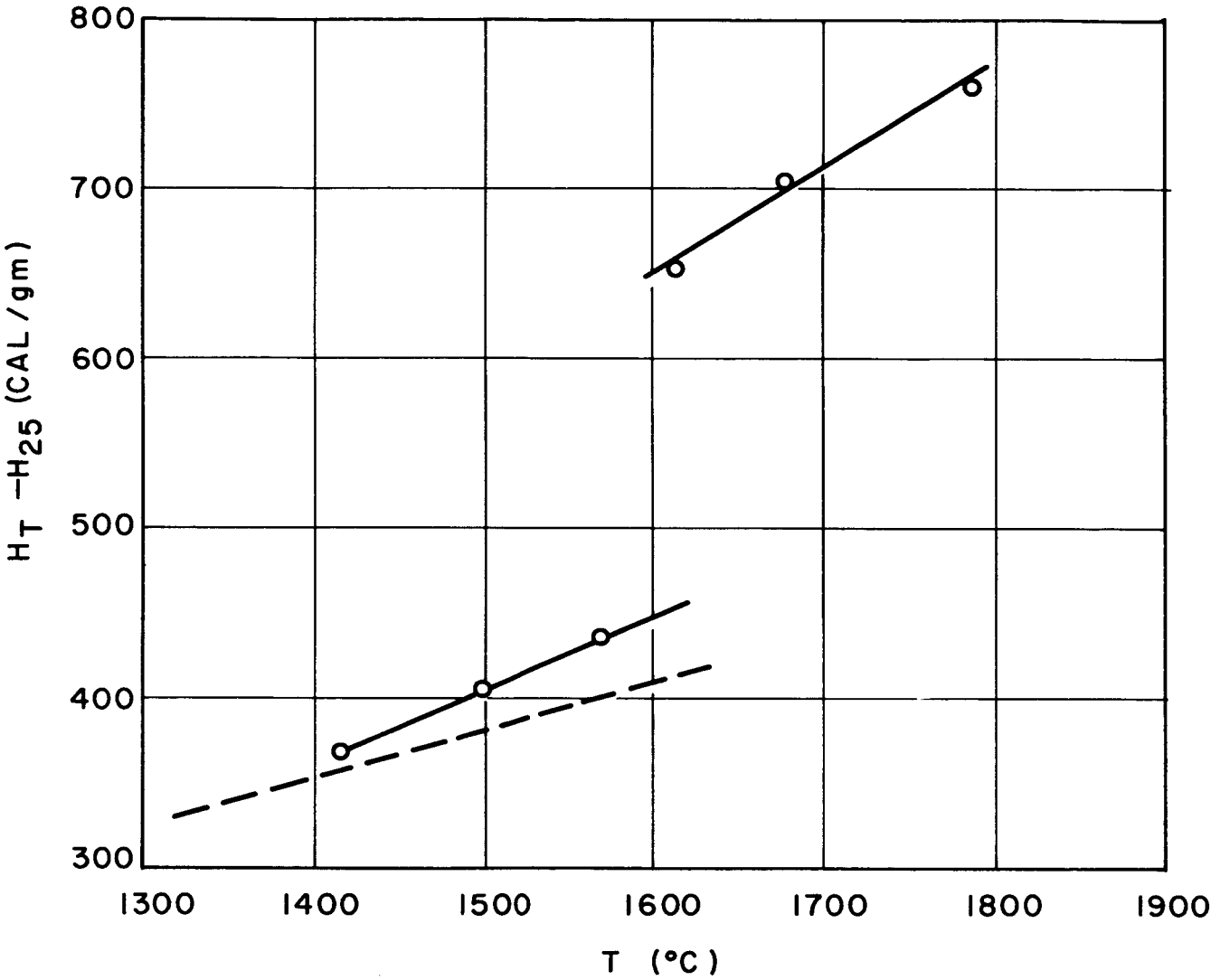

Figure C-14. Experimental Enthalpy Data for $4TiO_2 \cdot 2BeO \cdot Al_2O_3$

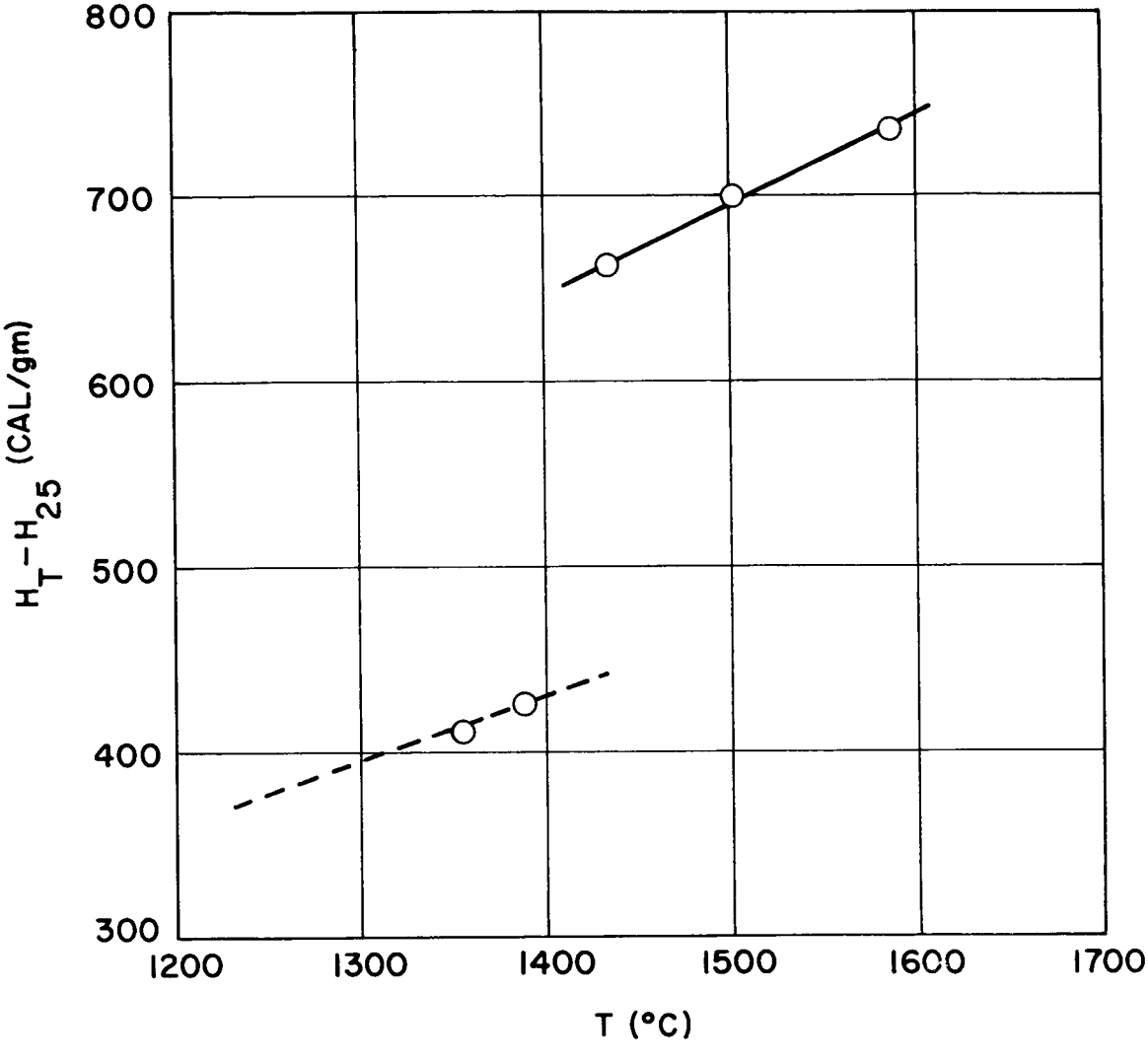

Figure C-15. Experimental Enthalpy Data for 3BeO·2CaO

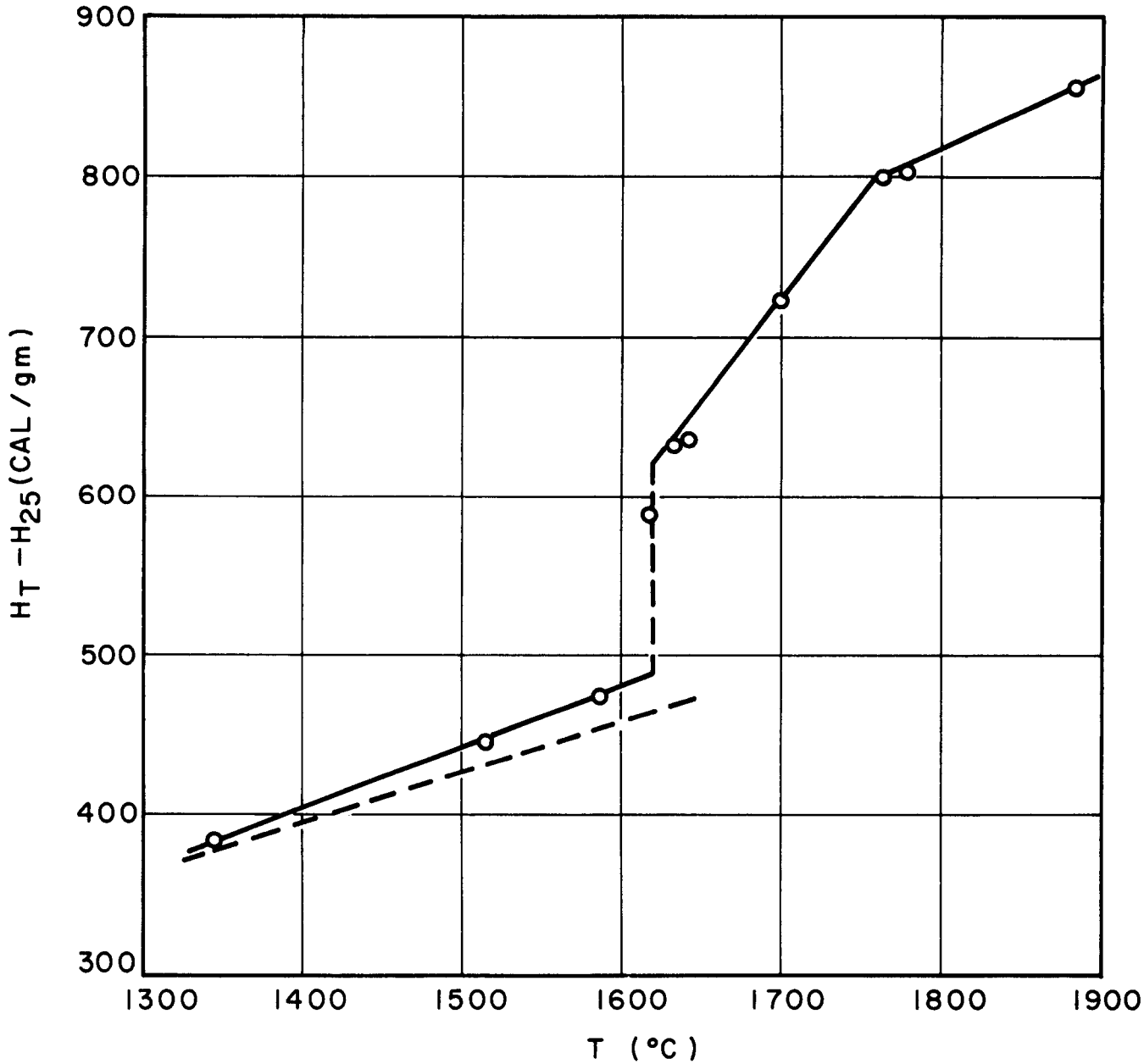

Figure C-16. Experimental Enthalpy Data for $3BeO \cdot Al_2O_3 \cdot 2TiO_2$

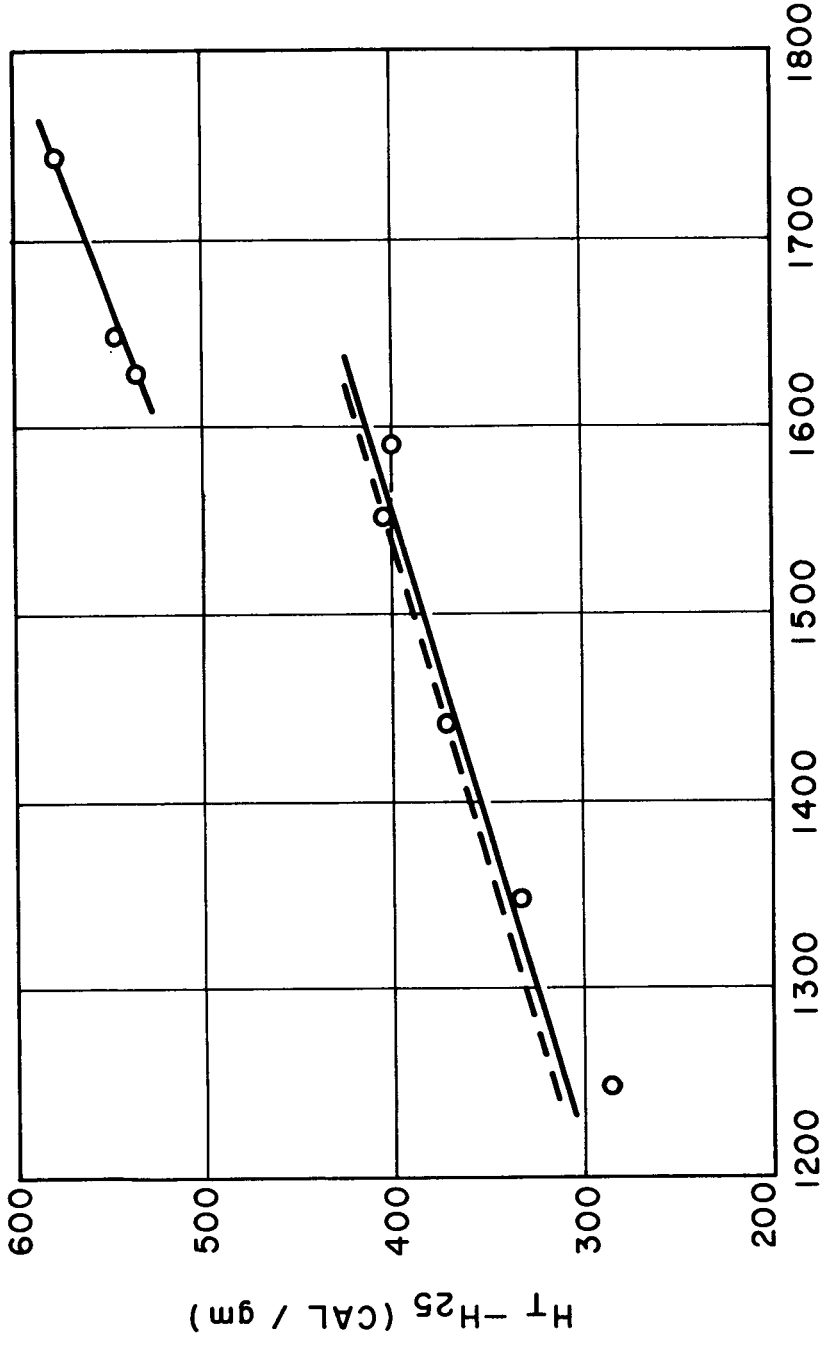

Figure C-17. Experimental Enthalpy Data for $CaO \cdot Al_2O_3$

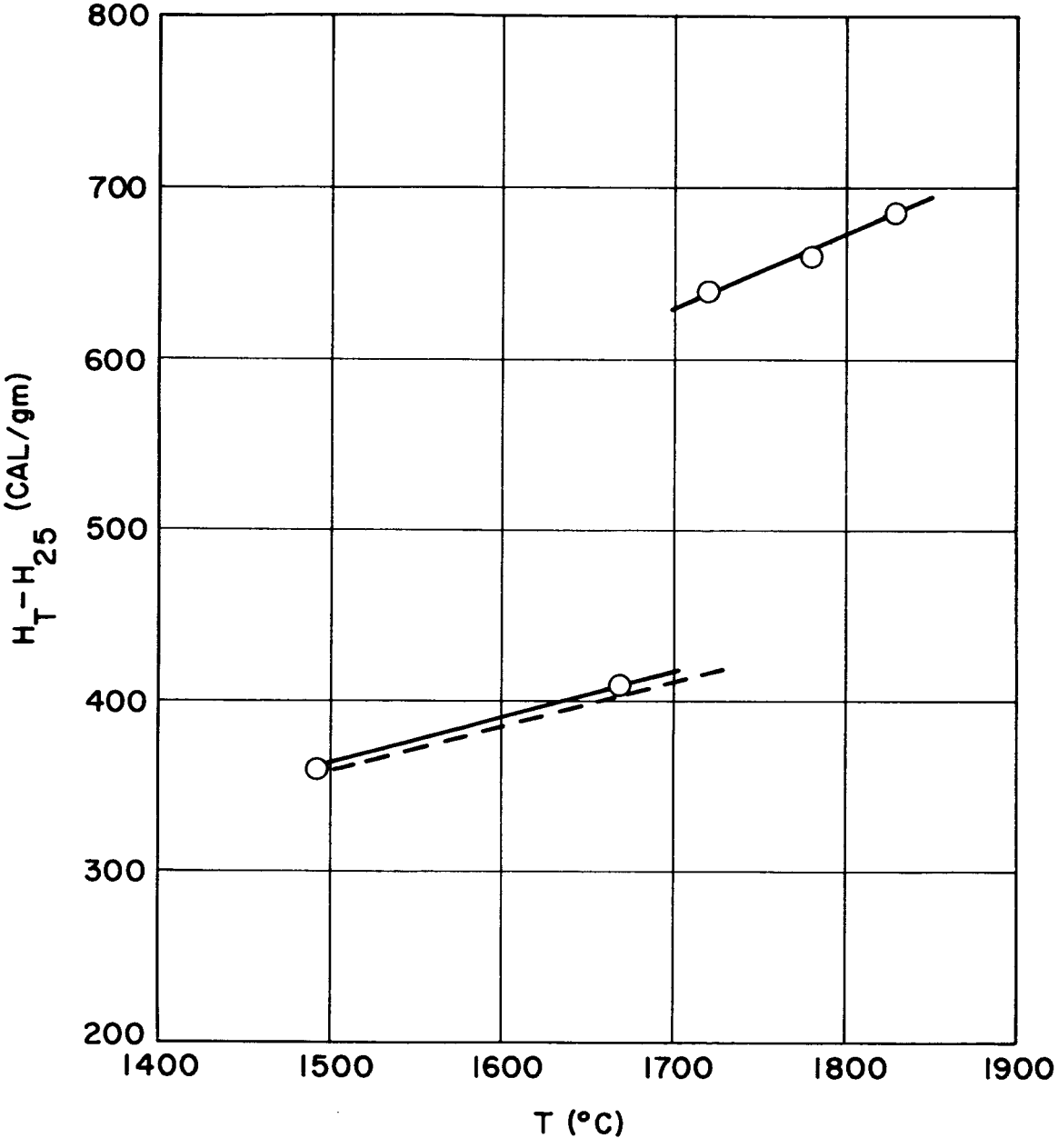

Figure C-18. Experimental Enthalpy Data for $4MgO \cdot 5BeO \cdot 3ZrO_2$

APPENDIX D

APPENDIX D

HIGH TEMPERATURE CERAMICS

A particular reference of great interest is "The Technology of High Temperature Ceramics" by Louis Navias of the General Electric Company's Research Laboratory. In this report, Dr. Navias has taken the large field of refractory materials melting points and presented the data in graphical form. Several of these are reproduced here for quick survey purposes as might apply to this study. The graphs are prepared in a steady progression form for ease of reference. For this purpose, Dr. Navias only considered those refractory materials with melting points higher than 1500°C with a few other lower melting materials included for comparison.

Figure D-1 is a graphical presentation of refractory oxides. The chart in Figure D-2 is intended to show that of the lower melting metals, their oxides are relatively high melting and lie above them whereas the reverse is true of the higher melting metals. Figures D-3 and D-4 are typical and nontypical phase diagrams, respectively, for high melting oxides.

The liquidus temperatures for various oxide combinations are shown in Figures D-5 and D-6. It is interesting to note that, in the normal concept of high-temperature use, these lower melting binaries are not attractive to the ceramist in the usual sense.

The large circle around a point in these graphs with the designated name shows the melting point of that oxide and the other points show the lowest melting (eutectic) temperatures of binary combinations. Note that all oxide combinations with BeO lower the melting point markedly (from 2530°C to as low as 1450°C with CaO or more than 1000°C). CaO, ZrO_2 and ThO_2 in combination with BeO also show interesting melting temperature lowering in several instances.

The melting point data in graphical form are also presented in Figures D-7 through D-14 for other refractory materials including the borides, carbides,

nitrides, silicides, fluorides and sulfides. A final graph, Figure D-15 shows the range of melting points for all of the refractory materials. In summary, there are at least 153 refractory materials of all kinds with melting points in the range 1500°C. to 4000°C.

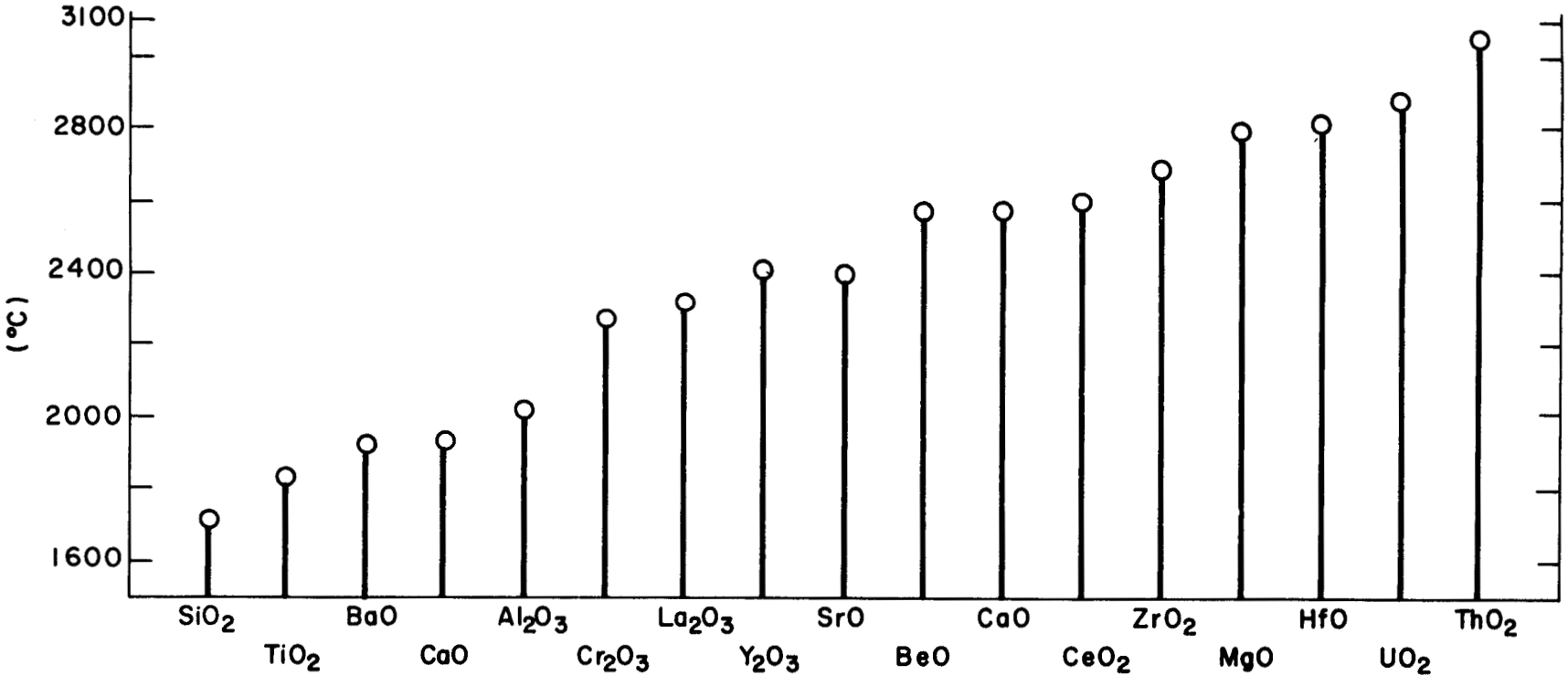

Figure D-1. Melting Point of Oxides (from several sources)

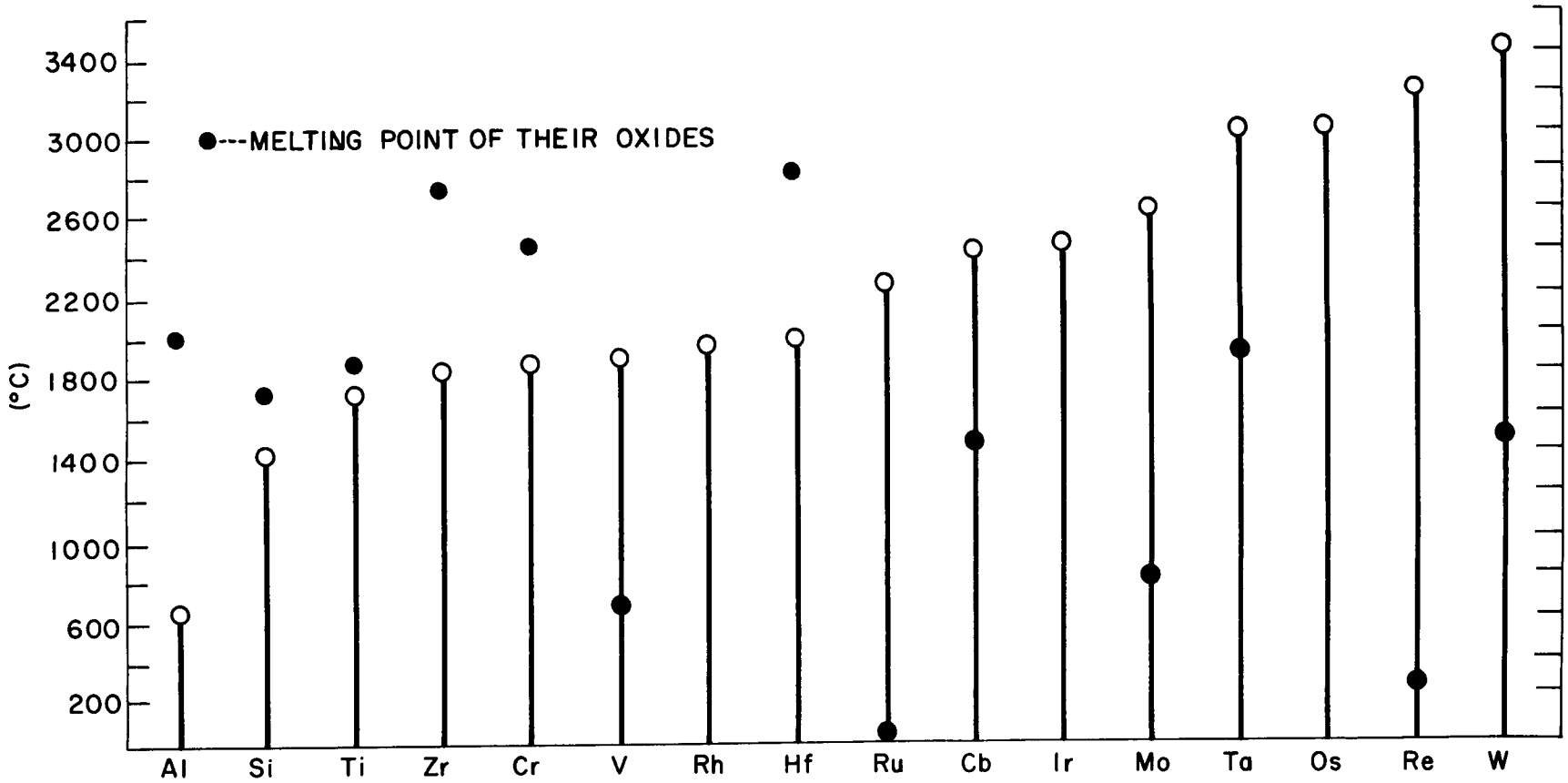

Figure D-2. Melting Point of Refractory Metals (Jaffee-Modified)

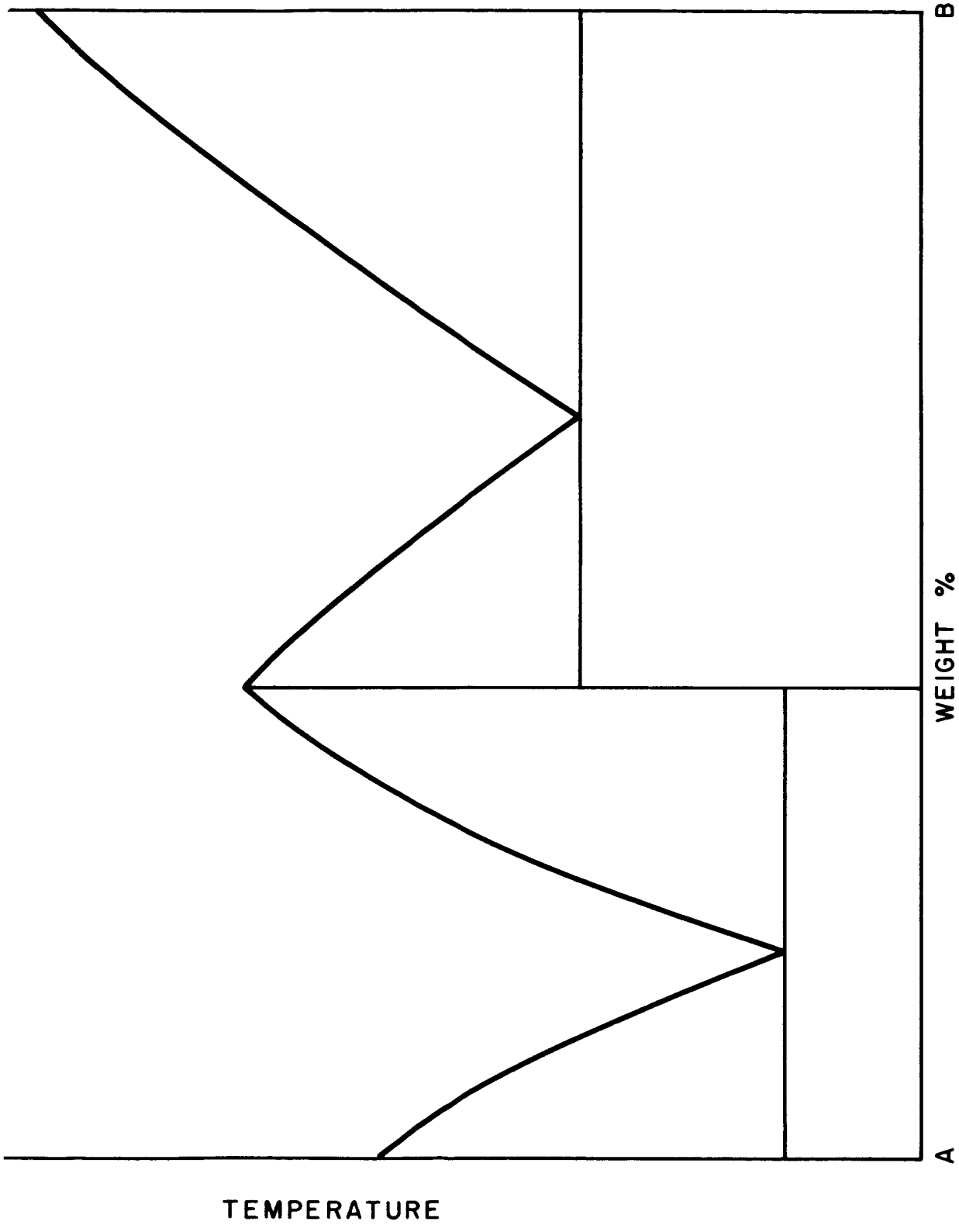

Figure D-3. Typical Phase Diagram for High Melting Oxides

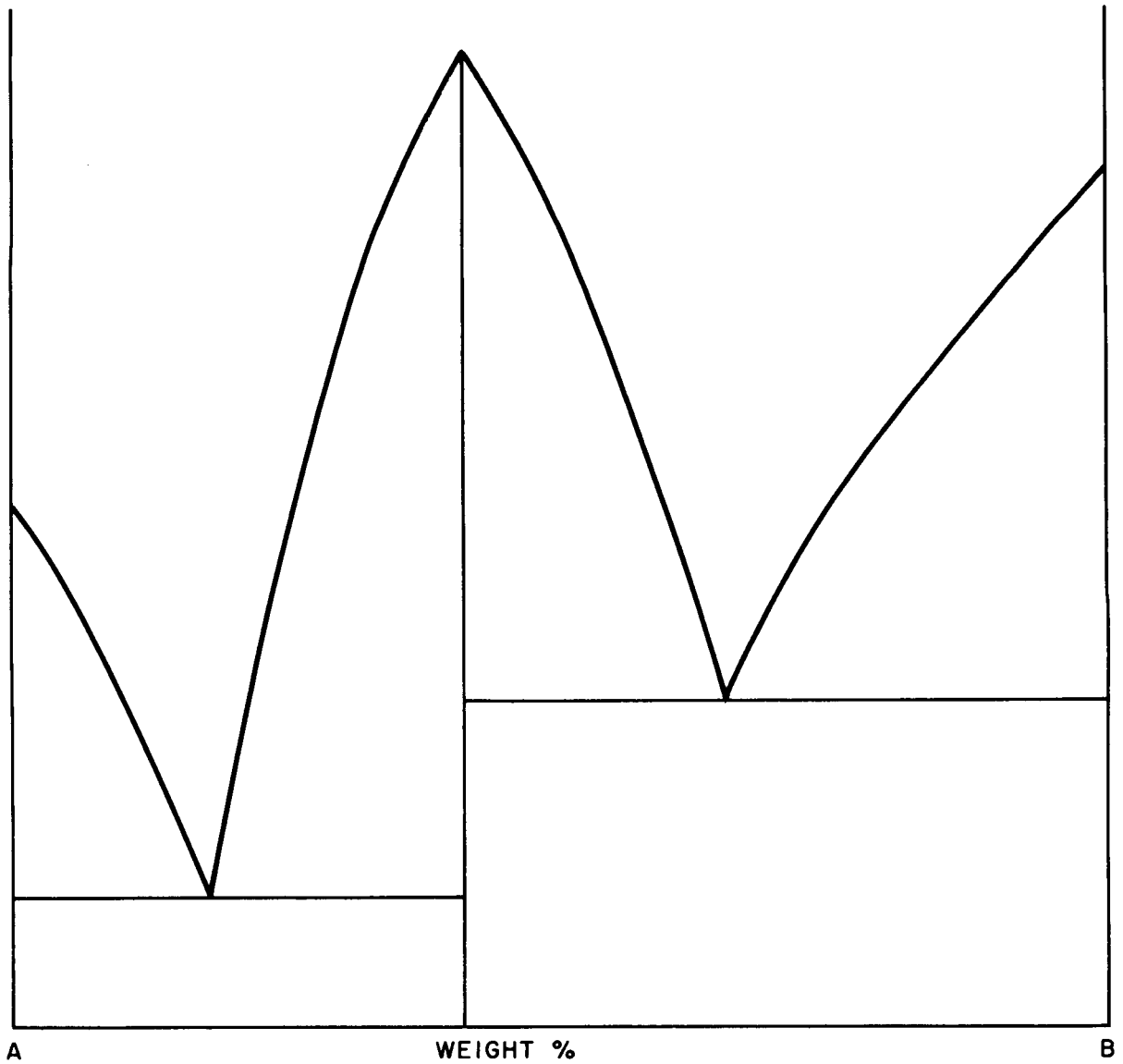

Figure D-4. Non-Typical Phase Diagram for High Melting Oxides

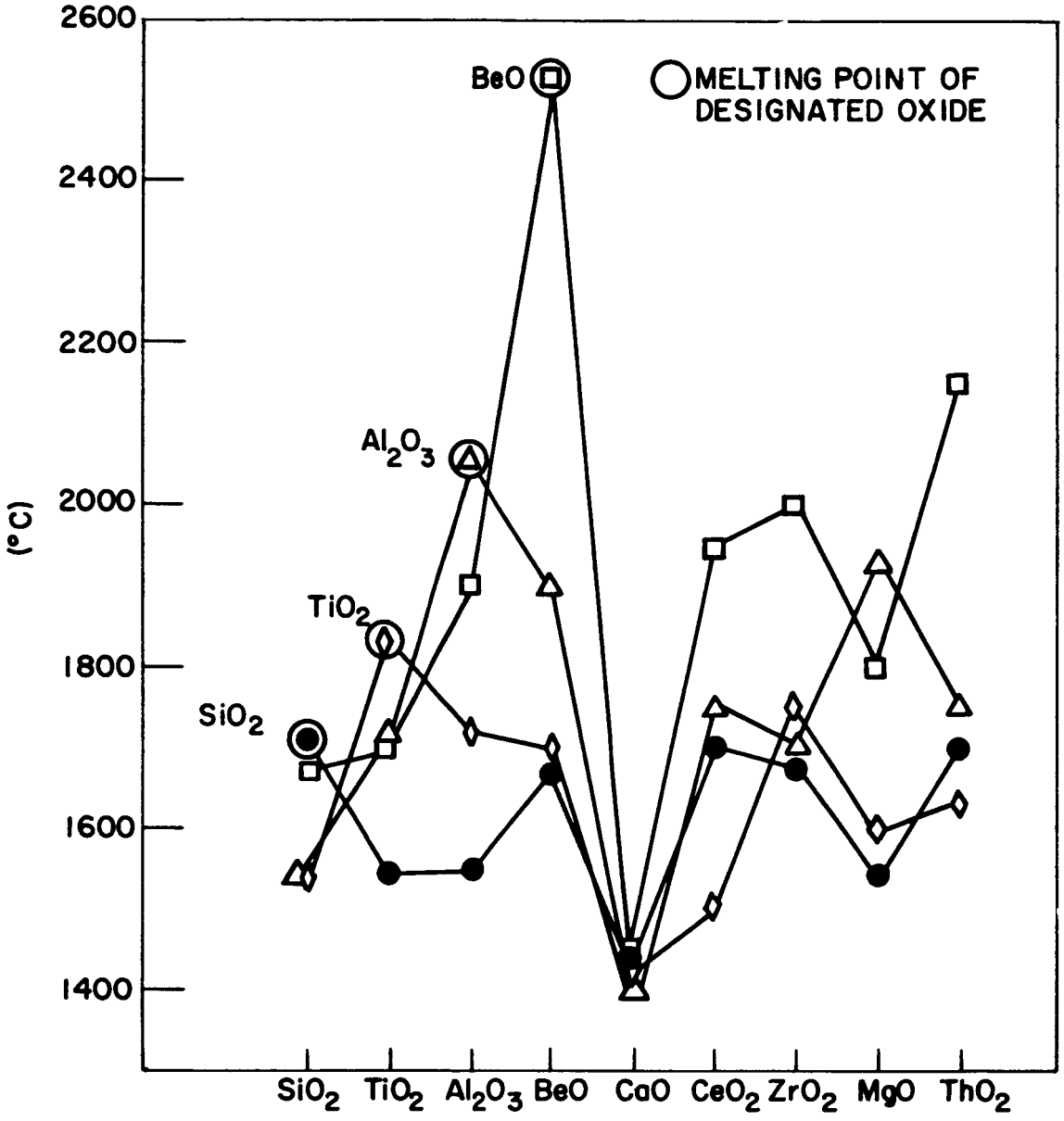

Figure D-5. Liquidus Temperature (^{o}C) for Various Oxide Combinations (After Kingery)

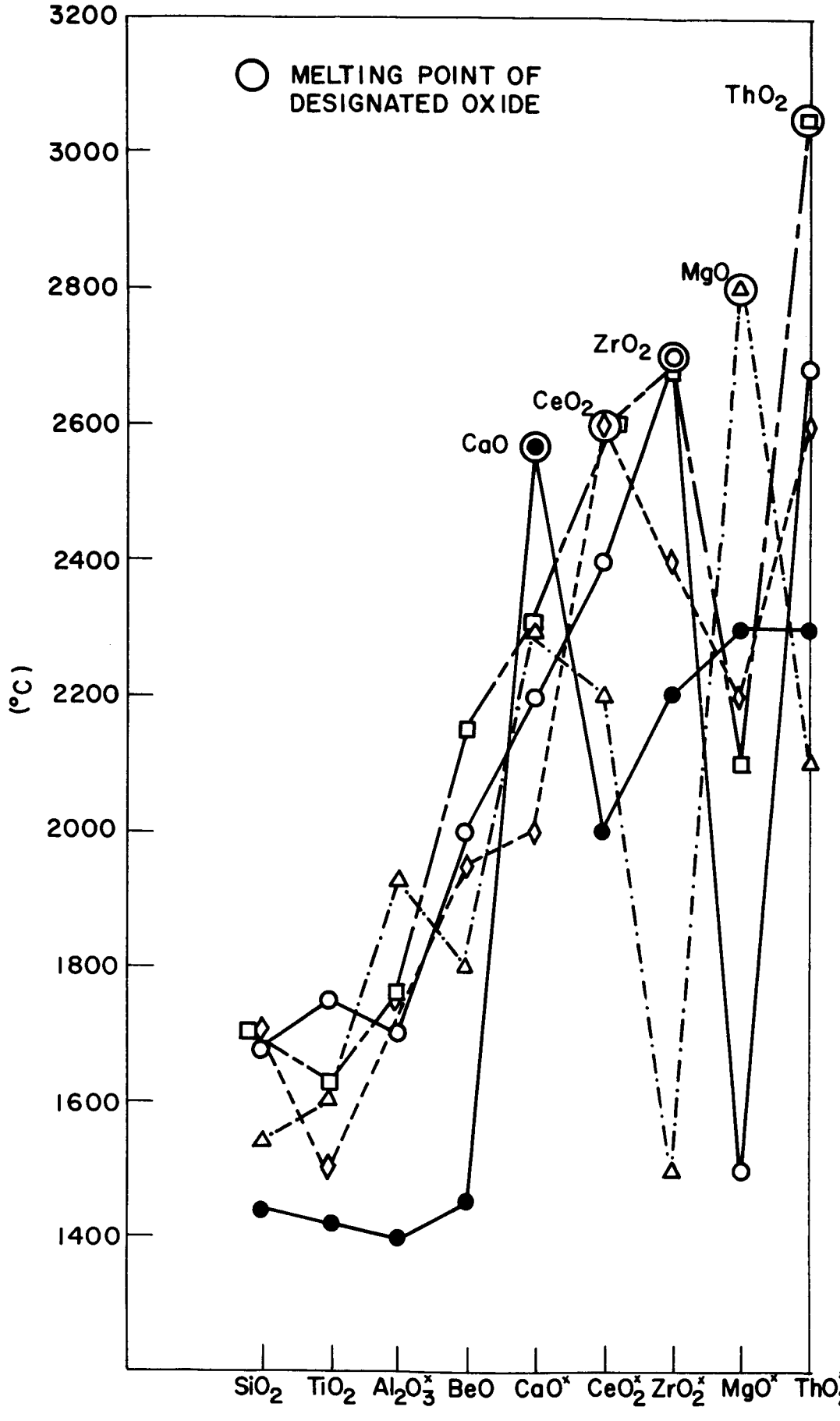

Figure D-6. Liquidus Temperature (^{O}C) for Various Oxide Combinations (After Kingery)

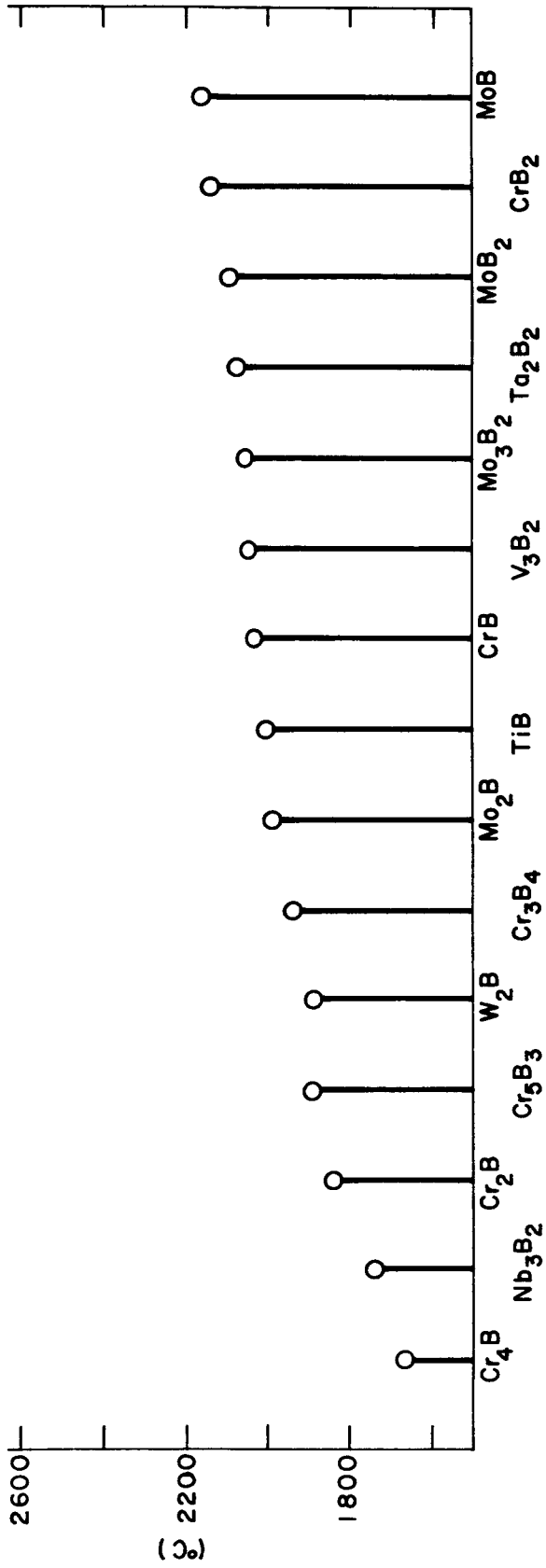

Figure D-7. Melting Point of Borides (Lower Temperature Group) (After Westbrook)

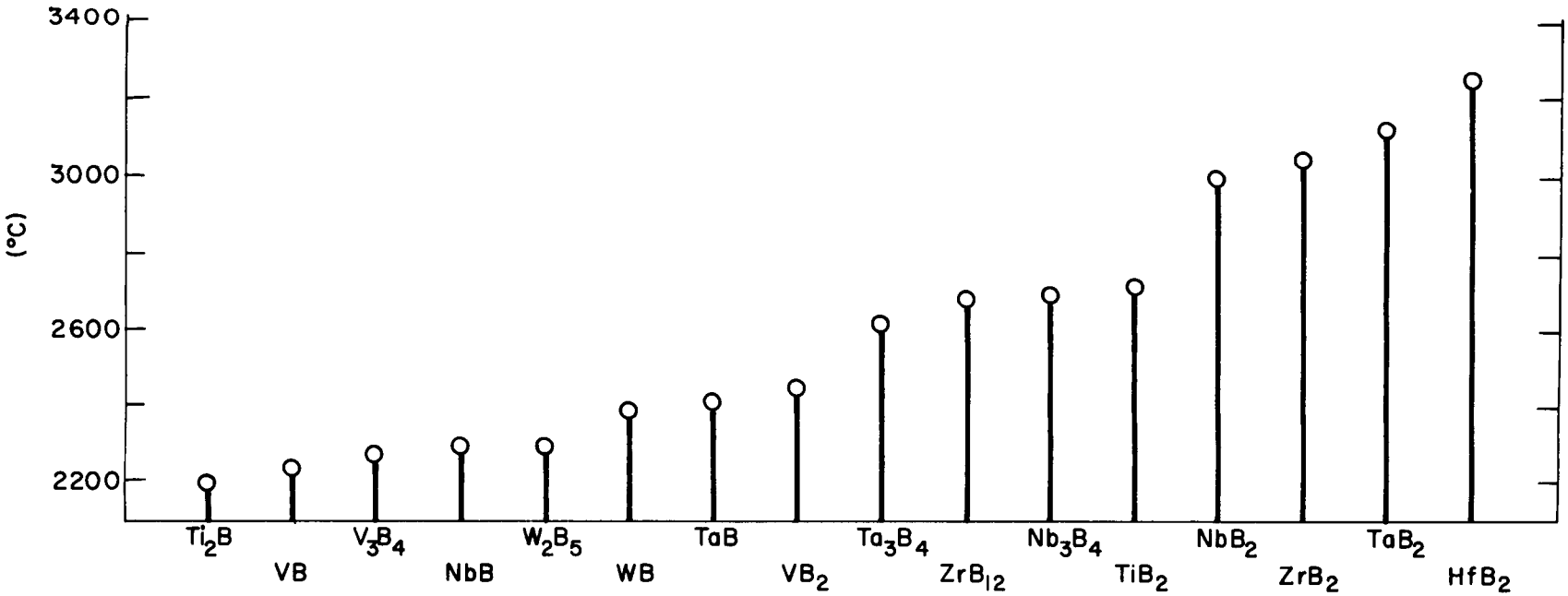

Figure D-8. Melting Point of Borides (Higher Temperature Group) (After Westbrook)

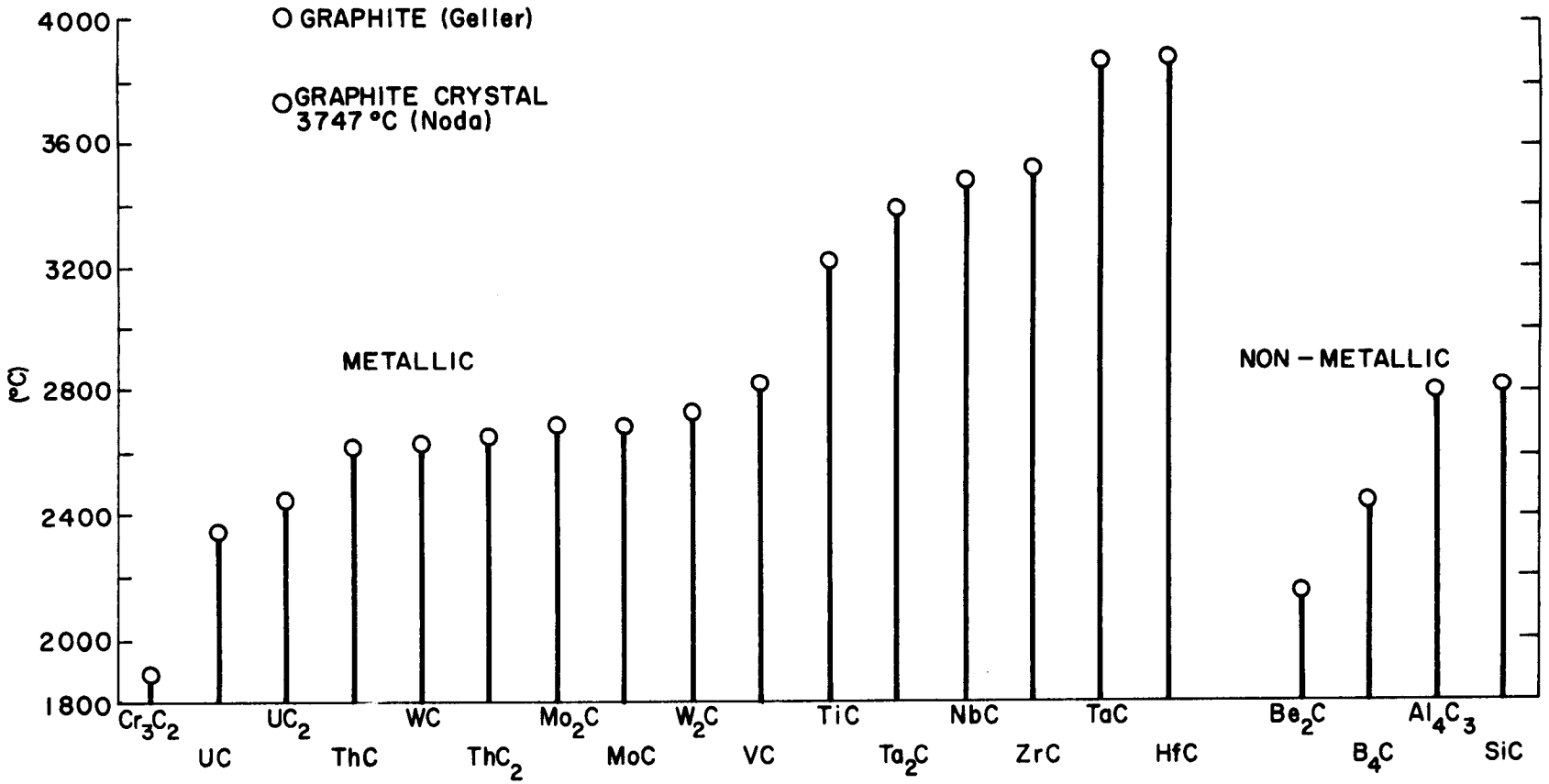

Figure D-9. Melting Point of Carbides (from L. M. Litz)

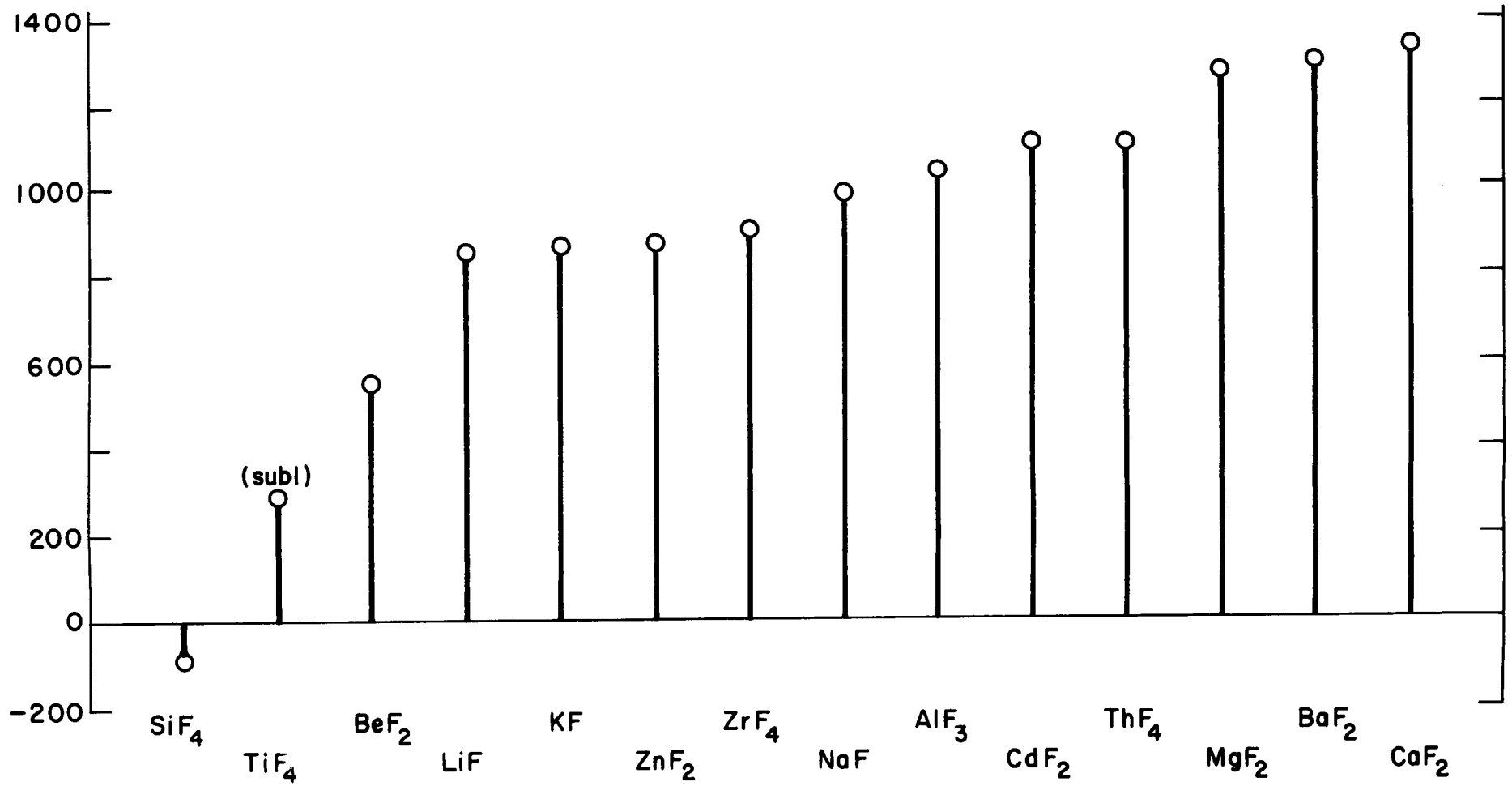

Figure D-10. Melting Point of Fluorides

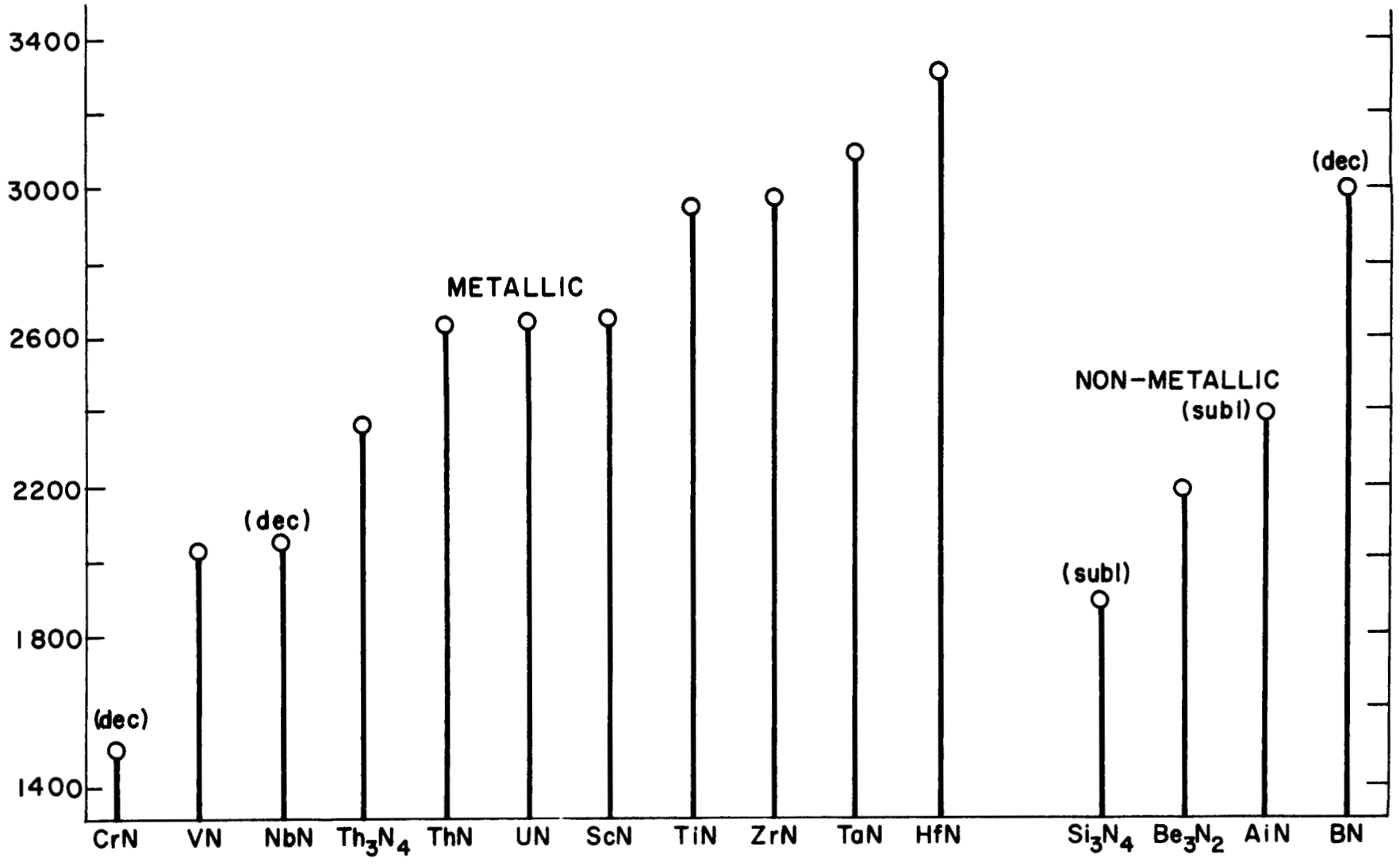

Figure D-11. Melting Point of Refractory Nitrides (After Litz)

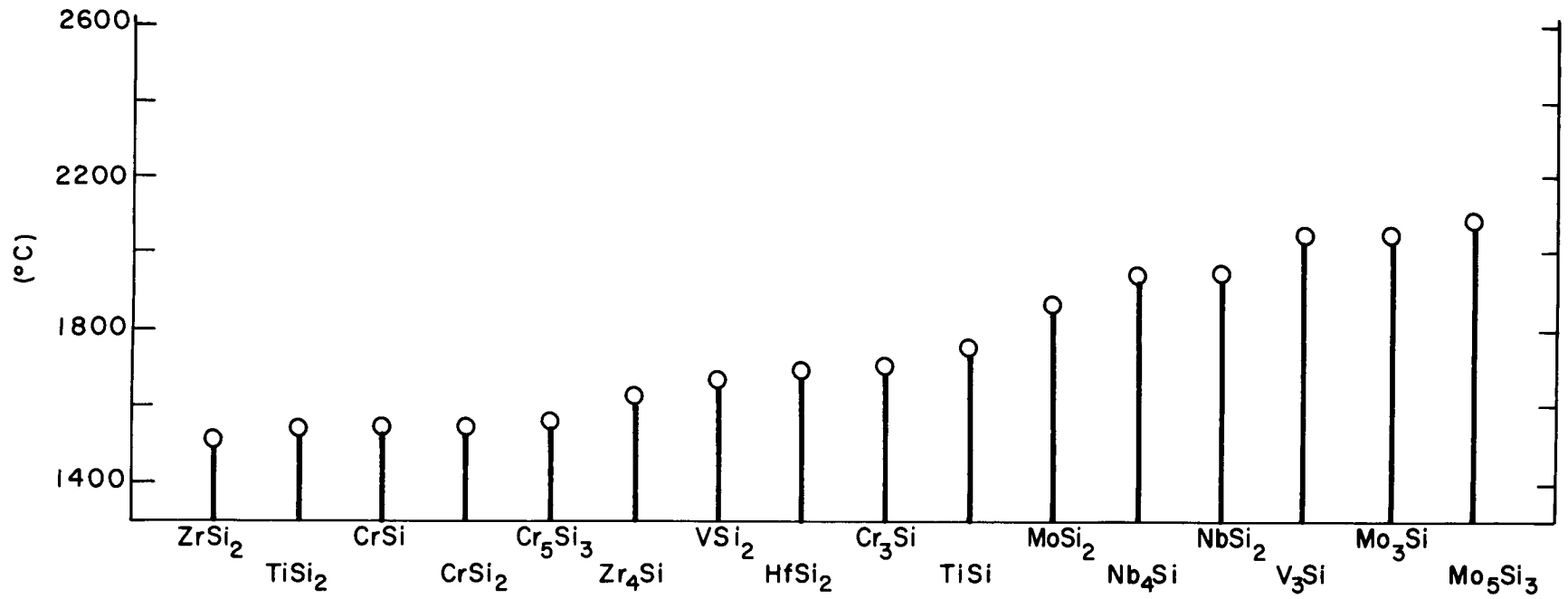

Figure D-12. Melting Point of Silicides (Lower Temperature Group) (After Westbrook)

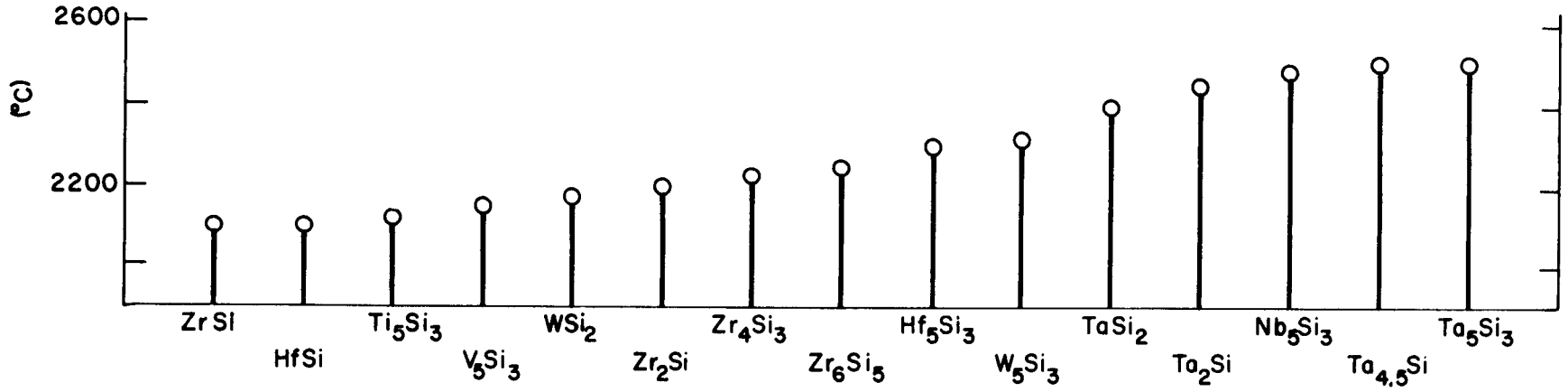

Figure D-13. Melting Point of Silicides (Higher Temperature Group) (After Westbrook)

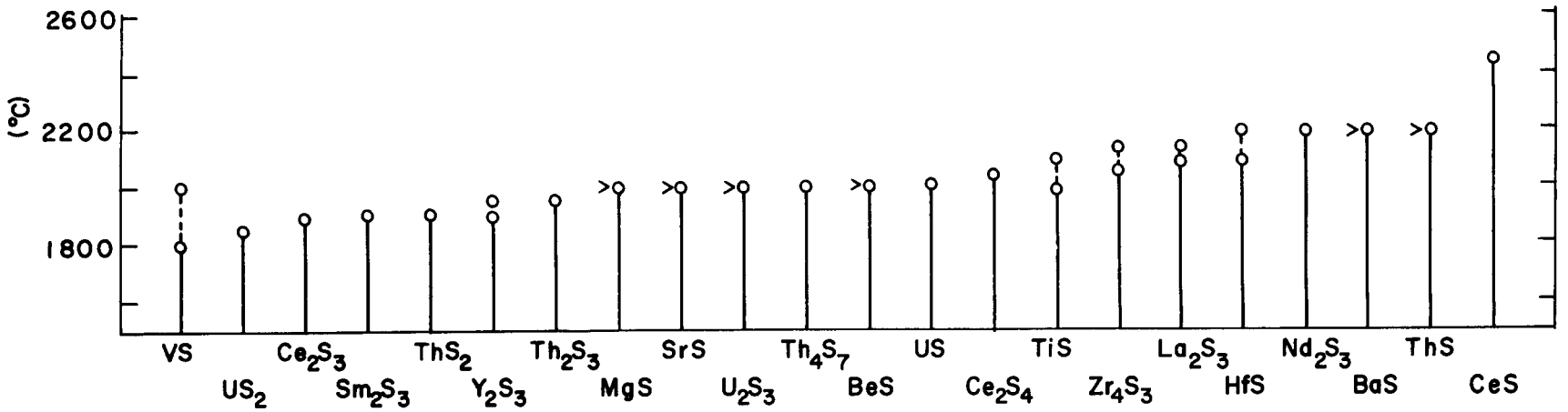

Figure D-14. Melting Point of Refractory Sulfides (After Litz)

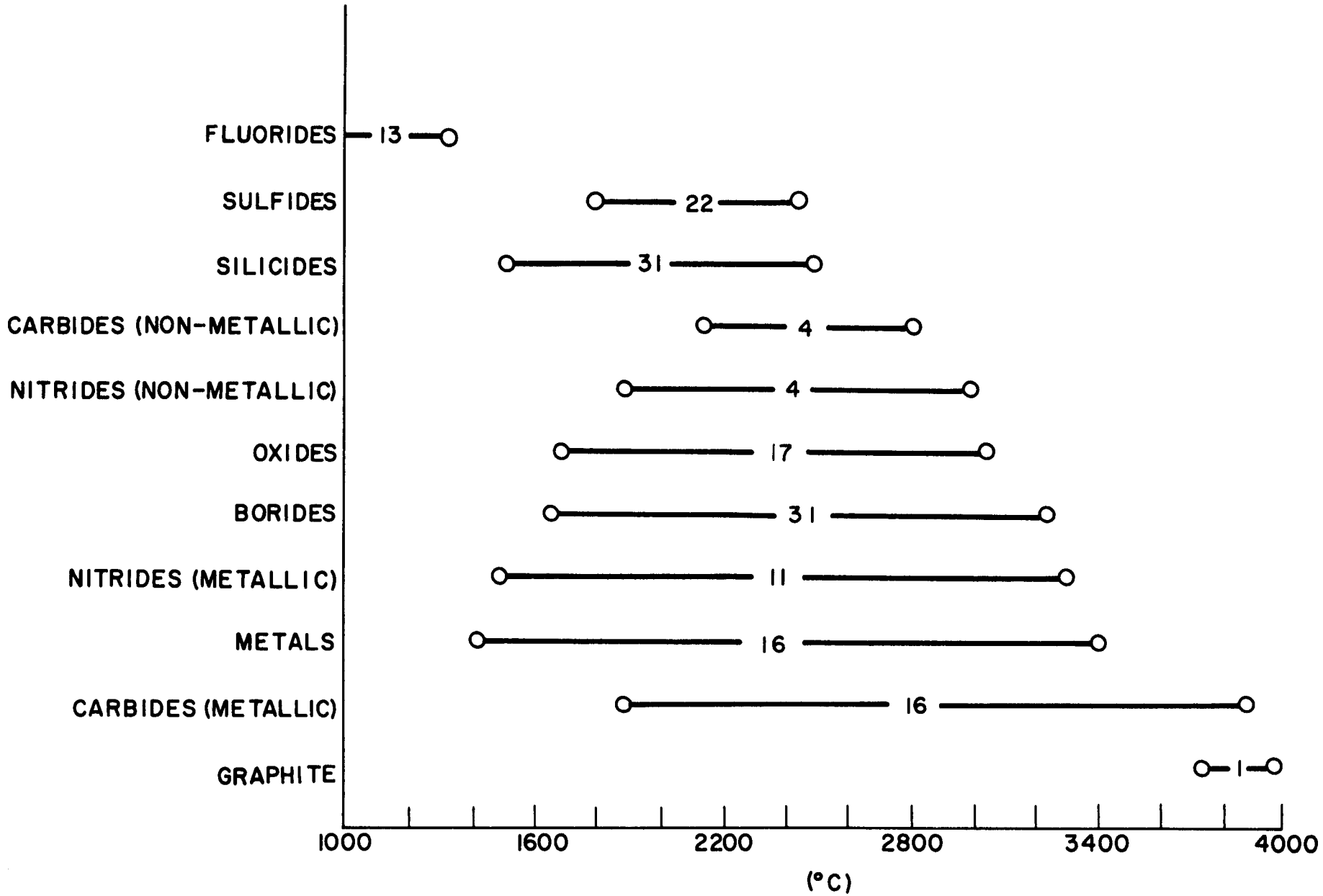

Figure D-15. Range of Melting Points of Refractory Materials